

SEISMIC DESIGN OF INDUSTRIAL RACK CLAD BUILDINGS

by

A. B. M. Rafiqul Haque

A THESIS SUBMITTED IN PARTIAL FULFILLMENT
OF THE REQUIREMENTS FOR THE DEGREE OF

MASTER OF APPLIED SCIENCE

in

The College of Graduate Studies
(Civil Engineering)

THE UNIVERSITY OF BRITISH COLUMBIA
(Okanagan)

April 2012

© A. B. M. Rafiqul Haque, 2012

ABSTRACT

Rack clad building (RCB) is a type of warehouse building system built using steel storage racks. Generally, these structures are larger and taller compared to regular storage racks commonly seen in superstores. These are built in a way that the peripheral frame can be used to support cladding. These structures possess some unique properties such as the members are built using thin walled perforated steel sections and the beam column joints utilizes teardrop connector in down isle direction. The hysteretic behavior of these connections is usually pinched type. Due to these properties the structure shows unique behavior under lateral loading. Until now very little research work has been carried out to determine the seismic performance of these structures. As RCB is a new type of structure, there exists no guideline in the current building codes for designing these structures against seismic loading. Here, a force and a direct displacement based design (DDBD) procedure have been adapted for designing RCB structures in the down isle direction. Finally, the performances of RCB frames designed under these two different methods have been compared and an optimum design method has been recommended for such type of structures.

PREFACE

A portion of this research work has been submitted to peer-reviewed journals for publication. All analytical modeling, literature review and mathematical calculations presented in the following journal papers have been solely carried out by the author. The thesis supervisor was responsible for the research guidance and review of the work produced by the author.

List of Publications Related to this thesis

Haque, A.B.M.R. and Alam, M.S. (2011). “Direct Displacement Based Design of Industrial Rack Clad Buildings.” tentatively accepted, *Earthquake Spectra*, EERI.

Haque, A.B.M.R. and Alam, M.S. (2011). “Direct Displacement Based Design of Industrial Rack Clad Buildings”, Submitted to BAH Enterprises Inc, Oakville, ON.

Haque, A.B.M.R. and Alam, M.S. (2011). “Force Based Design of Industrial Rack Clad Buildings.” Prepared for submission, *Journal of Structural Engineering*, ASCE.

Haque, A.B.M.R. and Alam, M.S. (2011). “Comparison between force and direct displacement-based design of industrial rack clad buildings.” Under preparation, *Journal Constructional Steel Research*, Elsevier.

TABLE OF CONTENTS

ABSTRACT	ii
PREFACE	iii
TABLE OF CONTENTS	iv
LIST OF TABLES	viii
LIST OF FIGURES.....	x
LIST OF NOTATIONS	xv
ACKNOWLEDGEMENTS	xix
DEDICATION	xx
CHAPTER 1: INTRODUCTION AND THESIS ORGANIZATION.....	1
1.1 General	1
1.2 Objective of the study	3
1.3 Scope of this research.....	4
1.4 Thesis organization	5
CHAPTER 2: OVERVIEW OF THE CURRENT STATE-OF-THE-ART	7
2.1 General	7
2.2 Advantages of RCB structures	8
2.3 Disadvantages of RCB structures.....	10
2.4 Comparison between RCB and steel storage racks	10
2.5 Consequence of failure.....	11

2.6	Difficulty in developing of a uniform guideline	12
2.7	Lateral force resisting system.....	13
2.8	Experimental and analytical studies	16
2.9	Component tests	20
2.10	Full scale tests	24
CHAPTER 3: DIRECT DISPLACEMENT BASED DESIGN OF RCB.....		26
3.1	General	26
3.2	Kinematic assumptions	28
3.3	Design steps.....	30
3.4	Case study	42
3.5	Section property calculation.....	42
3.6	Experimental results in literature	45
3.7	Hysteresis damping calculation.....	49
3.7.1	Effective damping.....	51
3.8	Displacement spectra.....	54
3.9	Calculation	55
3.9.1	Initial beam end rotation	55
3.9.2	Seismic weight calculation	60
3.9.3	Input data table.....	61
3.9.4	Preliminary calculation	62
3.9.5	Lateral force vector calculation	62

3.9.6	Final steps of calculation	63
3.10	DDBD of RCB frames with increasing number of stories.....	67
3.11	Results	71
3.12	Summary	75
CHAPTER 4: FORCE BASED DESIGN OF RACK CLAD BUILDINGS		76
4.1	General	76
4.2	Response modification factor calculation in literature.....	81
4.3	Current standard in rack Industry	84
4.4	Response modification factor.....	85
4.5	Overstrength factor.....	86
4.6	Force reduction factor calculation.....	89
4.7	Performance evaluation.....	101
4.8	Summary	107
CHAPTER 5: COMPARISON BETWEEN FBD AND DDBD OF RCB		109
5.1	General	109
5.2	Force vs. displacement based design.....	110
5.3	Frame design	113
5.4	Force based design	114
5.5	Direct displacement based design	114
5.6	Performance comparison.....	115
5.7	Summary	123

CHAPTER 6: CONCLUSIONS.....	125
6.1 Summary	125
6.2 Limitations of this study.....	126
6.3 Conclusion.....	126
6.4 Recommendations for future research.....	127
REFERENCES	130
APPENDICES.....	138
Appendix A: Incremental dynamic analysis output	138
Appendix B: Screenshots of the DDBD spreadsheet	143

LIST OF TABLES

Table 3.1: Mechanical properties of the RCB column section	45
Table 3.2: Relative section property of perforated column with respect to an intact column	45
Table 3.3: Mechanical properties of the beam selected for equation validation.....	58
Table 3.4: Beam end moment coefficient (γ) calculation.....	59
Table 3.5: Input data for DDBD.....	61
Table 3.6: Preliminary calculation	62
Table 3.7: Lateral force vector calculation.....	63
Table 3.8: Stiffness and base shear calculation.....	63
Table 3.9: Column base moment calculation	64
Table 3.10: Design bending moments for beams	65
Table 3.11: DDBD data of different height RCB frames.....	68
Table 4.1: Overstrength and ductility factor calculation from pushover analysis	89
Table 4.2: Connector design for different frame heights	90
Table 4.3: R_d values for four storied by four bay moment resisting frame.....	92
Table 4.4: R_d values for six storied by four bay moment resisting frame.....	92
Table 4.5: R_d values for eight storied by four bay moment resisting frame	93
Table 4.6: R_d values for ten storied by four bay moment resisting frame.....	93
Table 4.7: α and β coefficient proposed by Lai & Biggs (1980).....	96
Table 4.8: R^* & T^* values proposed by Riddell et al. (1989).....	96

Table 4.9: Force reduction factor for four storied by four bay frame 96

Table 4.10: Ductility overstrength and R_d values of 16 RCB frames 98

Table 5.1: Beam-to-column connector design data for the designed frames 115

Table A.1: Incremental dynamic analysis data for Northridge earthquake..... 139

Table A.2: Incremental dynamic analysis data for Kobe earthquake 140

Table A.3: Incremental dynamic analysis data for Emeryville earthquake 141

Table A.4: Incremental dynamic analysis data for Loma Prieta earthquake 141

Table A.5: Idealized (V_y) and elastic (V_e) base shear values from IDA..... 142

Table A.6: Force reduction factor (R_d) values from incremental dynamic analysis 142

LIST OF FIGURES

Figure 1.1: A rack clad building under construction.....	2
Figure 2.1: Basic components of a steel storage rack (adapted from Saar Lagertechnik GmbH (2010)).....	7
Figure 2.2: A typical RCB beam column joint (adapted from Saar Lagertechnik GmbH (2010)).....	9
Figure 2.3: Scene of the accident (left: front view with the original position of the rack indicated by yellow rectangles, right: side view) adopted from Affolter et al. (2009)	12
Figure 2.4: Experimental beam-to-column joint hysteresis (adapted from Beattie (2006))	14
Figure 2.5: Typical RCB box beam sections.....	16
Figure 2.6: A typical rack column.....	22
Figure 3.1: Flow chart of direct displacement-based design method.....	27
Figure 3.2: Kinematic assumptions of the semi rigid frame structure in down-isle direction (adapted from Filiatrault et al. 2006a)	29
Figure 3.3: Pushover analysis of RCB frames with and without gravity load	33
Figure 3.4: Standard damping vs. ductility curves (adapted from Priestley et al. 2007)	36
Figure 3.5: Displacement spectrum for Vancouver (soil class C) for different damping (%)	37
Figure 3.6: A sample connector moment rotation backbone plot using “Power model” (Prabha et al. 2010)	42

Figure 3.7: (a) Cross section of an RCB column and (b) FE model of an upright with perforation.....	44
Figure 3.8: Cantilever test model of the beam-to-column connection in FE software	47
Figure 3.9: Applied quasi static load.....	48
Figure 3.10: Simulated moment rotation behavior.....	49
Figure 3.11: Damping vs. ductility plot with connector hysteresis.....	53
Figure 3.12: Comparison between author's and Priestley et al. (2007)'s damping ductility plot of Takeda et al. (1970) hysteresis model	54
Figure 3.13: Site specific S_a-T response spectrum for Vancouver for different soil classes.....	55
Figure 3.14: Connector to beam relative stiffness vs. beam end moment coefficient	60
Figure 3.15: Chosen four bay and four pallet high RCB model for trial design.....	61
Figure 3.16: Trial moment rotation backbone curves of the connector	66
Figure 3.17: Change in base shear to weight ratio with change in number of stories.....	69
Figure 3.18: Change in seismic base shear demand with respect to number of stories	69
Figure 3.19: Change in total overturning moment with respect to number of stories.....	70
Figure 3.20: Change in maximum beam design moment with respect to number of stories	71
Figure 3.21: Response spectra of ten earthquake records matched with Vancouver response spectrum (PGA values shown inside bracket)	72
Figure 3.22: Displacement spectra of ten earthquake records matched with Vancouver soil class "C" response spectrum	73

Figure 3.23: Roof displacements and their values percentage higher (value inside bracket) than DDBD displacement profile..... 74

Figure 4.1: Relationships between force reduction (R_d), overstrength (R_o), response modification factor (R) and displacement ductility (μ) (adapted from Mwafy and Elnashai, 2002) 77

Figure 4.2: Flow chart of force based seismic design procedure 80

Figure 4.3: Comparison between the ductility reduction factor (R_d) and the definition of R_d (adapted from Mwafy and Elnashai, 2002) 86

Figure 4.4: Selected frames for incremental dynamic time history analysis (a) four story (b) six story (c) eight story and (d) ten story..... 87

Figure 4.5: Overstrength factor calculation for RCB moment resisting frames using pushover analysis 88

Figure 4.6: Beam-to-column connector backbone curve used for the analysis 91

Figure 4.7: Comparison of base shear-roof displacement curve from incremental dynamic and pushover analysis for a four storied RCB frame 94

Figure 4.8: Force reduction factors for different earthquake records 95

Figure 4.9: Pushover analysis of four storied frame with different bay widths 99

Figure 4.10: Pushover analysis of six storied frame with different bay widths 100

Figure 4.11: Pushover analysis of eight storied frame with different bay widths..... 100

Figure 4.12: Pushover analysis of ten storied frame with different bay widths..... 101

Figure 4.13: Roof drift of the four storied RCB frame from NLTHA 102

Figure 4.14: Roof drift of the six storied RCB frame from NLTHA 103

Figure 4.15: Roof drift of the eight storied RCB frame from NLTHA..... 104

Figure 4.16: Roof drift of the ten storied RCB frame from NLTHA..... 104

Figure 4.17: Maximum and residual interstory drift ratio of the four storied RCB frame
from NLTHA 105

Figure 4.18: Maximum and residual interstory drift ratio of the six storied RCB frame
from NLTHA 106

Figure 4.19: Maximum and residual interstory drift ratio of the eight storied RCB frame
from NLTHA 106

Figure 4.20: Maximum and residual interstory drift ratio of the ten storied RCB frame
from NLTHA 107

Figure 5.1: Roof drift of the four storied RCB frame from NLTHA 117

Figure 5.2: Roof drift of the six storied RCB frame from NLTHA 117

Figure 5.3: Roof drift of the eight storied RCB frame from NLTHA..... 118

Figure 5.4: Roof drift of the ten storied RCB frame from NLTHA..... 118

Figure 5.5: Maximum interstory drift ratio of the four storied RCB frame designed using
FBD and DDBD methods 119

Figure 5.6: Maximum interstory drift ratio of the six storied RCB frame designed using
FBD and DDBD methods 120

Figure 5.7: Maximum interstory drift ratio of the eight storied RCB frame designed
using FBD and DDBD methods..... 120

Figure 5.8: Maximum interstory drift ratio of the ten storied RCB frame designed using
FBD and DDBD methods 121

Figure 5.9: Residual interstory drift ratio of the four storied RCB frame designed using
FBD and DDBD methods 122

Figure 5.10: Residual interstory drift ratio of the six storied RCB frame designed using
FBD and DDBD methods 122

Figure 5.11: Residual interstory drift ratio of the eight storied RCB frame designed using
FBD and DDBD methods 123

Figure 5.12: Residual interstory drift ratio of the ten storied RCB frame designed using
FBD and DDBD methods 123

Figure B.1: Input data table of the excel spreadsheet 143

Figure B.2: Preliminary calculation table of the excel spreadsheet 144

Figure B.3: Story forces calculation table of the excel spreadsheet..... 145

LIST OF NOTATIONS

D_{max}	Maximum displacement of the base shear vs. displacement curve
d_b	Depth of beam
d_c	Depth of connector
E	Modulus of elasticity of steel
E_d	Energy dissipated by damping (Area inside hysteresis loops).
E_{se}	Maximum strain energy.
F_i	Story force at level i
F_t	Extra force at roof level
g	Acceleration due to gravity 9.80665m/s^2
h_{pi}	Is the elevation of the center of gravity of the i^{th} pallet with respect to the base of the storage rack
H_c	Height of the column
H_n	Height of building to roof level
H_i	Height of mass i in building design
h_i	Height of Story i,
I_b	Second moment of area of the beam
i	Integer
K_{be}	Stiffness of the doubly curved beam under lateral loading
K_{bu}	Effective rotational stiffness between the beams and uprights

K_c	Connector stiffness
K_e	Effective stiffness
K_u	Effective rotational stiffness at the base of each upright
l_b	Center to Center span length of the beam
M_{ci}	Column bending moment
M_{by}	Yield moment of the beam
M_{cy}	Yield moment of the connector
M_u	Ultimate bending moment of the connector calculated using power model
m_e	Effective mass
m_i	Mass at Story i
n	Number of Stories in multi-story building
n_s	Shape parameter, usual range of value 1 to 4
R	Response modification factor
R_d	Ductility related force reduction factor
R_o	Overstrength factor
R_{ki}	Initial stiffness of the connector calculated using power model
R_ξ	Reduction factor applied to displacement spectrum for damping ξ
S	Elastic section modulus
S_a	Spectral acceleration
S_d	Spectral displacement

T	Time period
T_e	Effective time period
t_u	Thickness of column
V_{base}	Base shear force
V_c	Column Shear force
V_d	Design base shear force
V_E	Elastic Structure base shear demand
V_{max}	Maximum base shear of the base shear vs. displacement curve
V_y	Actual/Idealized base shear capacity
W	Gravity load on the beam per unit length
W_{pi}	the weight of the i^{th} pallet supported by the storage rack
γ	Beam-end moment co-efficient
β_{hyst}	Hysteresis damping (%), represented as percentage of critical damping
β_{eff}	Effective damping (%) , represented as percentage of critical damping
β_{el}	Elastic damping (%), represented as percentage of critical damping
Δ	Target Displacement
Δ_i	Displacement at mass i
Δ_i''	Acceleration at mass i
Δ_c	Design Displacement at critical mass
$\Delta_{i,\omega}$	Reduced displacement at mass i

Δ_y	Yield displacement
Δ_{max}	Maximum/Ultimate displacement
δ_i	Dimensionless inelastic mode shape at mass i
δ_c	Value of Dimensionless inelastic mode shape at critical mass
μ	Displacement Ductility
μ_d	Design Ductility
θ_{be}	Beam end rotation
θ_{cy}	Yield rotation of the connector
θ_c	Code drift limit
θ_d	Design drift ratio
θ_i	Initial beam end rotation due to gravity load
θ_0	Reference rotation
θ_p	Plastic Rotation
θ_r	Relative rotation in radians
θ_y	Yield Rotation
ξ	Equivalent viscous damping ratio
ω_θ	Higher-mode drift reduction factors for DDBD of frames

ACKNOWLEDGEMENTS

I am extremely grateful to almighty Allah for helping me to bring my thesis into reality. I also greatly appreciate the support and mentoring of my supervisor Dr. M. Shahria Alam in completing my research. His knowledge, guidance and care were always there through my graduate studies at UBC. I also thank Dr. Abbas Milani, Dr. Solomon Tesfamariam, Dr. Ahmad Rteil and Dr. Kasun Hewage from whom I gained valuable knowledge and learned efficient techniques which I applied in my thesis.

UBC has provided an excellent educational and work environment through their systematic and efficient management system which was essential for my research. Also, I would like to acknowledge the financial support that I received from UBC and Natural Sciences and Engineering Research Council of Canada (NSERC). Additionally I acknowledge the support of our industrial partner BAH enterprises Inc. for providing technical support and knowledge when I needed them.

I am also grateful for the excellent research group where I was placed in. The highly experience research group mates provided excellent support in my research through criticism, discussion and technical knowledge. Thanks to my wonderful colleagues like Muntasir Billah, Nurul Alam and Samy Reza for this excellent experience.

Lastly, I would like to express my deepest gratitude to my parents who were always there for me through the ups and downs of my life. Also, I would like to thank my wife for excellent mental support and love. I also thank to almighty Allah for providing me a daughter who is the inspiration for all of my work.

Dedicated to my parents

Mr. Miah Mahmudul Haque

and

Mrs. Rokeya Haque

CHAPTER 1: INTRODUCTION AND THESIS ORGANIZATION

1.1 General

Recently, there has been a growing interest in building warehouse structures from steel storage racks. These structures are known as rack supported building or rack clad building (RCB). Generally, these structures are larger and taller compared to storage racks commonly seen in superstores. These are built in a way that the peripheral frame can be used to support cladding. These buildings provide the highest density storage solution with a very low construction cost, lead time and building footprint. Due to increasing land price and demand for fast construction, rack supported building is the optimal choice now a days in warehouse industry. These structures possess some unique properties for instance, the members are built using thin walled perforated steel sections where the beam column joints generally utilizes semi-rigid boltless connectors known as teardrop connectors in their moment-resisting frames. The hysteretic behaviour of these connections is pinched type and experiences high strength degradation under cyclic loading. Due to these unique properties, RCB structures show different behaviour under lateral loading compared to regular steel frame structures where the construction method is different. FEMA 460 (2005) and RMI (2008) provide design, installation, component testing and maintenance guideline for steel storage racks but no similar guideline exists for RCB structures. The steel storage racks have been extensively studied in the recent years, but until now very few or no research works have been carried out to determine the seismic performance of RCB structures. As the number of superstores and warehouses are increasing and public access to them is becoming frequent, safety is becoming a major concern. Now-a-days, these structures are an integral part of everyday public activity; therefore, the importance of

establishing a proper design guideline for such structures is critical. As rack structures are generally located inside of a larger structure, wind forces were generally ignored. In places where racks are attached to the main structure, often there is reluctance in considering seismic loading as well.

RCB warehouses by definition are type of warehouses in which the shelving facility is part of the building structure. In RCBs the shelving facility not only supports the load of the stored goods but also the load of the building envelope such as wind and snow. Most of these structures implement automated storage and retrieval system using advanced robotic equipment for handling merchandise (AR Storage Solutions 2012). Figure 1.1 shows a typical rack clad building under construction.



Figure 1.1: A rack clad building under construction

RCB structures need to be properly designed against lateral forces as they pose higher risk towards public safety compared to conventional steel storage racks. Although the National Building Code of Canada (NBCC 2005) recognizes the seismic risk of rack storage systems and

recommends that seismic provisions be provided while designing these types of structures, it has no guideline for designing RCB structures against seismic loading.

1.2 Objective of the study

The objective of this research is to develop a seismic design guideline to assist structural design practitioners for designing RCB structures. In order to fulfill this objective two different well-established seismic design methodologies have been adapted in this study namely, force and direct displacement based design. In particular, this study will focus on

1. Development/adaptation of force based design (FBD) for RCB frames. In this research some important design parameters such as ductility related force reduction and overstrength factor will be determined. These parameters will be used for calculating seismic design base shear for RCB structure and also proportioning member size.
2. Development/adaptation of displacement based design (DDBD) for RCB frames. This objective will be achieved by adapting DDBD method developed by Priestley et al. (2000) for RCB frames. Necessary equations and figures have been developed for the need of this design method and are presented in this study.
3. Determination of more suitable design method for RCB frames among the selected two design methods. Here, the seismic performance of RCB frames designed as per force and displacement based design approach will be evaluated.

1.3 Scope of this research

In order to achieve the above mentioned objectives of this study a literature review was carried out to learn about the behavior of RCB frames. As only a handful study exists on RCB frames, the author has carried out extensive study on the fundamental building blocks of RCB structure, which is known as steel storage rack. The steel storage racks have essentially the same elements of RCB structures except they are much smaller in size, non-self-sustaining and does not support roof or cladding on them. But the fundamental building blocks such as beams, columns and braces are similar for both structures. To achieve the stated goal in the objectives the followings were carried out:

1. Finite element models were built in SAP2000 (2010) environment. For accurate modeling the effect of perforations which exists on rack columns were taken into consideration by appropriate mechanical property reduction factors. The beam-to-column joint hysteresis behaviour of RCB frame was taken from the experimental study of Beattie (2006). This behaviour was incorporated in the finite element model using link elements. Later nonlinear static and incremental dynamic analysis (IDA) was carried out for the calculation of overstrength (R_o) and ductility related force reduction factor (R_d) respectively.
2. For the adaptation of displacement based design an equation has been developed using direct integration method for the calculation of yield rotation of RCB frames. Using this equation, finite element model and nonlinear time history analysis (NLTHA) ductility vs. damping has been established for RCB moment resisting frame (MRF). Using the developed equation, damping vs. ductility curve and

displacement response spectrum some RCB MRF has been designed and finally their performance was evaluated using NLTHA.

3. Using the above mentioned two methods some RCB frames were designed and their performance has been analyzed using nonlinear time history analysis under several earthquake records. After the analysis the performance data has been compared to determine the better performing design method among the two.

1.4 Thesis organization

This thesis is organized in six chapters. In the present chapter a short introduction, objective and scope of the research is presented. The content of this thesis is organized into the following chapters:

In **Chapter 2**, a comprehensive literature review on RCB and steel storage rack structure has been presented. First the frame system is reviewed; their similarity and dissimilarity to standard steel structure has been discussed. Later their behaviour under standard gravity and lateral loading condition is reviewed. At the next step the individual frame component like rack columns and beam-to-column connector behaviour is discussed. Finally the two design methods under consideration have been thoroughly reviewed.

In **Chapter 3**, Direct displacement based seismic design has been adapted for RCB structures and the performance of the designed frame has been evaluated using time history analysis of ten earthquake records.

In **Chapter 4** Force based seismic design has been developed for RCB frames. The value of force reduction factor and overstrength factor has been calculated by using incremental dynamic

time history and nonlinear static analysis respectively. Finally an RCB frame was designed using these factors and its performance was evaluated using nonlinear time history analysis of ten earthquake records.

Chapter 5 demonstrates a comparative study of performance of RCB frames designed under direct displacement and force based method. For this study two RCB frame with similar geometric property has been designed under two methods and their performance has been carried out using nonlinear time history analysis under ten earthquake records.

Finally, **Chapter 6** presents the conclusion of this research. Some recommendations for future research on this topic have also been suggested in this chapter.

CHAPTER 2: OVERVIEW OF THE CURRENT STATE-OF-THE-ART

2.1 General

Rack clad building system has become very common in the warehouse industry due to their low cost, constructability and movability. These structures are made of thin walled perforated steel sections. These structures are built from steel storage racks which are used as primary building blocks for RCB structures. According to CSA A344.2 (2005), steel storage racks are considered unusual structures because of their semi-rigid frames and proprietary connectors. These structures show higher performance in carrying gravity load compared to those of regular steel and concrete structures as they usually carry 20 to 50 times higher load compared to their self-weight. Figure 2.1 shows the basic components or primary building block of a RCB structure.

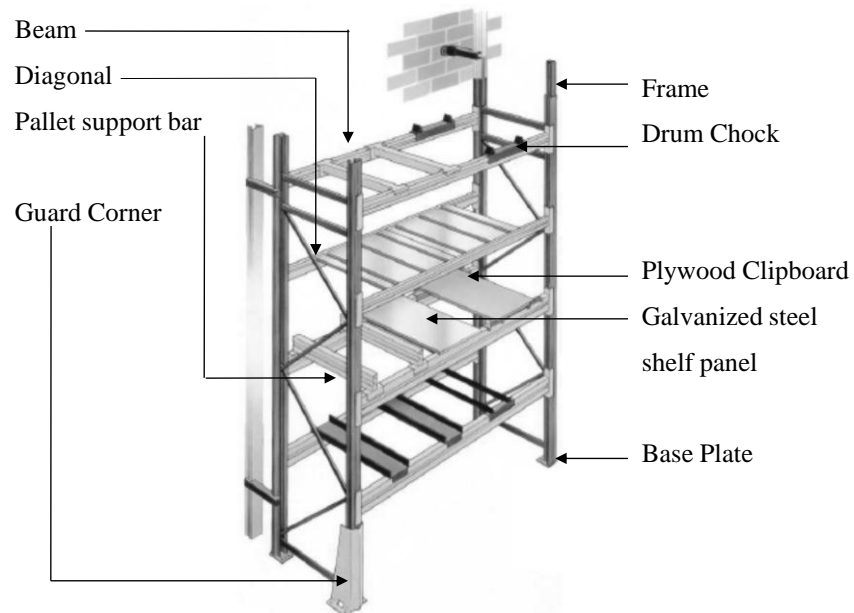


Figure 2.1: Basic components of a steel storage rack (adapted from Saar Lagertechnik GmbH (2010))

Like multi-story buildings, RCB structures can be built to considerable heights (Kilar et al. 2011). RCB structures in zones of high seismicity can experience large lateral loads, which pose additional risk from shedding of merchandise (Sideris et al. 2010; Alhan and Gavin 2005). They are usually made of thin-walled cold-formed steel section where columns are generally open sections made of perforated steel plates having one axis of symmetry. Beams are usually closed box sections (Godley 1997; Freitas et al. 2010; Filiatrault et al. 2010; Ng et al. 2009). The frame is built from connecting columns and beams. Usually the span is kept fairly uniform and for this reason the structural elements can almost entirely be made in the manufacturing plant and can be brought at site for assembly.

2.2 Advantages of RCB structures

There is substantial amount of cost savings in rack clad building construction as no additional warehouse building is required for holding wall and roof. There is no height restriction as RCB's are not built inside warehouses so they can be utilized with maximum capacity. The clients do not need to do anything during installation as the system is manufactured and installed with entire components. Another advantage of RCB is that the system can be disassembled and moved to another place if required by the client. The beam column joints usually employ semi rigid boltless connectors also known as teardrop connectors (Figure 2.2) which gives the flexibility of adjusting story height if required (Beattie 2006) compared to general steel structures which use bolted/welded moment frames. This flexibility of story and span height adjustment is very attractive to the owners (Temesist 2011).



Figure 2.2: A typical RCB beam column joint (adapted from Saar Lagertechnik GmbH (2010))

As no welding or riveting work is required and most of the preparation can be done before bringing the structural component on site, RCB can be classified partially under modular steel building (MSB) category. Annan et al. (2009) stated that MSB is a rapidly evolving alternative to traditional steel buildings. MSB's are designed and finished at one location and transported to be used in another location for use. The completed MSB units are connected horizontally and vertically at site. MSBs have been typically used for building hotels, apartments, schools, dormitories and correctional facilities up to six stories tall which have typical design repetition. RCB is an engineered modular steel building system which can be constructed 40% faster than the traditional ones (Frazier Industrial, 2011). Not only the construction method of RCB is economic but also the structure itself is cost-effective compared to those of traditional buildings.

Another advantage of these structures is good salvage value. Due to the use of semi-rigid boltless connectors, structural elements can be salvaged without almost any damage when required which ensures great salvage value. This is another reason for which these structures are getting popular day by day in the warehouse industry.

2.3 Disadvantages of RCB structures

Although these structures have advantages with respect to constructability there are some major disadvantages. The semi rigid beam-to-column connections used for these structures have very low moment-rotation stiffness compared to welded or bolted connections. The moment-rotation hysteresis of this type of beam-to-column connection is usually pinched shaped and the reloading stiffness under cyclic loading degrades rapidly compared to bolted or welded connections as shown in Bernuzzi and Castiglioni (2001). As a result, the energy dissipation through hysteresis reduces significantly after few cycles during earthquakes. Until now few research works have been done on the hysteresis behaviour of these connectors used in RCB frames. Most of the research work (Filiatrault et al. (2006), Beattie (2006)) has been done on steel storage racks which are primary building blocks of Rack Clad buildings but at a smaller scale.

2.4 Comparison between RCB and steel storage racks

The similarities between RCB and steel storage racks are that they use essentially same primary building blocks. The beams, columns, braces, beam-to-column connectors and column to base-plate-connectors are generally the same. The key difference between the steel storage rack structures and RCB structure is that the former one requires a larger structure (Primary structure) for its protection from wind or earthquake load. Generally, steel storage racks are installed inside of a larger warehouse structure so that the wind load is resisted by the primary structure. Also racks are generally connected at a higher frame location with the primary force resisting system of the main warehouse structure; therefore, their response under seismic loading is limited by the response of the primary structure. Since the RCB frames are much larger and

self-sustaining, the environmental load calculated for their design such as wind or earthquake loading can be significant which is not usually taken into consideration for steel storage racks placed inside of another building. This is why large RCB structures also employ braces in their down-isle direction.

2.5 Consequence of failure

Failure of steel storage racks which are basic components of RCB structures can have fatal consequence. Affolter et al. (2009) investigated such an incident where a high storage rack collapse in a depot for building materials without any preceding warning or indication. As a result a warehouse worker was killed from the impact of falling building materials. It happened during the warehouseman's operation with forklift which he was operating to move pallets from one place to another. The scene of the accident is shown in Figure 2.3. It was found from Affolter's analysis that the failure occurred due to overloading of a column, where the manufacturer's recommended capacity was 50 kN and the column was loaded up to 68kN just before the accident. If the design guideline had implemented higher factor of safety, this incident could have been avoided. For RCB structures, the consequence of a primary load carrying member's failure can have serious consequences as a large number of people may work inside these structures, which will result in a higher number of death and injury.



Figure 2.3: Scene of the accident (left: front view with the original position of the rack indicated by yellow rectangles, right: side view) adopted from Affolter et al. (2009)

2.6 Difficulty in developing of a uniform guideline

The difficulty in developing a uniform seismic design guideline for RCB structure is primarily due to the fact that large variation of different types of beam-to-column connectors are present in the market. These different types of connectors show different types of hysteretic behaviour under cyclic loading, which makes it very difficult for researchers to arrive at a single force reduction or overstrength factor for such structures. Also RCB structures can be made of moment resisting frame (MRF) only or a combination of braces and MRF as well depending on the structures size, load and seismic force demand. There can be many different configuration with respect to bracing type and their location on the frame. In this study, only the down-isle frames have been considered for brevity and the braced frames will be studied in our future research.

2.7 Lateral force resisting system

In rack industry, the columns are known as uprights. The frame system consists of upright posts with holes at regular interval for connecting beams on one side and braces on the other side, which can be seen in Figure 2.2. They rely on portal frame action in the down-aisle direction and frame action in the cross-aisle direction to resist lateral loads. The basic components of steel storage racks are shown in Figure 2.1. The story height of rack structures can vary depending on the stock required to be stored as described by Beattie (2006). Often braces and cables are used in the down aisle direction to reduce the horizontal deflection due to lateral load.

The moment resisting frame system used in the down-aisle direction of steel storage racks uses teardrop beam to upright connection, although the connection appears similar to steel moment-resisting frames defined in the 2003 NEHRP recommended Provisions FEMA (2004), it behaves quite differently than the connection system commonly used in buildings (Filiatrault et al. 2006).

Generally, moment resisting connections in buildings are designed to cause inelastic deformations in the beams away from the beam column joint, but in this type of structure inelastic behavior occurs directly in the beam-to-column connections. Besides, there is a significant difference between the behavior under positive and negative bending moment as the connector used at the beam column joint often is unsymmetrical (Filiatrault et al. 2006). The researchers also found out that although the system exhibits highly nonlinear behavior up to very large relative rotations between the beams and columns, it remains almost elastic because the behavior does not cause permanent deformation in the beams and uprights.

The inelastic rotation capacity of beam-to-upright connection is significantly high, for example the connection hysteresis adapted from Beattie (2006) used in the analysis has exceeded 0.068 radians and according to FEMA-460 (2005), rack design sometimes requires connectors with rotation capacity up to 0.2 radians. Figure 2.4 shows the moment rotation hysteresis test result of a RCB beam column joint done by Beattie.

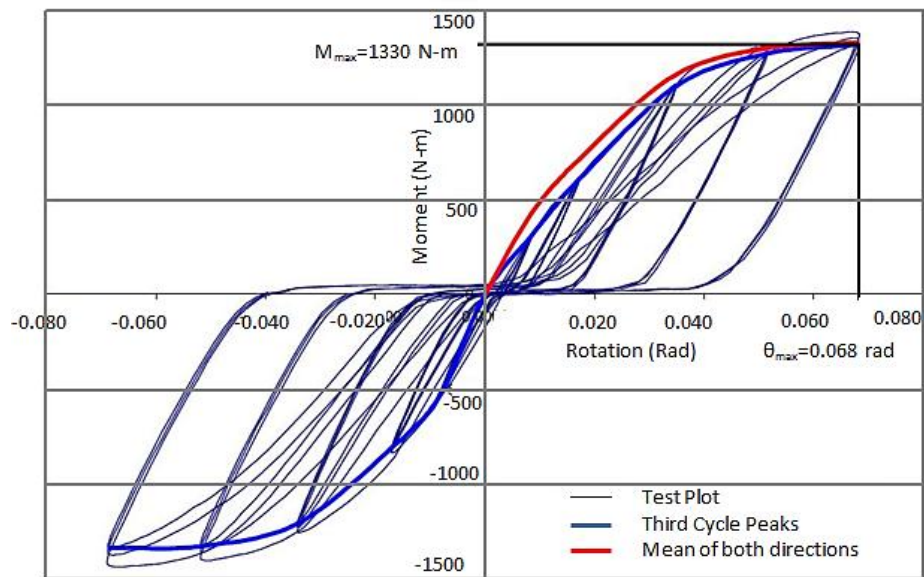


Figure 2.4: Experimental beam-to-column joint hysteresis (adapted from Beattie (2006))

Filiatrault et al. (2006a) also found out from experimental study that it can be as high as 0.2 radians. In contrast, building moment-resisting connections have inelastic rotation capacity of around 0.04 radians for special moment-frame systems. As these structures have low story heights with long fundamental time period compared to general building structures, the rotational demand at the beam column joint also become very large to withstand strong earthquake ground motion.

All nonlinear deformation for rack structures occurs at the connector rather than in the frame members. Therefore, it is easy to push back the structure in its original position after a seismic

event. The downward wedging action of the lugs or studs under gravity loading provides a self-centering ability to the racks, which helps the racks to easily recover their initial positions (Beattie 2006). Beattie also presented a design guideline for high level storage rack structure with public access. The guideline has been developed for New Zealand building code after a thorough study of the existing overseas standards. He has also performed extensive nonlinear analysis of computer model and carried out laboratory testing of racking components. Beattie (2006) also provided stocking recommendation for storage racks in his study. The design guideline suggests that for both cross isle and down isle direction the maximum ductility used for design should be 1.25 and in no case should go beyond 3.0 for down isle direction except if a detailed study suggested otherwise. A beam-to-column joint/connector moment-rotation hysteresis (Figure 2.4) is also presented in his paper from cantilever testing of the beam-to-column joint. The hysteresis shows significant pinching and strength degradation, which is very different from the general steel structure's beam-to-column joints. Finally, he recommended that the structural element behaviour should always be tested first before using the guideline.

The other structural elements such as the posts are generally made of 1.8mm, 2mm, 2.6mm and 3mm thick cold formed steel. The shape of the section is commonly known as Ω sections. Beams are generally rectangular box section as shown in Figure 2.5 with thickness varying from 1.5mm to 1.8mm. The beam depth ranges from 72mm to 150mm. The width is generally 50 mm. Braces are generally made of 'C' sections typically 45mm x 30mm x2mm, and 60mm x 30mm x 4mm. Sometimes cables are also used as tension only braces. The structural connection between the braces and the frame intersection points are usually pinned joints.

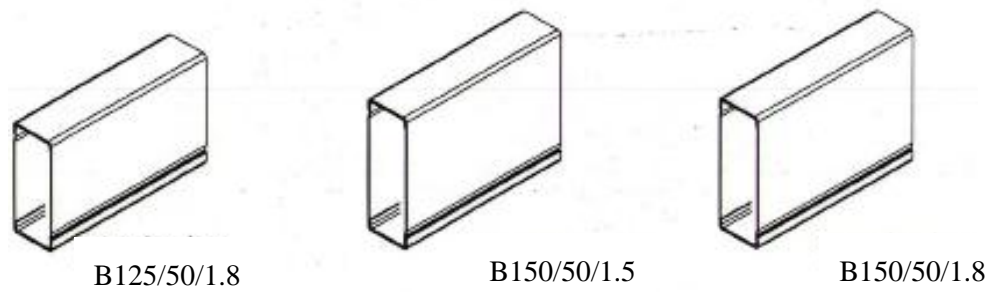


Figure 2.5: Typical RCB box beam sections

2.8 Experimental and analytical studies

Performance based seismic design is the state-of-the-art in structural engineering. The goal is to design structures in such a way that it performs exactly as it is designed for. This is achieved by controlling displacement or damage of the structure by taking damage related parameters directly into account during the design process. Filiatrault et al. (2006) have developed a performance based seismic design guideline for steel storage racks in their study. They have developed a simple analytical model to capture the behaviour of steel racks under seismic excitation in down isle direction. For the analytical model they assumed that the beam column joint and the column base plate connection have lower moment rotation stiffness than that of the beams and columns. Under lateral loads, the connections experience nonlinear response where the beams and columns essentially remain elastic. The researchers verified their assumptions using shake table testing of the rack structures. Finally, they presented a worked out example on the developed displacement based design of rack storage structure and found out that their analytical model can predict base shear demand within 10% accuracy of the experimental result. This analytical model has been used and further improved in this thesis for the direct displacement based design.

Fundamental or natural time period is another very important parameter for the seismic design of all types of structures. The current seismic design method calculates the seismic force demand by using the fundamental time period. A detail analysis was carried out by Bajoria et al. (2010) for calculating fundamental time period of steel storage racks under different loading condition. They have used experimental as well as finite element analysis to calculate the time period of different types of racks built with various beam end connectors. A total 18 types of beam end connectors have been used in this study. 3D finite element models were built in ANSYS with different height, bay lengths and with/without loads to compare the change in time period due to changes made with these parameters. Bajoria et al. (2010) also presented a simple analytical method for calculating the time period of rack structures. The results of the finite element analysis and the analytical result were compared and it was shown that the variation in the result is not significant. They concluded that there is no need to make detail 3D models as the analytical equations can accurately predict the fundamental time period of the structure. They also found out that the finite element simulation of the experiment can also predict the beam end connector stiffness accurately which makes the need for laboratory experiment redundant. Based on the above mentioned findings, and as there was no laboratory facilities available, only analytical study was carried out in this research. The analytical model presented in Bajoria's paper is taken from the work of (Filiatrault et al. 2006). The limitation of this study is that they only checked their finite element model results against analytical model, which is not satisfactory. A comparison with pull back tests results of the frame could have been more appropriate.

Determining the maximum safe content load for steel storage rack is a cumbersome process. It is also very difficult to determine this maximum safe storage load by conventional code

specified response spectrum analysis method. Alavi and Gupta (2008) carried out a study in this area. Their study focused on the performance based design of a self-supporting proprietary storage rack system. The force resisting frame under consideration has bolted moment resisting frame (MRF) in one direction and a combination MRF and corrugated panel welded to columns in the transverse direction. They checked the performance of rack structure designed according to AISC-LRFD recommended elastic response spectrum analysis, which uses nonlinear static analysis based performance evaluation technique prescribed in FEMA 356 and FEMA 450. The objective of their study was to find out the maximum content weight up to which the structure performs satisfactorily. The result from their analysis shows that the performance based analysis and design is clearly superior to the elastic response spectrum analysis. The result obtained from 55 frame analysis suggests that more than half of the frames designed using conventional response spectrum analysis method were unsafe under seismic loading. So, relying on only code provided response spectrum analysis method can produce designs which can perform very poorly under actual seismic loading condition. The present study deals with direct displacement based design which is a performance-based design as suggested by Alavi and Gupta (2008).

Mass eccentricity of rack supported building is a very important consideration for seismic design. As the pallets are usually loaded from one end, this can result in eccentric storage load to the structure, which can be detrimental during seismic loading. This is why it is necessary to find out the common mass eccentricity values of rack supported buildings and also their effect on the seismic design. Kilar et al. (2011) have carried out a study on rack supported warehouse structure for both fixed support and base isolated variant. The structural force resisting system of the warehouse is dependent on two steel braced frames connected at two ends of the structure. The structural design was carried out using the proposed European Racking Federation Guideline

Pr FEM 10.2.08 (2005). First a mass eccentricity study was carried out by distributing the pallet loads in the most unfavorable plan locations of the structure and it was found out that the maximum eccentricity occurred at a lower occupancy level of 27%. Kilar et al. (2011) concluded that the minimum eccentricity of 5% suggested by the Euro code 8 (2004) is not conservative for these structures. From the parametric study they found out that the most critical occupancy is not 100% but in-between 55% and 85%. Extended N2 based pushover and nonlinear dynamic analysis (NLDA) was also carried out on the structure using SAP2000 software. FEMA 356 (2000) based nonlinear hinges were used to capture the nonlinear behavior of the beam, column and braces. From the nonlinear analysis it was observed that the base isolated structure experienced a maximum interstory drift (ISD) ratio of 0.3% for all three earthquake records used for the analysis. On the contrary, the fixed base structure experienced a maximum ISD of 1.0%. A point to be noted that Kilar et al. (2011) found very good correlation between the ISD results of NLDA and the pushover analysis.

Collapse mechanism determination is another very important study area in structural engineering. By determining the most probable collapse mode we can design the structure to resist that specific failure mode. It has been observed by Bernuzzi and Castiglioni (2001) that generally collapse happens in a steel storage rack frame due to the interaction between plastic deformation of beam-to-column joints and frame instability. This is why the rack uprights/columns can hardly reach their ultimate strength. However, in some cases a plastic hinge may form approximately at the mid span of the beams. Bernuzzi and Castiglioni (2001) suggested that it is reasonable to assume energy dissipative zones of the steel storage racks located at the beam column joints, and the energy dissipation capacity depends on their hysteretic behavior.

2.9 Component tests

Failure mechanism of the beam-to-column connector is essential for understanding the behaviour of rack type structures. Aguirre (2005) has carried out cyclic load test on rack beam-to-column connectors and found out that only the hooks yielded during the testing procedure and the connectors became less redundant from that point. The bending moment redistributed towards the center of the beam span and as a consequence an earlier failure of the beam was observed. It was also observed that the hooks essentially act as fuses to prevent column failure so failure takes place at the beam only which is actually a better failure mechanism since column failure can lead to progressive collapse which can be catastrophic. Aguirre (2005) also found out that the shear forces have no effect on the moment rotation curve. As a result, no shear nonlinearity has been considered for the nonlinear time history analysis of RCB frames in this study. He also found out that these flexible connectors are more suitable for vertical loads as brittle failure was observed under seismic loading condition. He suggested that for seismic loading an alternative type of connector should be searched for.

Bernuzzi and Castiglioni (2001) carried out some cyclic loading tests on the beam-to-column connection of pallet racks beam-to-column connection and presented their results. They found out that the nodal zone/joint area showed satisfactory performance in terms of ductile behavior. They did not observe collapse although the rotation has exceeded values beyond general scope of design. They also observed that the connectors showed large amount of slippage during testing which means that during seismic loading the structure will experience large sway and consequently large second order effect. They also observed very different hysteresis shapes for different types beam-to-column connectors. For one specimen the hysteresis was fat and strength degradation rate was slow but for the other specimen the connection very rapidly degraded in

strength and became as weak as a hinge in the second loading cycle. In their earlier study Bernuzzi et al. (1989) concluded that the rack structures may supply a limited post elastic response but they reach the elastic limit at a very low value of horizontal force.

Global and local buckling of rack columns are very important failure criteria for seismic design of rack supported buildings. As the rack columns are usually made with thin walled perforated steel sections, they are very susceptible to local distortional buckling. The racks columns are usually made of thin walled perforated members, which are affected by different buckling modes such as local, distortional and global and by their mutual interaction (Hancock (1985), Davies and Jiang (1998)). A common upright/column section is shown in Figure 2.6 for reference. Casafont et al. (2011) carried out an experimental investigation on steel storage rack columns distortional buckling behavior under different length and support condition. They found out that only a certain length range is susceptible to distortional buckling failure, columns taller than this range are more prone to global buckling failure. The column length range where distortional and global buckling modes are combined is 1200 to 1500mm. In the present study the column length ranges from 1600mm to 1800mm which is out of this range and therefore, distortional buckling was not considered. Casafont et al. (2011) also suggested that the incorporation of distortional buckling in column design can slightly improve the standard procedure. The equation provided in RMI (2008) takes the effect of perforation, local and global buckling into account but no provision is provided for calculating distortional buckling strength. On the other hand the distortional global buckling is accurately taken into consideration by European racking code. They proposed a modified direct strength method to more accurately predict the distortional buckling strength of rack columns where good correlation between the prediction and observation was found.

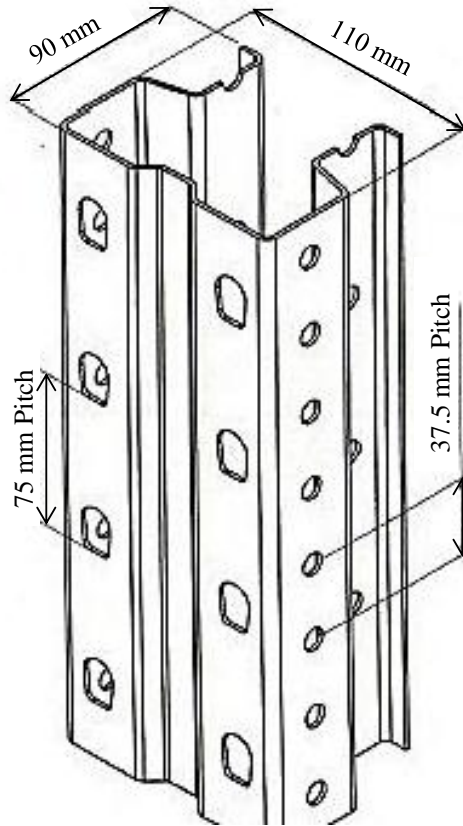


Figure 2.6: A typical rack column

Modeling of rack columns in finite element is a very difficult task. As they come with perforations, their load carrying capacity becomes difficult to predict. Designers are always faced with dilemma whether to use gross, nominal or actual cross sectional area in the analysis. Also their axial capacity depends on material and geometric nonlinearities. Freitas et al. (2005) carried out both experimental and finite element analysis of rack columns to determine their axial capacity by taking into account both geometric and material nonlinearities. In their finite element model they used three types of cross sections as follows, nominal, actual and gross. They calculated their axial load carrying capacity and finally compared the result with experimental result and capacity predicted by different code's equation. They found out that the load predicted by actual column model showed greatest resemblance to the experimental result. Also it was observed that the FE model with imperfection included in the model showed similar failure mode

compared to the experimental one which confirms the strong influence of imperfection on the failure mode. They also observed local web buckling and distortional mode during the experiment. Finally they have concluded that the equation provided by rack manufacturing institute (RMI) is conservative in predicting the load carrying capacity of the rack columns.

Cyclic test result of rack portal frames is particularly important for seismic design of rack supported buildings. Cyclic test result shows the performance of an actual beam column joint and their strength degradation under lateral loading. With this experimental result the designers can better predict the seismic performance of larger structure built using these frames. Gilbert and Rasmussen (2010) presented experimental cyclic test result of a cold form rack portal frame where beam to upright connection utilizes bolted moment connections. They also presented the nonlinear cyclic behaviour of bolted moment connections which was observed from the cyclic test. They found out that the bolted moment connections show significant looseness after a high initial rotational stiffness. They stated that the current research is not conservative as it focuses on structures not sensitive to second order P-delta effect and also do not take connector looseness into consideration. But they argued that the P-delta effect should be taken into consideration as it is required by the international racking specifications (RMI 2008; AS 4084; EN15512; FEM 2008) for unbraced frames. However, it was also noted that if the finite element analysis shows that the design load induced moment is less than the one which induces the slippage, then the looseness of the connection can be disregarded in the analysis, otherwise not. Based on the recommendation of Gilbert and Rasmussen (2010) P-delta analysis was carried out for all RCB frame analysis in this study.

Prabha et al. (2010) have carried out extensive studies on the behaviour of beam-to-column connector of steel storage racks. A total of 18 experiments were carried out to find out a relationship between moment and rotation behaviour of these connectors. Before carrying out the experimental investigation a detailed nonlinear three-dimensional cantilever test setup model was created in finite element software named ABAQUS. The results obtained from the finite element software were used for parametric studies. Finally, they carried out the experiments by varying some important parameters like beam depth, connector depth and column thickness and came up with a three parameter based power model for the connector moment rotation relationship which is presented later in this study. It was observed that the finite element model showed very good correlation with the experimental results.

2.10 Full scale tests

It is particularly important to understand the behavior of rack structures under seismic loading condition to determine the behavior of rack supported building under similar loading conditions. Seismic load is a type of dynamic or transient load with varying acceleration, displacement and velocity with respect to time. Chen et al. (1980) carried out a research to investigate the response of racks under dynamic loading condition, incorporating both shake table test and quasi-static cyclic loading on real storage rack frames. From the experiment they found out that the racks performed much better in the longitudinal direction compared to its transverse direction. Although the rack performed well against lateral loading their capacity came lower than that specified in 1976 UBC code's zone 4 demands. They found out that the ductility and energy dissipation capacity of the racks in the down isle direction is much larger than that of the transverse direction. This is why the rack can undergo large inelastic deformation

without suffering major damage in down isle direction. On the contrary the rack can undergo very low inelastic deformation in the cross isle direction. They also checked their experimental result with theoretical model and found good correlation.

Shake table testing of various types of steel storage racks has recently been performed by Filiatrault et al. (2006b) to find out fundamental time period and its dependency on beam end connector stiffness and interstory drift ratio under seismic excitation. They performed pullback, white noise and seismic tests utilizing different types of bolted beam-to-column connectors. They also modeled the frames in SAP2000 (2003) software prior to the experiment to predict connector stiffness from observed time period from the test. From this experiment it was found out that the rack structures connector stiffness is insensitive to the content weight. Also it was observed that with high root mean square (RMS) acceleration values, the beam column connectors show highly nonlinear behavior and their stiffness degrade significantly with the increase of acceleration. However, they found that after large amplitude of vibration the beam-to-column connector can recover almost all of its initial stiffness by simple “white noise” excitation. During this testing the observed transient interstory drift values were very high (3.8%-9.1%) compared to regular steel structures. Also, the residual interstory drift was significant (0.5% to 2.6%) but the racks did not lose their vertical load carrying capacity at these high drifts. They also found out that after a seismic excitation (below 0.3g acceleration), a substantial portion (at least half) of these residual drift can be recovered by low level white noise excitation. On the contrary, Filiatrault et al. (2007) found out from another experiment that steel storage rack incorporating boltless teardrop beam-to-column connectors was able to recover almost all of their initial stiffness without the need of any low-level white-noise excitation. The connectors automatically recovered their stiffness after the end of the experiment.

CHAPTER 3: DIRECT DISPLACEMENT BASED DESIGN OF RCB

3.1 General

This chapter presents a direct displacement based design (DDBD) procedure which is adapted for designing RCB moment resisting frame in the down isle direction. Despite force based design being the standard code of practice in North America, the building design is nowadays evolving towards performance-based approach (Ghobarah 2001). Such an approach is direct displacement based design.

Direct displacement-based design is a new concept in structural engineering, which unlike traditional force based design, uses the displacement and effective stiffness as the key controlling factors for seismic design. In direct displacement based design the word ‘direct’ indicates final design with very little or no iteration (Powell 2008). This method is able to achieve uniform performance level for all designed structures, which is the greatest advantage of DDBD over force-based design. A detailed DDBD design methodology flowchart is presented in Figure 3.1.

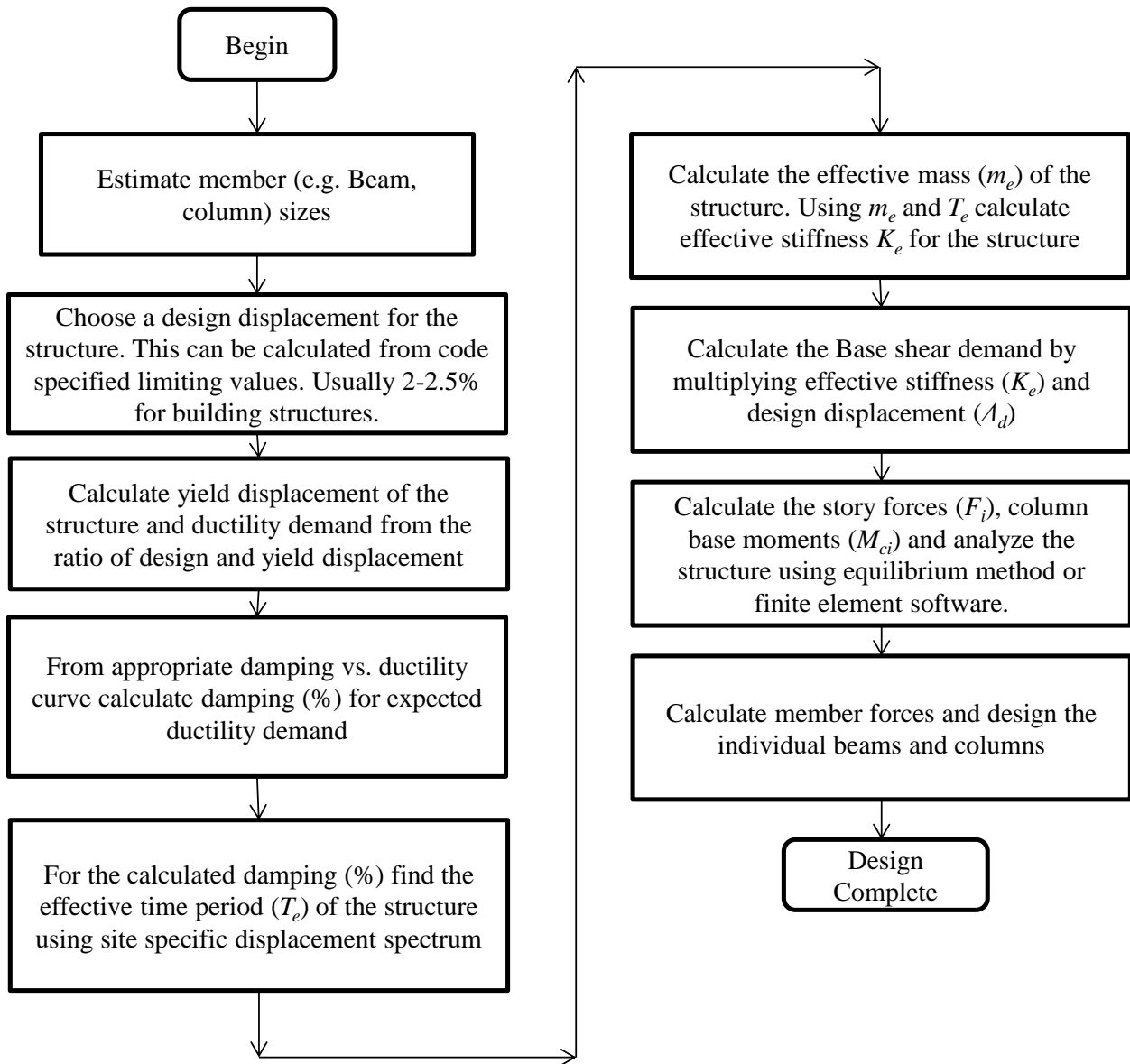


Figure 3.1: Flow chart of direct displacement-based design method

It is clear from the above steps that unlike force-based design this method takes displacement into account during the design, which is obvious as displacement is the indicator of damage, not strength. Recently, force-based design has also incorporated a displacement check at the end of the design to determine whether the displacement is within code specified limit.

3.2 Kinematic assumptions

In order to adapt DDBD for RCB structures the following assumptions are made. The following points were summarized from the experimental works of Filiatrault et al. (2006) and Priestley et al. (2007). Figure 3.2 graphically represents the assumption made underneath.

- Similar type of beam-to-column connection is used throughout the frame system.
- The beams are spaced uniformly with height.
- All moment-resisting connections of the racks experience almost identical rotations at all times. This mechanism is vital for a beam sway mechanism as described by Priestley et al. (2007). This assumption suggests that the connection rotational stiffness is somewhat smaller than the rotational stiffness of the beams and columns, thereby making the lateral deflection of the rack structure vary linearly with height. This assumption was validated by the shake-table testing by Filiatrault et al. (2006a). All plastic hinge rotations occur at the beam-to-column and base-column-to-slab connections. This assumption is only valid if the connector moment rotation stiffness is smaller than the members (beams and columns). This assumption was also validated by the shake-table testing (Filiatrault et al. 2006a). Also this is another fundamental requirement of DDBD's beam sway mechanism (Priestley et al. 2007).
- The overall seismic response can be rationally modeled as a single-degree-of-freedom (SDOF) system corresponding to an assumed first down-aisle mode of deformation of the rack (Filiatrault et al. 2006a). This assumption is a fundamental requirement of DDBD, which explicitly states that the design process is based on an assumed single degree of freedom

representation of the structure where floor displacements are related to a normalized inelastic mode shape (Priestley et al. 2007).

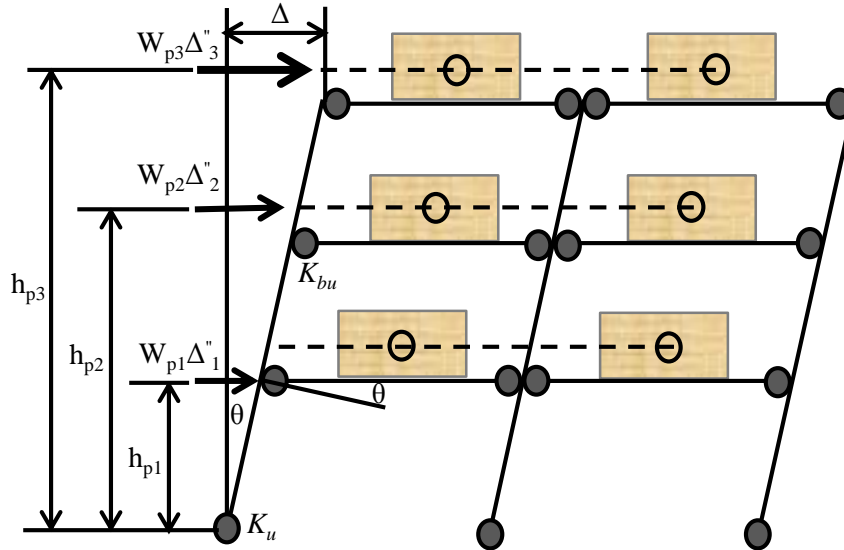


Figure 3.2: Kinematic assumptions of the semi rigid frame structure in down-isle direction (adapted from Filiatrault et al. 2006a)

It is expected that the connection moment versus rotation curves for various types of beam-to-column connectors have been developed based on cyclic load test and these design curves have been adjusted for uncertainty in the cyclic test data.

Aguirre (2005) also suggested that the proper method of analyzing these structures is taking account of the nonlinear properties of the connection. He also stressed that it will be a serious mistake if we analyze these structures assuming rigid beam-to-column connections. He found out that the nonlinear structural displacement was more than twice than that of the standard rigid structural model.

On the basis of an extensive experimental analysis Baldassino and Bernuzzi (2000) suggested that in most cases the beam-to-column joints should be modeled as hinges, if they are classified in accordance with Eurocode 3 criteria. However, he also stated that the beam-to-column

connectors also provide significant amount of lateral stiffness to the frame. For this reason a semi continuous frame model is always preferred for a more refined and optimal analysis for design. From a parametric investigation it was also confirmed that there is a significant response of the base-plate joint on the overall response of the rack. For this reason it is necessary to use test data related to the behaviour of column base-plate connection. Baldassino et al. (n.d.) suggested that the model of rack structures should take nonlinearity of beam-to-column and column-to-base plate connection into account. On the other hand the performance of the column-to-base plate was found to be significantly dependent on the axial load.

3.3 Design steps

The direct displacement based design steps are discussed below.

Step 1: determination of the design displacement, Δ_d

Design displacement can be calculated from the design drift ratio,

$$\theta_d = \theta_y + \theta_p \leq \theta_c \quad (3.1)$$

The design drift ratio (θ_d) is composed of elastic (θ_y) and plastic (θ_p) component, which has an upper code drift limit, θ_c . As per NBCC 2005, for general structures other than post disaster buildings and schools the design drift limit should be less than 2.5% of the height. The critical location of θ_d is generally at the lowest Story in frame structures (Priestley and Calvi 2008). In many cases it is more appropriate to select a design ductility limit of,

$$\mu_d = \frac{\theta_y + \theta_p}{\theta_y} \quad (3.2)$$

So,

$$\theta_d = \mu\theta_y \leq \theta_c \quad (3.3)$$

While designing for damage control limit state, the limiting value of design ductility (μ_d) should be 67% of the ultimate ductility capacity (μ_c) (Priestley et al. 2007), the latter can be calculated from pushover analysis of a RCB frame.

Step 2: design story displacements

The design floor displacements of the frame can be related to the normalized inelastic mode shape, which can be calculated using the guideline provided in Priestley et al. (2007).

Step 3: estimate damping from expected ductility demand vs. damping curve

Design displacement ductility can be calculated from equivalent SDOF design displacement and yield displacement from this equation, $\mu = \Delta_d / \Delta_y$, where yield displacement can be calculated using the following equation.

$$\Delta_y = \theta_y h_e \quad (3.4)$$

Here, the effective height, h_e can be calculated using guidelines provided by Priestley et al. (2007). θ_y can be assumed to be composed of the yield rotation of the connector (θ_{cy}), rotation of the beam end while connector experience yield moment (θ_{be}) and initial rotation of the connector due to gravity load (θ_i). The following expression is proposed in this study, which can be used to calculate the yield rotation.

$$\theta_y = \theta_{cy} + \theta_{be} - \theta_i \quad (3.5)$$

θ_{be} can be calculated using the following equation.

$$\theta_{be} = \frac{M_{cy}}{K_{be}} \quad (3.6)$$

Here K_{be} is the stiffness of the doubly curved beam under lateral loading. And the stiffness can be calculated using the following expression.

$$K_{be} = \frac{6EI_b}{l_b} \quad (3.7)$$

Where,

Δ_y = Yield displacement at the height of the resultant seismic force

θ_{cy} = Yield rotation of the connector (from experimental moment rotation curve). To determine θ_{cy} , first bilinear idealization of the moment rotation curve should be done. From the idealized moment rotation curve θ_{cy} the corresponding connector yield moment M_{cy} can be determined.

M_{cy} = Yield moment of the connector calculated from idealized bilinear moment rotation plot.

I_b = Second moment of area of the beam around horizontal axis.

l_b = Bay length of the beam

E = Modulus of elasticity of steel

W = Total seismic weight on the beam per unit length, typically this value is the sum of the dead load and 66% storage load. The storage load can be further reduced by a factor of 0.8 considering the dislodging of the crates during seismic excitation (Beattie 2006).

Initial connector rotation (θ_i) of the semi rigid end of the beam under gravity load can be calculated using the following equation proposed by the author where the detailed calculation is shown in section 3.9.1.

$$\theta_i = \frac{wL^2}{12(K_c + \frac{2EI_b}{L})} \quad (3.8)$$

Equation 3.8 gives the end rotation of a spring supported beam under gravity loading; this is a general expression that can be used for different stiffness values and support conditions like hinge, semi rigid and rigid connections.

Equation 3.5 is empirical in nature. It was determined from the pushover analysis of RCB frames shown in Figure 3.3.

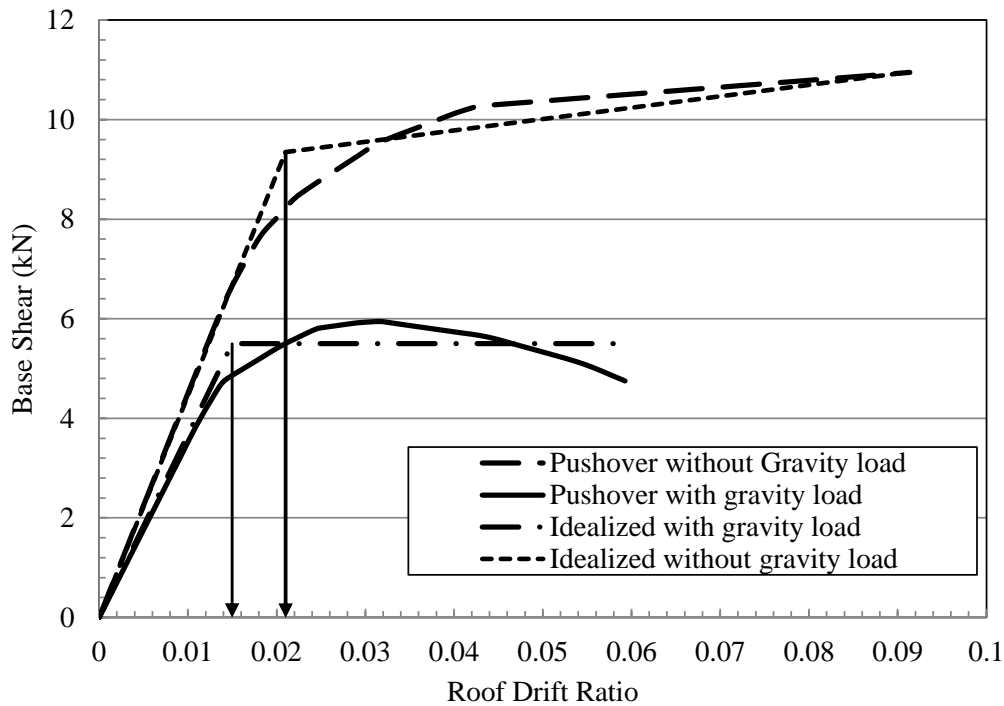


Figure 3.3: Pushover analysis of RCB frames with and without gravity load

It was observed that when the analysis is carried out without any gravity load, the yield rotation can be calculated using the equation proposed by Filiatrault et al. (2006a) as shown below.

$$\theta_y = \theta_{cy} + \theta_{be} = 0.017 + 0.0035 = 2.05\%$$

The calculated values of θ_{cy} and θ_{be} are given in Table 3.5. This result matches with the result obtained from the pushover analysis shown in Figure 6. But when the same analysis was carried out on a loaded structure, it showed very different load deflection behavior compared to unloaded one, which can be seen in Figure 6. Also it was observed that the loaded structure exhibits a very low base shear capacity compared to the unloaded structure. Also due to P- Δ effect, at the end of the pushover curve there is a downward slope which is not present in the pushover curve of the unloaded structure. Under close examination it can be seen that the loaded structure has very early strength degradation at 4.8kN. This stiffness degradation can be associated to yielding and strength degradation of the structural elements under the combined effect of gravity and lateral load. When a structure with very low beam-to-column joint stiffness is loaded with large gravity load, the initial beam end rotation due to this heavy load becomes very large. This rotation creates a sagging deflection on the beam. When the structure is loaded laterally the beams assume a doubly curvature shape. Due to the initial end rotation, if near end of the beam is aiding towards the attainment of double curvature, the far end is resisting towards it. The near end has to cover fewer angles to achieve yield rotation, on the other hand the far end has to rotate a larger angle for yielding, and this is because the external force has to cancel out the initial rotation due to gravity load in order to create a hogging moment in the far end. Due to this phenomenon the structure experiences an early yield which can be seen in the pushover

curve show in Figure 6. As the yield displacement changes for the loaded structure, the equation for calculating the yield displacement also has to take this phenomenon into account. This early yielding can be approximately calculated using Equation 3.5. Using this equation the calculation for yield rotation is carried out as shown below.

$$\theta_y = \theta_{cy} + \theta_{be} - \theta_i = 0.017 + 0.0035 - 0.00584 = 1.46\%$$

The calculated values of θ_{cy} , θ_{be} and θ_i are given in Table 3.5. From the pushover analysis of the gravity loaded structure, the approximate yielding was observed at around 1.5% roof drift, which is very close to the calculated value from equation 3.5. This change in yield rotation depends on the stiffness of the connector. As these structures use semi rigid connectors, the initial end rotation from the analysis became large. For a much stiffer structure, like a concrete or general steel frame structure this initial end rotation will be infinitesimal and thus will not have any significant effect on the analysis, but for RCB structures with very low connector stiffness it cannot be ignored. This assumption is also confirmed by other researchers, for example Castiglioni et al. (2009) presented the results of the “Storage Racks in Seismic Areas” project, which was carried out reduce the design and safety related limitations of building storage racks in seismic regions. In this journal they argued that the general testing procedures for beam-to-column connections only take displacement into consideration under lateral loading but in reality both downward and lateral forces act at the same time which is hybrid in nature. Considering this limitation they used an innovative testing procedure for their research, which is capable of capturing the hybrid loading condition present in real life situation. They found out that the innovative procedure showed different behavior in terms of displacement symmetry and connection opening and close-out behaviour. For innovative technique the displacement

accumulation was asymmetric and connection only closed out at the bottom part unlike traditional experimental technique.

From the design displacement ductility calculated above, the damping (%) can be estimated using standard damping vs. ductility curves shown in Figure 3.4. The damping vs. ductility relationship establishment is an important step for RCB design using DDBD. RCB structures unique joint behavior warrant a completely different relationship between these parameters which is unlikely to match with general steel structures. For this research a ductility demand vs. damping curve has been generated utilizing the moment rotation hysteresis data published by (Beattie 2006). As these curves are for demonstration of design method development and not based on experiment, they should be used with caution and engineering judgment. The real world design should be based on experimental result of the specimen under consideration. The calculations for generating these curves are discussed later in detail.

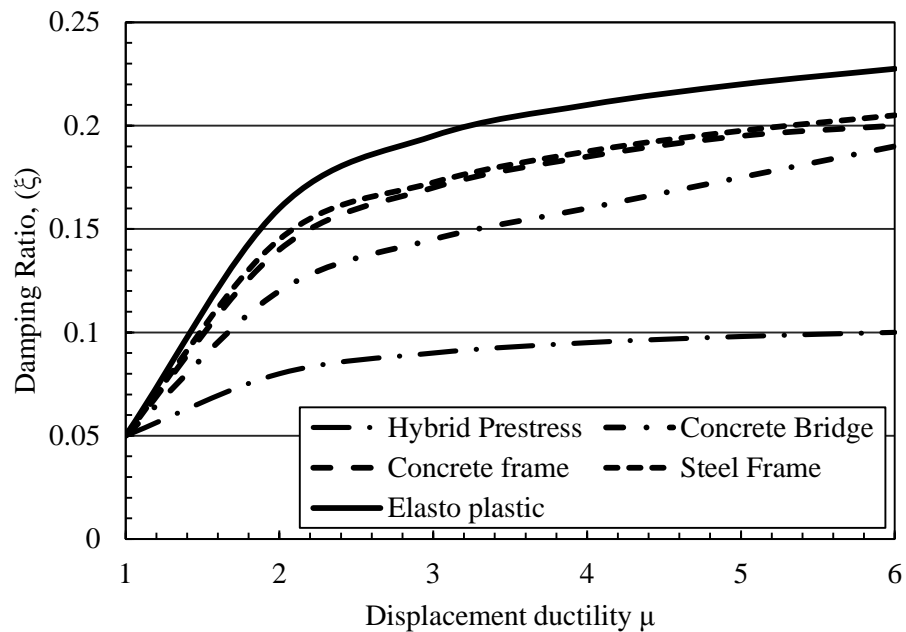


Figure 3.4: Standard damping vs. ductility curves (adapted from Priestley et al. 2007)

Step 4: determine effective time period (T_e) from displacement response spectra

From the known design displacement and damping (%) and utilizing the displacement spectra of the site under consideration the effective time period of the structure can be calculated.

A standard displacement spectrum is shown in Figure 3.5.

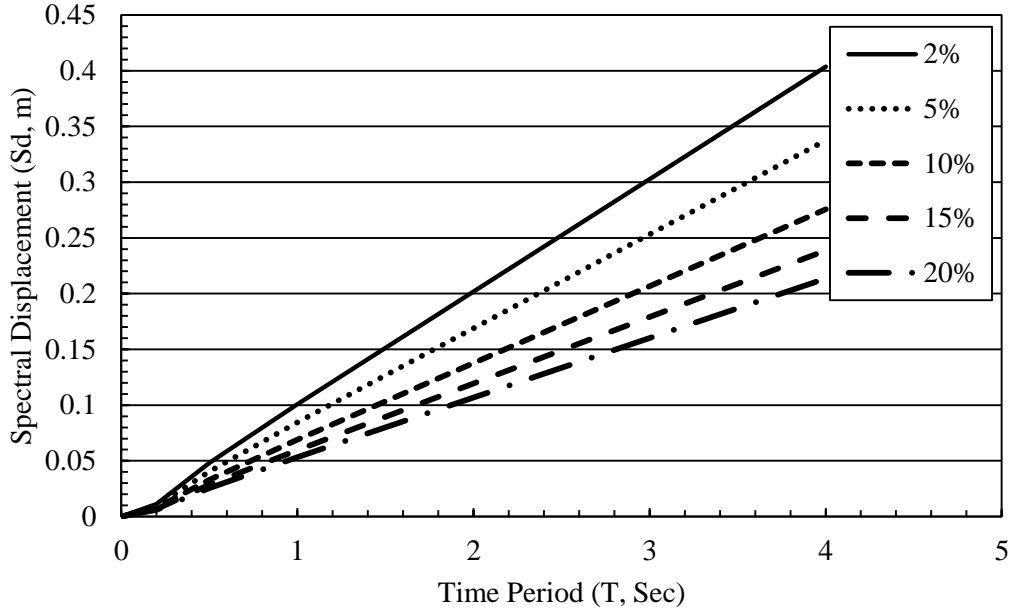


Figure 3.5: Displacement spectrum for Vancouver (soil class C) for different damping (%)

This displacement response spectra has been generated from NBCC 2005 acceleration time period spectra using the relation, $S_d = \frac{T^2 * S_a * g}{4 * \pi^2}$, Where S_d is the spectral displacement, and S_a is the spectral acceleration. To convert the 5% damped response spectrum to other damping values the following factor can be used as per Euro code 8.

$$R_\xi = \left(\frac{0.10}{0.05 + \xi} \right)^{0.5} \quad (3.9)$$

$$S_{d\xi} = S_{d5\%} * R_\xi \quad (3.10)$$

Where,

ζ = Viscous damping ratio

Step 5: Determine the effective stiffness, K_e

Effective stiffness can be calculated using the relation,

$$K_e = \frac{4\pi^2 m_e}{T_e^2} \quad (3.11)$$

Where,

m_e = Effective mass (Priestley et al. 2007).

T_e = Effective time period

Step 6: determine the demand base shear, V_b

Demand base shear can be calculated using the following relation.

$$V_{base} = K_e \Delta_d \quad (3.12)$$

Step 7: distribute the base shear force

The base shear calculated in the last step should be distributed in proportion to the product of the mass and displacement using equations provided in Priestley et al. (2007)

Step 8: analyze the structure

The building should be analyzed using the force distribution determined in step 7 to determine the required strength at the plastic hinge locations. This analysis requires the adoption

of member stiffness appropriate for the member ductility level. As it was discussed earlier that in the case of RCB structures all the nonlinear behavior occurs at the beam column joint (while Unbraced) and at the column base plate connection, it will be sensible to reduce the connector and base plate stiffness to secant stiffness. This reduction can be easily achieved by dividing the initial stiffness with the design ductility factor (Priestley et al. 2007).

The desired mechanism of inelastic deformation for RCB frames involves the formation of flexural plastic hinges at the column-to-base-plate connection and at the beam-to-column joint connector. This is known as ‘beam sway’ mechanism. This mechanism is preferable to column sway or soft story mechanism as the latter can result in catastrophic failure of the structure. In beam sway mechanism the greatest number of beam column joints experience plastic deformation and thus, the energy dissipation maximizes. This mechanism also ensures plastic hinge rotations that are very nearly identical to the inelastic story drift. In order to avoid column sway mechanism the column strength has to be higher than the beam strength. It should be ensured that in places other than the base or roof, plastic hinges are not formed in the columns. So, column flexural strength other than these locations should be set sufficiently higher to avoid any type of nonlinear behavior. Also, as shear failure is a brittle type failure, which is catastrophic in nature, the shear strength in both beams and columns should be set sufficiently higher so that shear failure cannot occur.

Before applying the force vector calculated in earlier step, as per the method described in Priestley et al (2007), the base shear force should be distributed in the ground floor columns so that the interior columns get twice the shear force than the exterior ones. Then the bending moment at the base of the columns should be calculated using the following equation,

$$M_1 = 0.6V_cH_c \quad (3.13)$$

Where,

V_c = Shear force on the column due to lateral force

H_c = Height of the column

Next, the frame should be modeled with hinged base and the calculated moment should be applied at the base with the rotational direction resisting the overturning moment generated by the force vector. And the beams should be modeled with appropriate moment rotation springs with secant stiffness at the beam-to-column joint. After completing the procedure, the model should be analyzed using linear static procedure. The resultant bending moment at the critical locations should be used to design the members.

Using the calculated bending moments the suitable connectors can be selected or current design can be revised using the power model (Prabha et al. 2010). This “power model” for connector can predict the initial connector stiffness and ultimate moment capacity based on some structural parameters, such as thickness of the column base plate, depth of the beam and depth of the connector. Although it is easy to guess the size and type of connector using the power model, its use should accompany component testing because the model utilizes a mathematical function which predicts connector moment rotation behavior based on empirical equation. As empirical equations cannot flawlessly predict the actual behavior, this model should not be used alone in the final design. The power model equations are presented in Equation 3.14 to 3.16 and a sample connector moment-rotation plot is illustrated in Figure 3.6. Initial stiffness is calculated using equation 3.14,

$$R_{ki} = 1791.05t_u + 235.14d_b + 208.48d_c \quad (3.14)$$

Ultimate moment is calculated using equation 3.15,

$$M_u = 272d_b^2 - 48.8d_b + 4.81 \quad (3.15)$$

Equation 3.16 can be used for moment-rotation curve plotting,

$$M = \frac{R_{ki}\theta_r}{\left(1 + \frac{(\theta_r)^{n_s}}{\theta_0}\right)^{\frac{1}{n_s}}} \quad (3.16)$$

Where,

t_u = Thickness of column, m

d_b = Depth of beam, m

d_c = Depth of connector, m

θ_0 = Reference rotation, M_u/R_{ki}

θ_r = Relative rotation in radians

n_s = Shape parameter, usual range of value 1 to 4

Figure 3.6 was plotted with t_u (0.003 m), d_b (.10 m) and d_c (.30m) and shape parameter, n_s equal to 1.

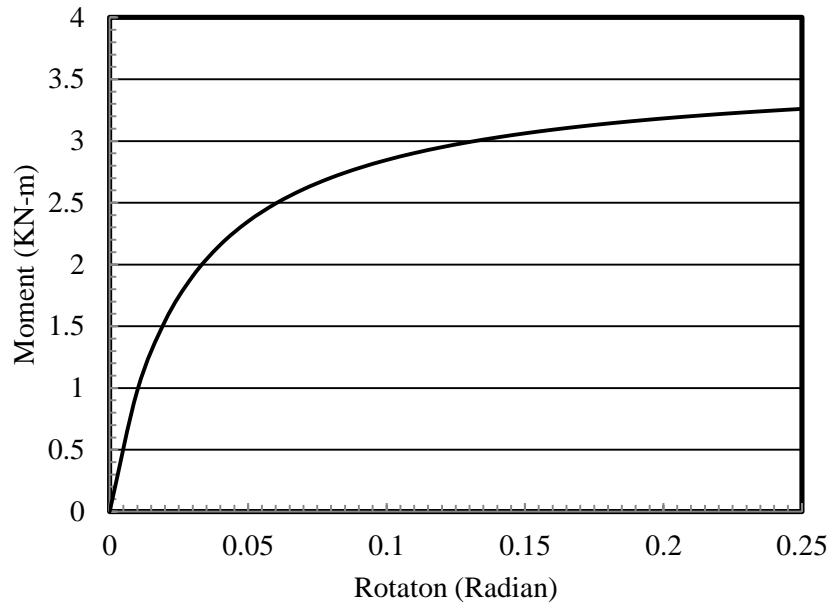


Figure 3.6: A sample connector moment rotation backbone plot using “Power model” (Prabha et al. 2010)

Step 8: design the structure

Design of the structural members should be carried out using limit state design requirement of the relevant structural steel design code.

3.4 Case study

To demonstrate the direct displacement design process, an existing RCB building design was collected from the industrial research partner. Some structural drawings and storage loading values were supplied by them. Based on the drawings, finite element model was generated using SAP2000 (2010) software.

3.5 Section property calculation

The RCB uprights contain perforations at regular interval. Modeling a large frame using perforated column section requires the use of shell elements, which is extremely time consuming and tedious work. To expedite the modeling process approximate section properties of the

perforated upright section were calculated partially using FE model and hand calculation. And a relationship has been developed between the section with and without perforation. The calculated property modifiers are second moment of area, shear area, cross sectional area and torsional constant. The cross sectional area modifier is taken as the ratio between the axial stiffness of the perforated and the gross upright section. This axial stiffness ratio was found by dividing the axial deformation of the perforated column with that of the intact column in finite element environment under the same axial loading condition. Moment of inertia modifiers were calculated by dividing the tip deflection of a cantilever un-perforated column with the deflection of a perforated column of same length using a selected point load at the beam end. Similarly, torsional constant reduction factor was calculated using a torsional load applied at the end of both perforated and un-perforated cantilever columns of same length and finally from the ratio of the beam's rotation angle. Last of all, shear area reduction factor was calculated as follows, first the shear area for two perpendicular axis of the cross section was calculated using SAP2000 (2010)'s section designer, which takes the area of the web and flanges projection (if any) in the direction of shear under consideration.

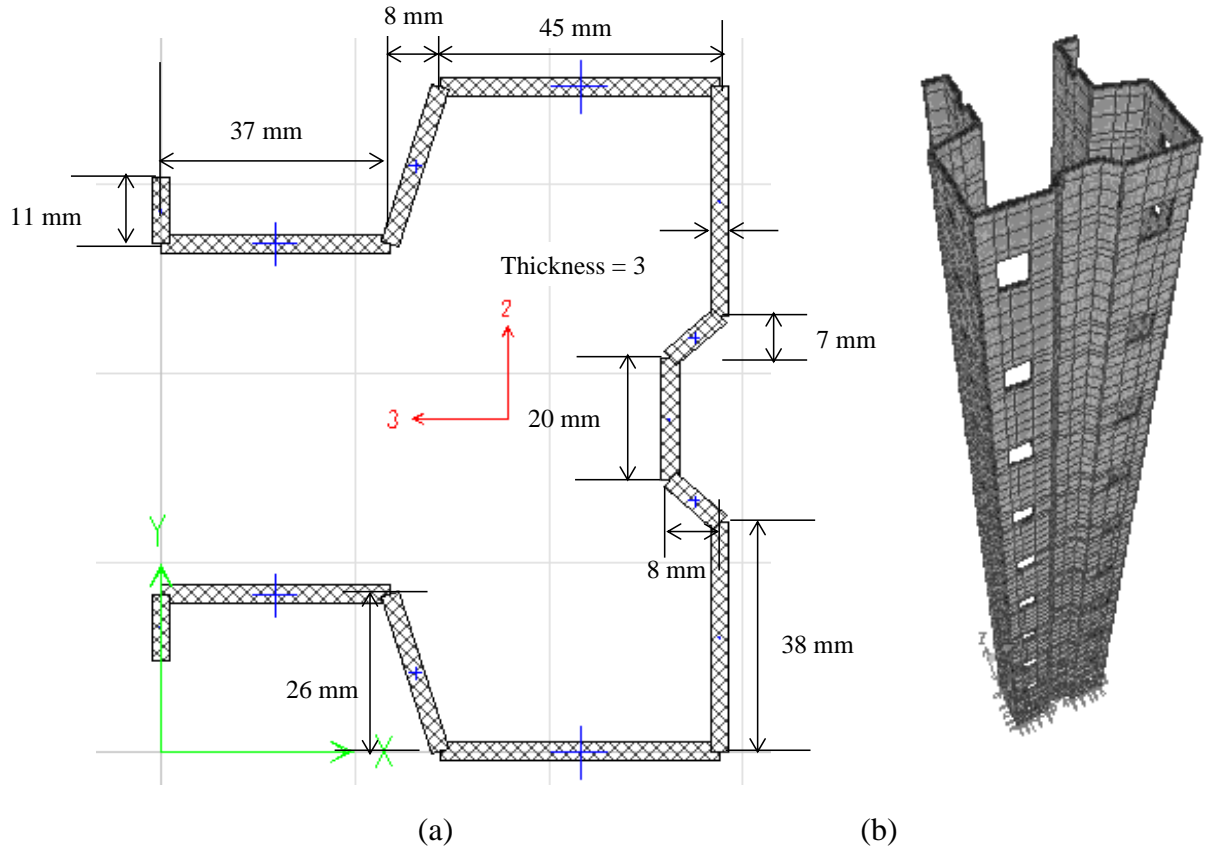


Figure 3.7: (a) Cross section of the RCB column and (b) FE model of an upright with perforation

In the next step this shear area was reduced by subtracting the area of perforations from it. Finally this reduced shear area was divided by the shear area of un-perforated column section and thus the shear area modification factor was calculated. Figure 3.7(a) shows the cross section of the upright, which is built using the section designer module of SAP2000 (2010) whereas Figure 3.7(b) illustrates the detailed shell element based model of the column. Table 3.1 shows the mechanical property of the column section shown in Figure 3.7(a) used for this study.

Table 3.1: Mechanical properties of the RCB column section

Mechanical Property	Value	Unit
Cross Sectional Area, A	1053.26	mm ²
Torsional Constant, J	3117.16	mm ⁴
Moment of Inertia around 3 axis, I_{33}	1651176	mm ⁴
Moment of Inertia around 2 axis, I_{22}	1029853	mm ⁴
Shear area in 2 direction, A_{s2}	406.16	mm ²
Shear area in 3 direction, A_{s3}	587.53	mm ²
Radius of gyration around 3 axis, r_{33}	39.64	mm
Radius of gyration around 2 axis, r_{22}	31.26	mm

Using the above mentioned section property modifier calculation procedure the data shown in Table 3.2 were calculated. By utilizing the data presented in Table 3.2 the section properties presented in Table 3.1 were modified inside SAP2000 (2010) software.

Table 3.2: Relative section property of perforated column with respect to an intact column

Mechanical Property	Ratio
Cross Sectional Area	88%
Moment of Inertia about 2-axis	90%
Moment of Inertia about 3-axis	88%
Shear area in 2 direction	76%
Shear area in 3 direction	89%
Torsional Constant	92%

3.6 Experimental results in literature

As a large number and different types of beam end connectors exist in the market, and also numerous combination of beam-to-column-connector is possible, theoretical evaluation procedure of the cyclic loading performance of the beam-to-column joints are not currently available. As a result, all the recently developed standards for steel storage rack type structure design require specific testing to assess the key parameters describing the response of key rack components i.e. beam-to-column joints and base-plate connections (Bernuzzi and Castiglioni

2001). As RCB structures are built using steel storage racks, similar situation exists also in the design phase. The component testing for RCB structures is much more important than individual steel storage racks as full scale building will be built in the former case. An RCB structure can have a much greater consequence of failure considering human life.

Many researchers have carried out beam column joint hysteresis analysis using single cantilever or double cantilever method. In Italy Bernuzzi and Castiglioni (2001) performed experimental investigations using two types of sample and found two different types of hysteresis behavior. Specimen A150s showed relatively fat hysteresis loops compared to B150S specimen. Also, the specimen B150S degraded severely after the first loop whereas specimen A150S retained strength for a greater no of cycles. The difference is due to the significantly larger and deeper tabs present in specimen A150S than that of specimen B150S. But at the end cycles, the degraded moment rotation behavior became as weak as a hinge as per EC3 classification for both specimens.

Due to this hinge type behavior, the above mentioned moment-rotation data was not used for the analysis. Figure 3.8(b) shows the hysteresis moment-rotation data for the beam column joint from a cantilever test done by Beattie (2006). This test result shows relatively much higher stiffness at the end cycles. This beam-to-column connector remained semi rigid till the end of the test. As, the author intends to utilize the semi rigid behavior of this connectors for the moment resisting frame in the down isle direction, this experimental result was chosen for the analysis.

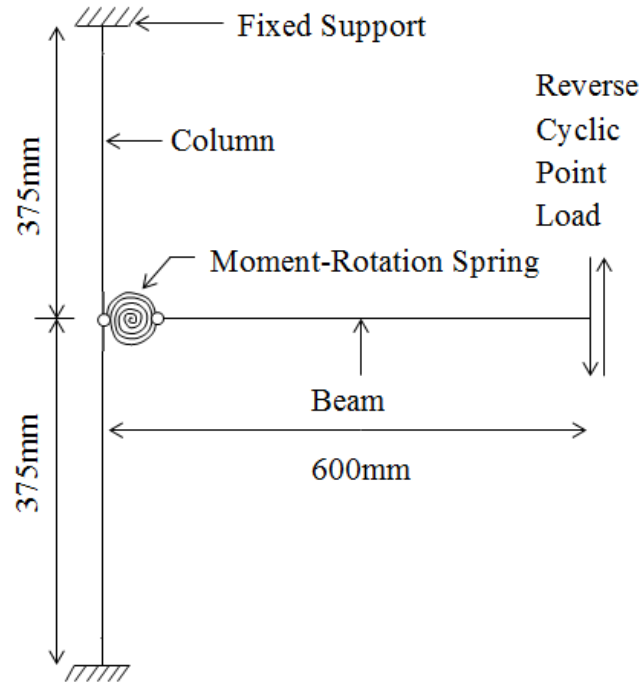


Figure 3.8: Cantilever test model of the beam-to-column connection in FE software

Using the hysteresis behavior adapted from Beattie (2006), a multi-linear plastic link model was generated using pivot hysteresis model developed by Dowell et al. (1999). The pivot hysteresis behavior best represents the moment rotation behavior of the RCB frames beam column joint under consideration, because the pivot model has the ability to model pinched hysteresis loops. So, this link has been used to simulate the joint hysteresis behavior of the frame. The model shown in Figure 3.8 was built in SAP2000 (2010) to verify the moment rotation behavior of the model. This model represents the experimental setup done by Beattie (2006). The parameters used for the pivot model of the link element in SAP2000 (2010) are $\alpha=100$, $\beta=0$, $\eta=5$ where the parameter α is used to define the primary pivot point, β is used for defining pinching pivot point and η is the softening or strength degradation parameter as defined in Dowell et al. (1999).

This simple cantilever model has a 600mm long cantilever beam connected to mid height of a 750 mm tall column. A zero length nonlinear plastic link element was assigned at the beam column joint, which represents the hysteresis behavior adopted from Beattie (2006). A point load of 2.28kN was applied in the downward direction at the free end of the cantilever beam and the quasi static loading history shown in Figure 3.9 was associated to it. The point load was calculated by dividing the maximum moment from the experiment with the length of the cantilever beam.

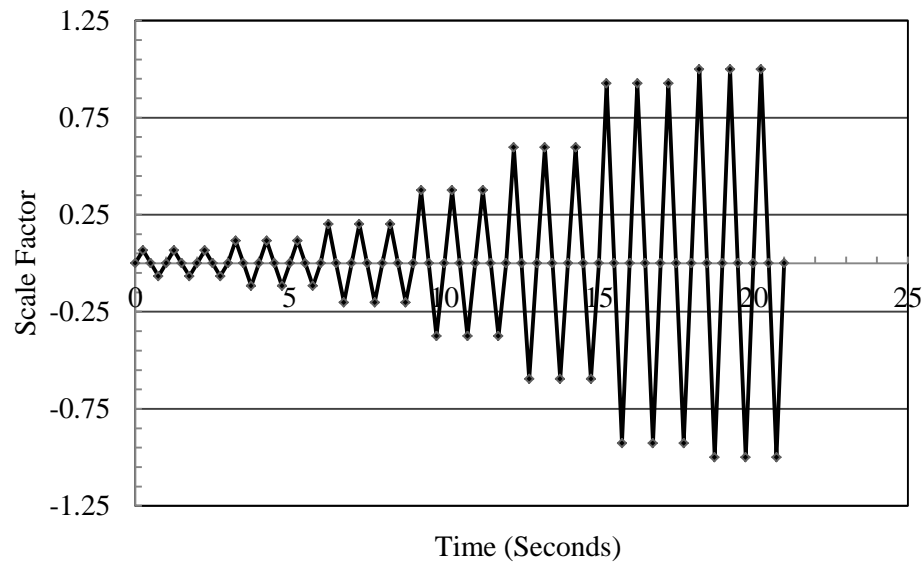


Figure 3.9: Applied quasi static load

By applying a point load at the end of the cantilever column and a cyclic load time history (Figure 3.9) the moment rotation hysteresis graph shown in Figure 3.10 was generated.

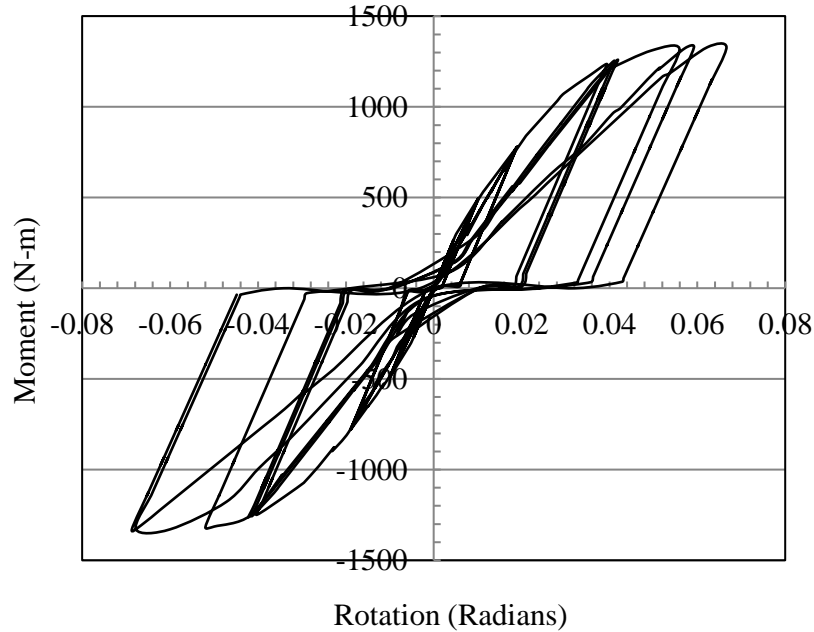


Figure 3.10: Simulated moment rotation behavior

The output hysteresis was found to be satisfactory as it matched the shape of the experimental curve shown in Figure 2.4 in terms of both bending moment and rotation. The experimental result done by Beattie (2006) shown in Figure 2.4, shows that the rotation at maximum moment (1,330 N-m) is 0.068 radians and also from the simulated response we can see that that at a maximum moment value of 1330 N-m the rotation is also 0.068 radians. Also both experimental and simulated response shows same (almost zero) residual rotation. This link was used for the model generation. As no base plate data was available for the analysis, the same moment rotation behavior is used to create the multi-linear plastic link for the base plate, which was used for the beam column joint (Filiatrault et al. 2006a).

3.7 Hysteresis damping calculation

The ductility versus equivalent viscous damping curve could be generated with large number of real earthquake accelerogram (Dwairi et al. 2007) data or small numbers of spectrum compatible artificial accelerograms, where the results of the elastic and inelastic analysis can be

separately averaged and compared (Priestley and Grant 2005). This analysis can be carried out with the aid of a substitute structure model (single degree of freedom representation). For this study a simple numerical method was used to generate an approximate ductility damping relationship, which utilized a simple three column based single Story frame model. For this model the joint hysteresis behaviour has been adapted from Beattie (2006). This hysteresis model was incorporated in the beam column joints of the finite element model of RCB frame. Using the finite element model a time history analysis was carried out with quasi static loading with varying amplitude and large number of cycles. This generated sufficient number of hysteresis loops at very small load factor increments, which were used for calculating hysteretic damping values.

The selected time history analysis type is nonlinear direct integration method. In direct integration method the modal responses are coupled, therefore, it is difficult to retrieve a symmetrical hysteresis curve from a complex multi-degree of freedom system, the above mentioned simple model was chosen so that higher mode effect can have less influence on the analysis. At each end of the beam, a zero length two noded nonlinear plastic link element was assigned. The support was modeled as a hinge to allow rotation but to restrain all translation. To introduce the semi rigid behavior at the base, a single joint link was assigned with the same beam-to-column joint hysteresis shape used for the beam column joint. A horizontal point load with a quasi-static loading time history was applied at the top of the middle column. A lateral load starting with 1.5 kN and subsequently 2.0, 3.0, 3.5, 4.0 and 5.0 kN was applied for the analysis, and then the corresponding joint displacement and base shear was monitored. The reason for using different values of horizontal loading is to produce sufficient number of points for the curve.

3.7.1 Effective damping

From the hysteresis loops the areas inside the curves were calculated along with the strain energy corresponding to maximum base shear and displacement. Then equation 3.17 was used to calculate the hysteresis damping as per Jacobsen (1960).

$$\beta_{hyst} = \frac{E_d}{4\pi E_{se}} \quad (3.17)$$

Where,

E_d = Energy dissipated by damping (Energy inside hysteresis loop).

E_{se} = Maximum strain energy. $(V_{max} * D_{max})/2$

V_{max} = Maximum base shear of the loop under consideration

D_{max} = Maximum displacement of the loop under consideration

After the hysteresis damping calculation, the effective damping was calculated using the following expression.

$$\beta_{eff} = \beta_{el} + \beta_{hyst} \quad (3.18)$$

Where,

β_{eff} = Effective damping (%) , represented as percentage of critical damping

β_{el} = 5%.

This 5% elastic damping is assumed to take into account damping due to hysteretic response of non-structural elements (Priestley and Grant 2005), relative sliding of shelf content (Beattie 2006) and initial non-linearity of the hysteresis data.

Where, β_{eff} is the effective damping (%), represented as percentage of critical damping. The joint hysteresis used for this study has nonlinearity in its elastic portion from the very first cycle and from the origin of the moment-rotation plane. So, it automatically took approximately 4% elastic damping into consideration, which is generally absent for traditional theoretical hysteresis rules (e.g. Elasto-Plastic, Takeda (1970) etc.) due to their linear response before yielding. For this reason, only an additional 1% elastic damping (β_{el}) was considered from the response of the merchandise/non-structural elements as per Beattie (2006); Priestley and Grant (2005). For plotting the curve of displacement ductility vs. effective damping, demand ductility was calculated by dividing the maximum displacement of each loop with the yield displacement Δ_y . The curve shown in Figure 3.11 was generated using the above mentioned method and this was used for the design exercise presented in the case study. It is recommended that the determination of accurate elastic damping value should be carried out using shake table testing.

A unique characteristic of the damping-ductility curve (Figure 3.11) is the near linear increase of damping with ductility which is not observed for other hysteresis rules (e.g. Elasto Plastic, Takeda etc.). For verification of the method used in this research, damping-ductility relationship was calculated for Takeda (1970) hysteresis model and very similar figure (Figure 3.12) was found compared to Priestley (2007). For this reason, the linear relationship may be attributed to the unique hysteresis shape of the RCB beam-to-column connection used in this study.

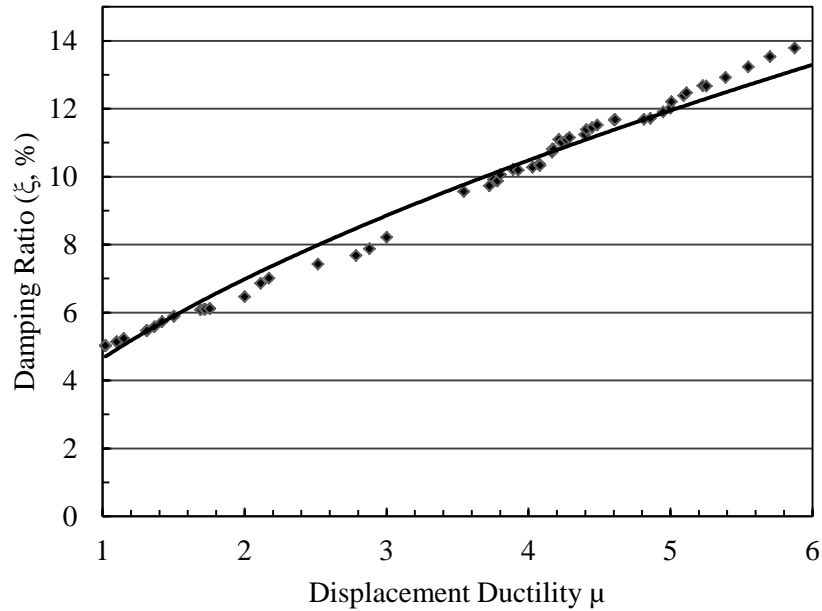


Figure 3.11: Damping vs. ductility plot with connector hysteresis

For tall RCB structures with large number of beam-to-column joints the contribution from the base plate will gradually become less significant, because, with increasing ratio of connector to base plate, the taller structures will have behavior governed by connector hysteresis only. So for multi-level RCB structures only the connector hysteresis shape will govern. For this reason the curve shown in Figure 3.11 was generated using only beam-to-column joint hysteresis data and this was used for the design exercise presented later in this chapter.

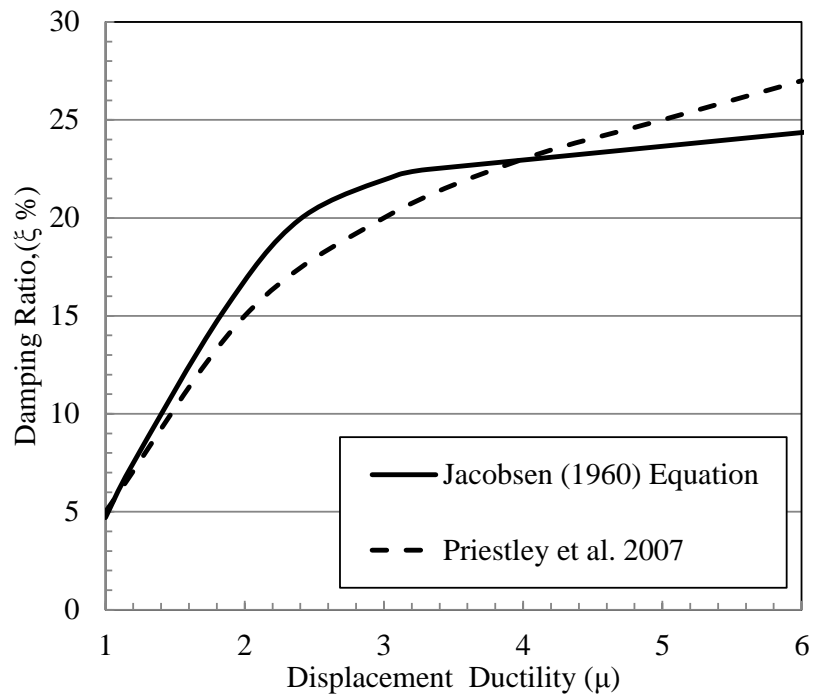


Figure 3.12: Comparison between author's and Priestley et al. (2007)'s damping ductility plot of Takeda et al. (1970) hysteresis model

But for low rise RCB structures where connector number to base plate number ratio is small, the base plate hysteresis will have significant effect on the global structural behavior. So, the ductility-damping curve should be generated using the combination base plate and connector link elements in the model.

3.8 Displacement spectra

To develop displacement spectrum, response spectrum for five soil classes were calculated as per NBCC 2005. Then using the relationship, $S_d = \frac{T^2 * S_a * g}{4 * \pi^2}$, the corresponding spectral displacement values were calculated.

Figure 3.5 shows a displacement spectrum for Vancouver (soil class C). Using the coefficient for transforming displacement spectrum (R_ξ) from 5% damped to other damping (%) values, five

different displacement spectra were calculated for soil class A to E defined in NBCC 2005. These displacement spectra have a maximum limit at four second time period as they were calculated from NBCC 2005 response spectrum (Figure 3.13) having data up to four seconds. For more accurate calculation, displacement spectra should be generated using statistical analysis of large number of earthquake records.

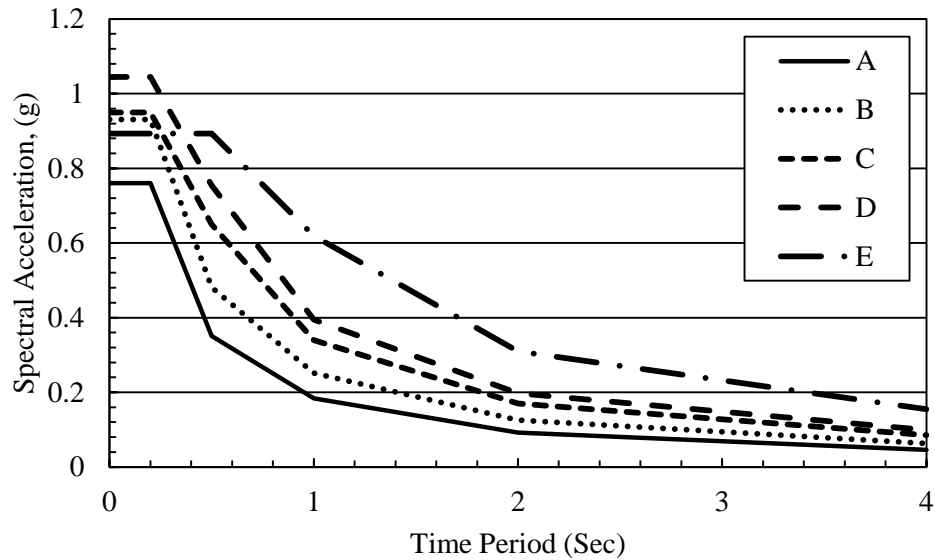


Figure 3.13: Site specific S_a-T response spectrum for Vancouver for different soil classes

3.9 Calculation

3.9.1 Initial beam end rotation

It is assumed that a single span beam with length L is supported on its both ends by springs with rotational stiffness k_c . A uniformly distributed gravity load w (kN/m) is acting on it. By integrating equation for load, equation for shear force can be derived, and by doing subsequent integration equation for bending moment, beam rotation and deflection can be determined. By using equations 3.19 through equation 3.31, the equation for beams with semi rigid support stiffness has been derived.

Load.

$$W(x) = -w \quad (3.19)$$

Shear force,

$$V(x) = -wx + c_1 \quad (3.20)$$

Where,

$$c_1 = \frac{wL}{2} \quad (3.21)$$

Bending moment,

$$M(x) = -\frac{wx^2}{2} + \frac{wLx}{2} + c_2 \quad (3.22)$$

So,

$$EI_b \theta(x) = -\frac{wx^3}{6} + \frac{wLx^2}{4} + c_2x + c_3 \quad (3.23)$$

And,

$$EI_b y(x) = -\frac{wx^4}{24} + \frac{wLx^3}{12} + \frac{c_2x^2}{2} + c_3x \quad (3.24)$$

At, $x = L$, deflection, $y = 0$

So,

$$-\frac{wL^4}{24} + \frac{wL^4}{12} + \frac{c_2L^2}{2} + c_3L = 0 \quad (3.25)$$

And as we know, Bending moment = Rotational stiffness x Rotation

Also at, $x = 0$, $M(0) = c_2$ and $\theta(0) = \frac{c_3}{EI_b}$

So, we can write,

$$c_2 = \frac{k_c c_3}{EI_b} \quad (3.26)$$

Substituting Equation 28 in equation 27 we get,

$$c_3 L + \frac{k_c c_3 L^2}{2EI_b} + \frac{wL^4}{24} = 0 \quad (3.27)$$

$$c_3 = -\frac{wL^4}{24\left(L + \frac{k_c L^2}{2EI_b}\right)} \quad (3.28)$$

We know, at $x = 0$

$$\theta_i = \frac{c_3}{EI_b} \quad (3.29)$$

Substituting Equation 30 in Equation 31 we get,

$$\theta_i = -\frac{wL^2}{12\left(k_c + \frac{2EI_b}{L}\right)} \quad (3.30)$$

If we disregard the sign, we can write

$$\theta_i = \frac{wL^2}{12\left(k_c + \frac{2EI_b}{L}\right)} \quad (3.31)$$

Here, c_1 , c_2 and c_3 are integration constants

3.9.1.1 Equation Validation

Equation 3.31 is validated using some simple calculations where the connector stiffness for a particular beam has been increased gradually and the resulting changes in some parameter values were recorded. The detail of the selected beam is given in Table 3.3. From these parametric values the ratio between $w*L^2$ and beam-end/connector moment (M_{ci}) was calculated which is also known as the support moment coefficient (γ).

Table 3.3: Mechanical properties of the beam selected for equation validation

Description	Value	Unit
Beam width (outside), a	0.05	m
Beam Depth(outside), b	0.1	m
Beam wall thickness, t	0.0015	m
Beam width (inside)	0.047	m
Beam Depth(inside)	0.097	m
Moment of Inertia around horizontal axis, I_{33}	5.92031E-07	m ⁴
Uniformly distributed load, w	2330	N/m
Length of the beam, L	2.25	m
Fictitious moment, $w*L^2$	11795.625	N-m ²
Connector Stiffness, K_c	Variable	N-m/rad
Modulus of elasticity of steel, E	2.00E+11	N/m ²
EI/L	5.26E+04	N-m

Some sample calculations of other important parameter values are presented in Table 3.4. It can be observed from this table that in the case of a lower ratio of connector stiffness (k_c) to beam stiffness (EI/L), the beam-end moment co-efficient is very high. For example if $k_c/(EI/L)=0.8$ then the moment co-efficient $\gamma = 42$, which means if a beam of length “ L ” is loaded with “ w ” load per unit length, then the beam-end support moment will be $wL^2/42$, which is very low compared to a fixed end condition ($wL^2/12$), but if the stiffness of the beam-to-column

connector increases, the moment co-efficient also decreases. For example, from the last row of Table 3.4 it can be seen that for $K_c/(EI/L)$ value of 248, the moment co-efficient became 12.1 which is almost 12 or similar to fixed end moment co-efficient. In this table θ_i is calculated using equation 3.31 and $M_{ci} = K_c * \theta_i$.

Table 3.4: Beam end moment coefficient (γ) calculation

K_c	θ_i	M_{ci}	γ	$K_c/(EI/L)$
42099.96	6.67E-03	2.81E+02	42.00	0.8
63149.95	5.84E-03	368.6133	32.00	1.2
105249.9	4.67E-03	491.4844	24.00	2
126299.9	4.25E-03	536.1648	22.00	2.4
147349.9	3.89E-03	573.3984	20.57	2.8
210499.8	3.11E-03	655.3125	18.00	4
420999.6	1.87E-03	786.375	15.00	8
736749.4	1.17E-03	860.0977	13.71	14
1010399	8.81E-04	8.90E+02	13.25	19.2
1199849	7.53E-04	9.04E+02	13.05	22.8
1578749	5.84E-04	9.22E+02	12.80	30
2525998	3.74E-04	9.44E+02	12.50	48
4209996	2.28E-04	9.59E+02	12.30	80
13050989	7.47E-05	9.75E+02	12.10	248

Figure 3.14 graphically represents the values calculated in Table 3.4. From this figure it is clear that the moment co-efficient curve becomes asymptotic to the value 12 when connector stiffness becomes 150 times more than the EI/L value of the beam. This figure validates the output of the equation 3.31 as it closely matches the co-efficient of the fundamental equation of statics.

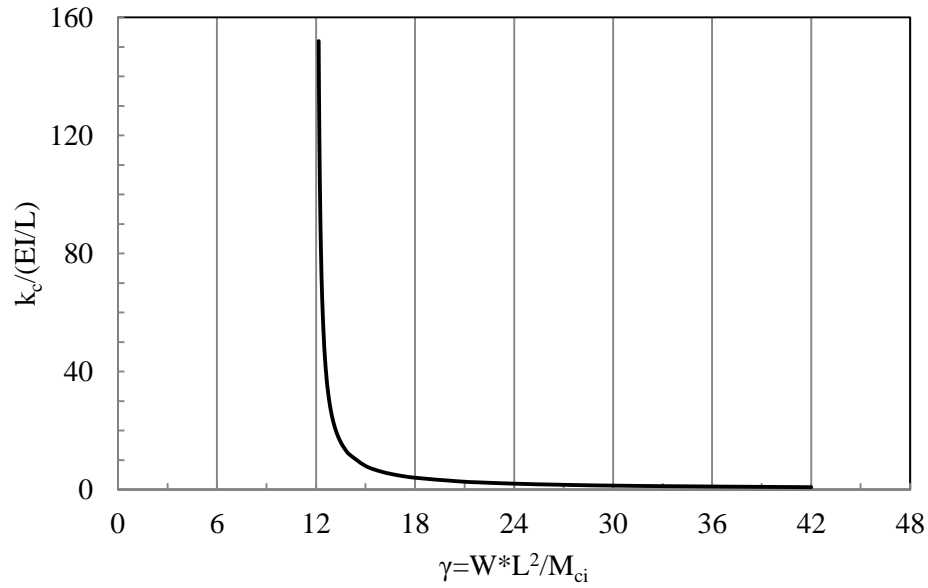


Figure 3.14: Connector to beam relative stiffness vs. beam end moment coefficient

3.9.2 Seismic weight calculation

The two dimensional frame shown in Figure 3.15 having a height of 6.57m was chosen for the analysis. The columns are 90mm x 110mm x 3mm open channel sections shown earlier in Figure 3.7(a) and beams are 50mm x 100mm x 1.5mm box sections. Each bay is 2.25m wide where the rack height is 1.77m at ground level and 1.6m for other levels. Live load was taken from the industrial partner and is considered as 4.35kN/m. This load was applied on the beam as a uniformly distributed load. Seismic storage load was calculated using recommendation provided by (Beattie 2006). Two reduction factors were used for the calculation of seismic storage loads, these are area reduction factor with a value of 0.8 and rigid mass factor with a value of 0.67 (Beattie 2006), which considers the disconnection of stock from the shelf under earthquake loading. The seismic zone is assumed to be Vancouver and soil class C. The detailed calculation is presented in the following section.

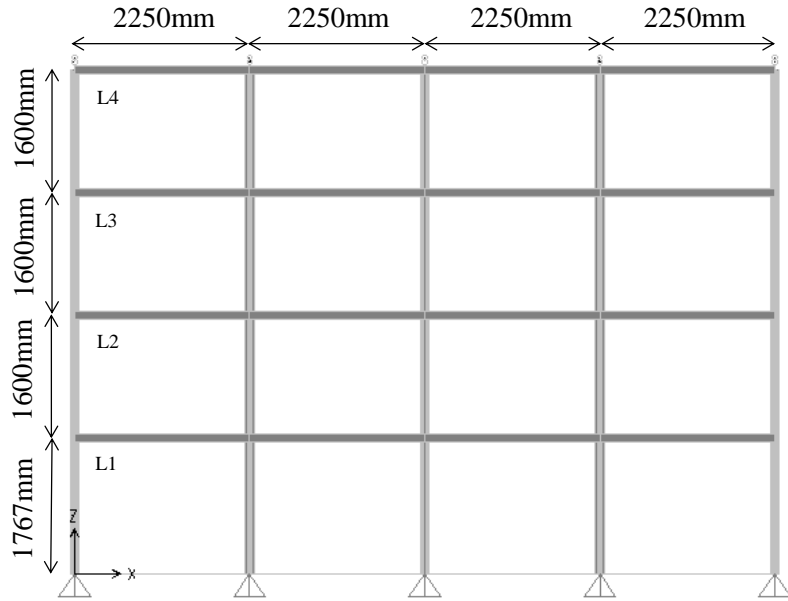


Figure 3.15: Chosen four bay and four pallet high RCB model for trial design

3.9.3 Input data table

A summary of the input data presented in Table 3.5 was used for the analysis.

Table 3.5: Input data for DDBD

Description	Value	Unit
Length of Beam, L_b	2.25	m
Depth of Beam, h_b	0.1	m
Width of the beam, w_b	0.05	m
Beam thickness, t	0.0015	m
Modulus of Elasticity, E_s	2.00E+11	N/m ²
Yield moment of the connector, M_{cy}	1120	N-m
Yield stiffness of the connector, k_{cy}	65882	N-m/rad
Seismic Load on the beam, w	2370	N/m
Code drift limit, θ_c	0.025	rad
Column dimension in direction of load, h_c	0.11	m

3.9.4 Preliminary calculation

By using the input data the preliminary calculations shown in Table 3.6 were carried out.

Table 3.6: Preliminary calculation

Description	Value	Unit
Second moment of Area of the beam, I_b	5.92E-07	m ⁴
Beam-end stiffness, $K_{be} = 6EI_b/L_b$	3.16E+05	N-m/rad
Rotation due to gravity load, $\theta_i = w \cdot l^2 / (12 \cdot (k_{cy} + 2 \cdot E \cdot I_b / L))$	0.00584	rad
Yield rotation of the connector, $\theta_{cy} = M_{cy} / k_{cy}$	0.017	rad
Beam-end rotation, $\theta_{be} = M_{cy} / k_{be}$	0.00355	rad
Yield rotation of the beam-to-column connection, $\theta_y = \theta_{cy} + \theta_{be} - \theta_i$	0.0147	rad
Critical Story displacement, $\Delta_c = \Delta_1$ (first Story)	0.04425	m
Critical Story normalized inelastic drift, δ_c	0.2694	m
Drift amplification factor, $\omega_\theta = 1.15 - 0.0034 \cdot H_n$	1	Unit less

3.9.5 Lateral force vector calculation

The calculations shown in Table 3.7 were carried out using the method discussed previously under “Design steps”. The last two columns represent the lateral force (F_i) and Story shear ($V_{s,i}$) with respect to height.

Table 3.7: Lateral force vector calculation

Story ,i	Height, H_i (m)	Story Mass, m_i (Tonne)	Inelastic mode shape vector, δ_i	Story Displacements, Δ_i	$\Delta_{i,\omega}$	$m_i\Delta_{i,\omega}$	$m_i\Delta_{i,\omega}^2$	$m_i\Delta_{i,\omega}H_i$	F_i (KN)	$V_{s,i}$ (KN)
4.00	6.57	2.13	1.00	0.164	0.164	0.34	0.056	2.23	6.88	5.85
3.00	4.97	2.13	0.76	0.124	0.124	0.26	0.032	1.28	4.06	9.31
2.00	3.37	2.13	0.51	0.084	0.084	0.17	0.015	0.59	2.75	11.65
1.00	1.77	2.13	0.27	0.044	0.044	0.09	0.04	0.16	1.45	12.88
Sum						0.86	0.11	4.26	15.13	

3.9.6 Final steps of calculation

Table 3.8 shows some important parameters of DDBD, which were calculated using the appropriate equations discussed in the ‘Design Steps’ section.

Table 3.8: Stiffness and base shear calculation

Description	Value	Unit
Substitute Structure effective height, h_e	4.94	m
Equivalent System yield displacement, $\Delta_y = \theta_{cy} * h_e$	0.07	m
Substitute Structure Design displacement, $\Delta_d = \theta_d * h_e$	0.123	m
Displacement Ductility demand, $\mu = \Delta_d / \Delta_y$	1.70	Unit less
Equivalent Viscous damping, ζ	6.4	%
Total mass of the structure, m	8.27	Tonne
Effective mass, m_e	6.99	Tonne
Effective time period, T_e	1.5	Sec
Effective Stiffness, $K_e = 4 * \pi^2 * m_e / T_e^2$	122.58	kN/m
Base Shear force, $V_{base} = K_e * \Delta_d$	15.13	kN
Extra lateral load on roof, $F_t = I * V_{base}$	1.51	kN
Base shear for distribution, $0.9 * V_{base}$	13.61	kN

After the distribution of story shear forces the support moments were calculated for the design of the base plate which is shown in Table 3.9. In this table V_{c1} and V_{c2} stand for exterior

and interior column shear force, respectively. Similarly, M_{c1} and M_{c2} stand for exterior and interior column base moment, respectively.

Table 3.9: Column base moment calculation

Description	Value	Unit
Exterior column shear, V_{c1}	1.89	kN
Interior column shear, V_{c2}	3.78	kN
Exterior column Design moment, $M_{c1}=0.6*V_{c1}*H_1$	2.01	kN-m
Interior column Design moment, $M_{c2}=0.6*V_{c2}*H_2$	4.02	kN-m

These support moments were assigned at the hinged column base of the SAP2000 (2010) model in the direction opposing the overturning moment generated by the applied lateral force vector. Moment-rotational springs were assigned at the end of the beam with a value equal to the secant stiffness of the beam-to-column joint moment rotation curve, which was calculated at the design ductility level (1.7 for this particular case). The secant stiffness value was calculated to be $65883/1.7$ N-m or 38750.9 N-m. After the above mentioned modification done on the model, a linear static analysis was carried out and the bending moments shown in Table 3.10 were found. The letters L1 to L4 represents the beam-end location of the frame shown in Figure 3.15. From these bending moments the critical design bending moment was found to be at the first story beam-end (L2). It should be noted that NBCC combination contains a linear addition of 100% Dead load, 100% Earthquake load and 50% live load.

Table 3.10: Design bending moments for beams

Location on frame	Design moments (lateral load only) (kN-m)	Design moments (NBCC load combination) (kN-m)
L4	1.44	1.86
L3	1.65	2.10
L2	1.85	2.29
L1	1.81	2.25

Priestley et al (2007) suggested that it is unnecessarily conservative to add the full gravity load moments to these seismic moments. If we add the gravity load moments, it will increase the cost and also reduce the lateral displacement below the intended design level. As, we can see from Table 3.10 that the NBCC load combination moments are larger than the lateral load moments so using the combination load will not increase the cost by a big margin. This is why the following calculations were carried out using the lateral load moments only.

To find out the suitable connector for this required design moment (1.98KN-m), the design moment was divided by a chosen yield rotation, θ_{cy} (0.017 radian). From this calculation the minimum required stiffness is 116.5KN-m/rad, which is much higher than that of the current stiffness. For the trial design a theoretical connector moment rotation curve shown in Figure 3.16 was chosen with an idealized initial stiffness of 132kN-m/radian. Using the idealized connector yield moment capacity of $132 \times 0.017 = 2.244$ kN-m and the initial stiffness of 132kN-m/radian, a re-iteration of the whole design process was carried out for the recalculated lateral load vector.

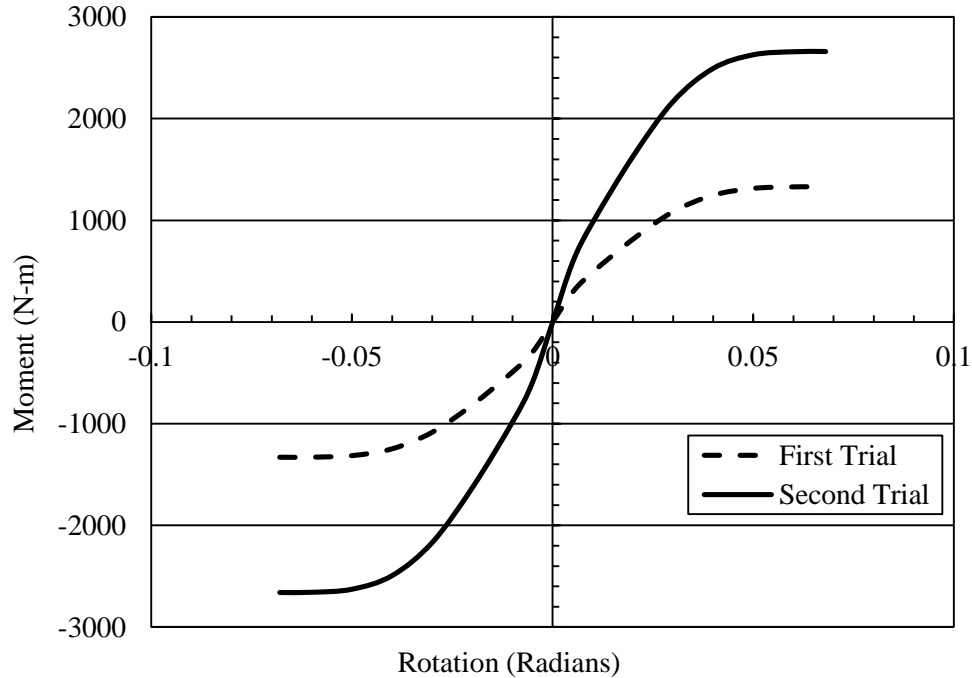


Figure 3.16: Trial moment rotation backbone curves of the connector

From the iterative analysis the maximum moment at beam end was determined as 2.19kN-m, which is less than the connector's capacity of 2.244 kN-m. So, the design is satisfactory. It was found out that due to a high moment demand, the rotational demand at yield of the connector also increased, which reduced the design ductility of the system to 1.26 from a previous value of 1.7. Because of the lower ductility demand, the damping percentage decreased to 5.4% from 6.4%, which eventually decreased the time period from 1.5 sec to 1.44 sec of the structure and increased the effective stiffness as well as the base shear demand. The final design of the RCB is given below. The section sizes were estimated based on the Power model (Prabha et al. 2010).

Beam section: Design revision is necessary for the attainment of higher stiffness of the connector. As it was found that the connector's stiffness is dependent on the beam-depth (Prabha et al. 2010). The required beam-depth was 150 mm for the required connector stiffness.

Column section: For this design the initial column plate thickness (3mm) was found satisfactory as per power model (Prabha et al. 2010).

Connector: Depth of the connector was determined with the help of the power model as discussed earlier. It was determined that a 450 mm deep connector is needed for the required stiffness.

3.10 DDBD of RCB frames with increasing number of stories

As RCB structures are normally built to a height range of 20m to 30m or more, a number of designs are carried out starting from four storied to twenty storied frames with an increment of two stories per design. The height of the RCB frames in this study ranges from 6.57m to 32.17m. This design was carried out as per the guideline presented in Priestley et al. (2007) and is known as equilibrium method. A point to be noted that the results from equilibrium frame analysis method can be slightly different from the finite element method in terms of story shear, forces and beam end moments. Table 3.11 shows the data compiled from the nine frame designs.

Table 3.11: DDBD data of different height RCB frames

Number of Stories	Height (m)	Total Weight (kN)	Base Shear (kN)	Base Shear/Weight	Total overturning moment (KN-m)	Total Story Shear	Maximum Beam design moment
4	6.57	81.13	13.30	0.16	67.83	40.98	2.07
6	9.77	121.72	15.62	0.13	112.05	68.37	2.59
8	12.97	162.30	17.65	0.11	165.17	101.35	3.03
10	16.17	202.87	17.25	0.09	199.21	122.67	3.02
12	19.37	243.45	17.87	0.07	245.48	151.53	3.18
14	22.57	284.02	18.34	0.06	292.10	180.62	3.29
16	25.77	324.60	23.68	0.07	429.00	265.61	4.28
18	28.97	365.17	29.70	0.08	603.12	373.79	5.40
20	32.17	405.74	36.40	0.09	818.92	507.96	6.65

The data represented in this table is also graphically represented in Figure 3.17 to Figure 3.20. Figure 3.17 shows the change in base shear to weight ratio with change in height/number of stories in RCB frame. It can be seen that the ratio decreased up to 16 storied frame but it started to increase after that. The reason behind this anomaly can be attributed to the unusually high spectral displacement demand of RCB structures. For the sixteen story frame it reached the maximum point of the Vancouver displacement spectrum which has a maximum time period of four seconds. After reaching this maximum value, the displacement is supposed to remain constant as per Priestley et al. (2007). For this reason the effective time period was considered to be capped to four second for subsequent frames. This is why the general base shear decreasing trend was changed and an increase of base shear to weight ratio was observed.

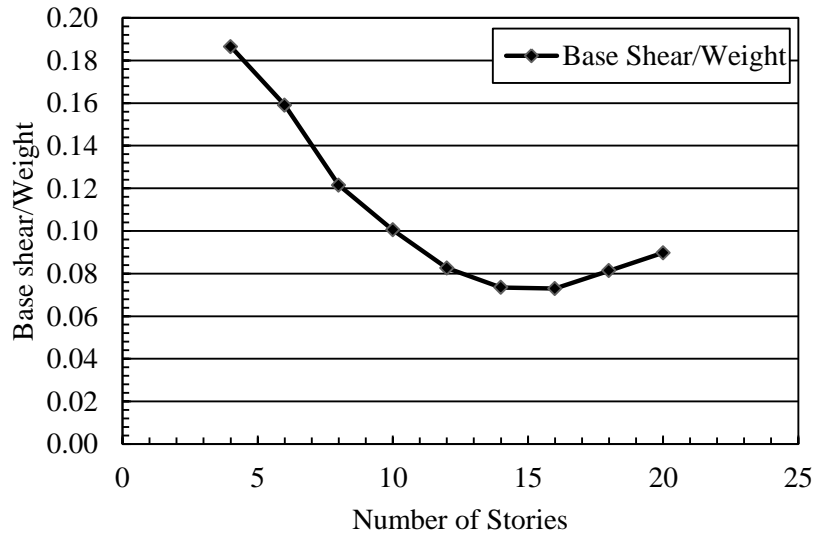


Figure 3.17: Change in base shear to weight ratio with change in number of stories

Figure 3.18 shows the change in base shear demand with the change in RCB frame height. It can be observed that the base shear demand rapidly increased from four to eight storied frame then from eight to fourteen storied frame the base shear is almost constant and after that it increases rapidly up to twenty storied frames.

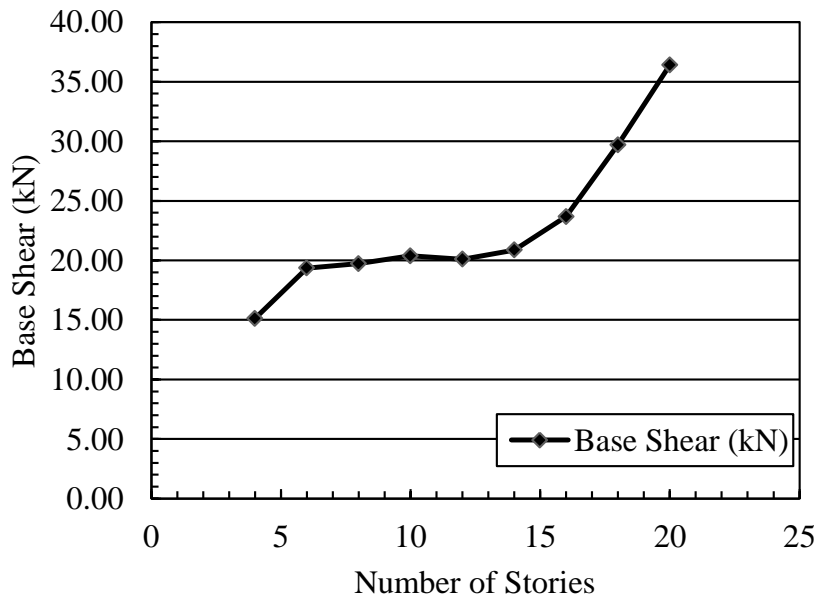


Figure 3.18: Change in seismic base shear demand with respect to number of stories

Figure 3.19 shows an increasing trend in change of total overturning moment with respect to change in frame height or number of stories. It can be observed that for up to fourteen storied frame the rate of increase in overturning moment is much lower than the higher frames.

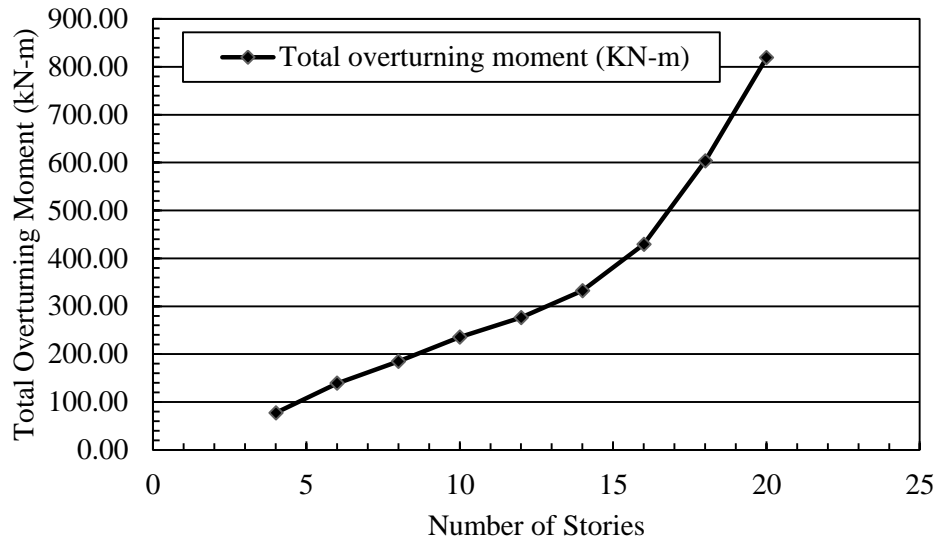


Figure 3.19: Change in total overturning moment with respect to number of stories

The Figure 3.20 shows one of the most important parameter for DDBD of RCB frames. This figure shows the maximum beam-end design moment and its change with respect to change in frame height. It can be observed that up to six storied frame the beam-end design moment is approximately equal to 3.2kN-m which is more than half of the beam's yield moment capacity (4.14 kN-m) but almost three times the beam-to-column connector capacity used in the preliminary design. But after six storied frames the beam-end design moment increases drastically and goes beyond the beam's yield moment capacity.

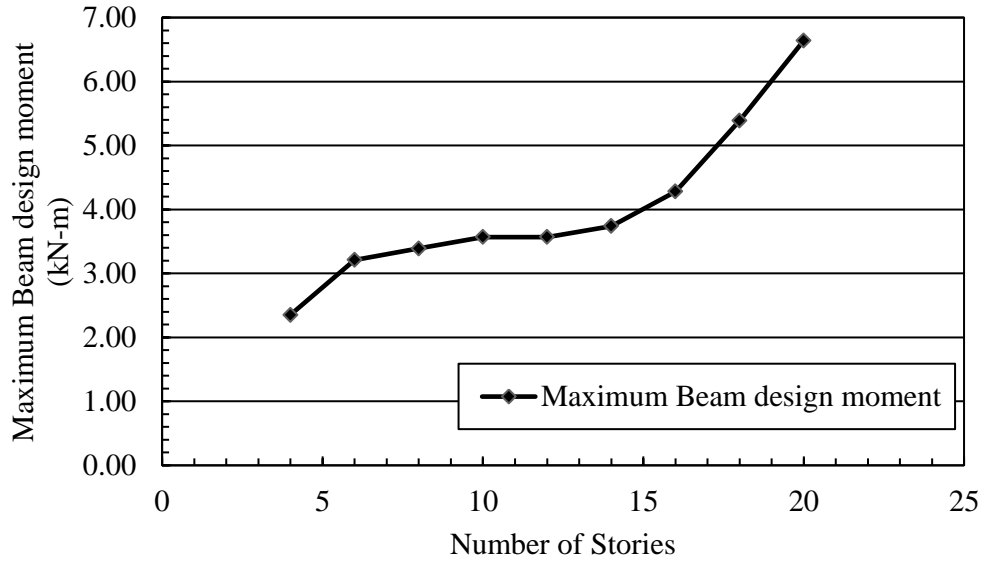


Figure 3.20: Change in maximum beam design moment with respect to number of stories

Similar study was carried out by changing frame width but no change in shape or trend was observed compared to the figures generated for story height changes except change in parameter values. This is because of the fact that as frame width increases it increases both stiffness, mass and base shear demand proportionately, so no change occurs in design moment or base shear/weight ratios.

3.11 Results

In the final iteration, the yield moment capacity of the connector was increased to 2.244 kN-m from 1.12 kN-m. Response spectrum analysis was carried out using Vancouver's response spectrum and the final ductility value calculated from the analysis and the roof displacement was 0.166m which close to the design roof displacement of 0.164m. This close match of the maximum response is due to the fact that the structure was designed using the displacement spectra converted from the acceleration versus time period response spectrum, not the displacement spectrum calculated using statistical analysis of the earthquake records.

The earthquake records were first scaled to match the Vancouver soil class ‘C’ response spectrum (Figure 3.13) using SeismoMatch (2011) software which uses the wavelets algorithm proposed by Abrahamson (1992) and Hancock et al. (2006). The scaled S_a - T response spectra are shown in Figure 3.21.

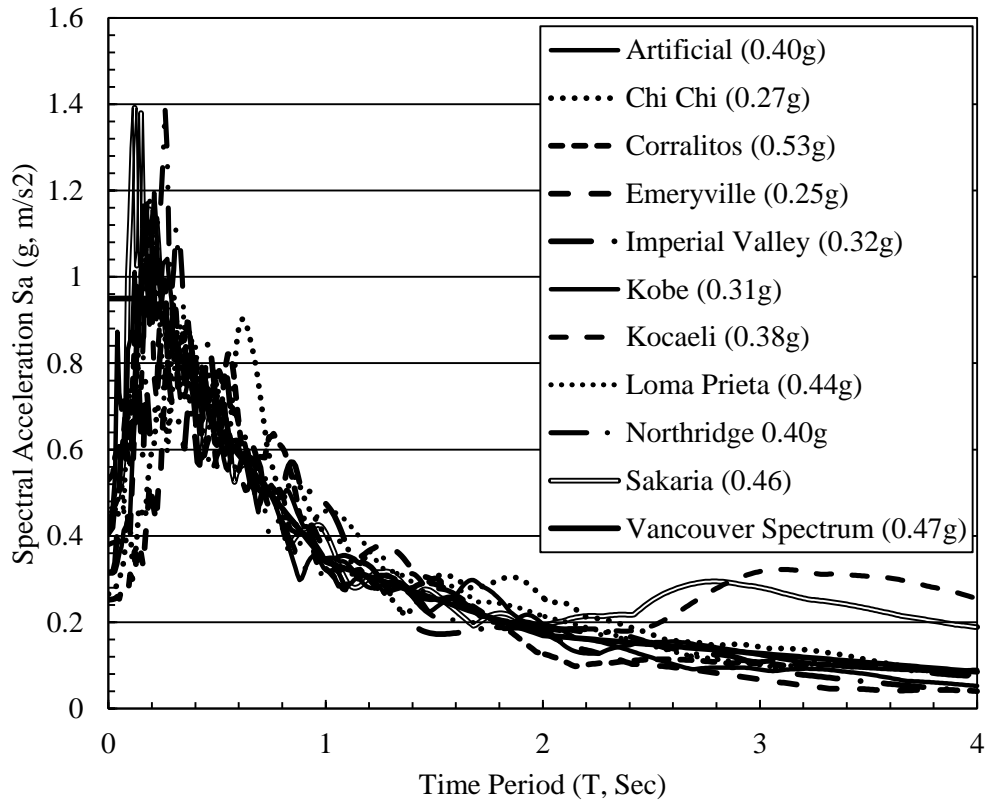


Figure 3.21: Response spectra of ten earthquake records matched with Vancouver response spectrum (PGA values shown inside bracket)

As displacement based design is dependent on the displacement spectra rather than the S_a - T response spectra, the displacement spectra of matched earthquake records are presented in Figure 3.22 for better understanding of the performance of the model frame under time history analysis.

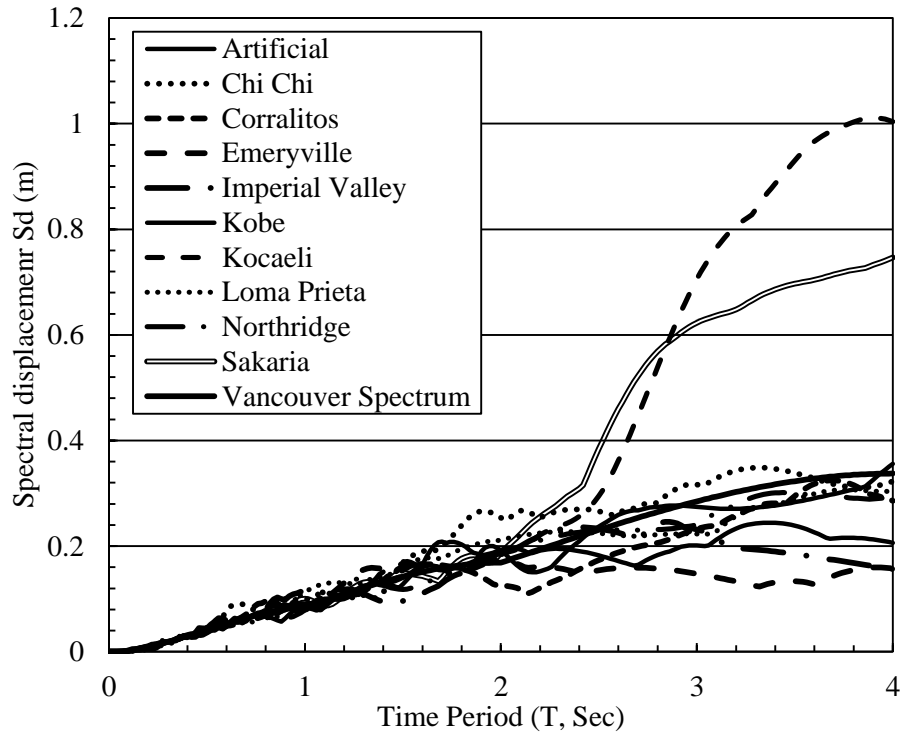


Figure 3.22: Displacement spectra of ten earthquake records matched with Vancouver soil class “C” response spectrum

Nonlinear time history analysis (NLTHA) was carried out with ten earthquake records and the results are shown in Figure 3.23. Then NLTHA was carried out on the RCB frame model built with nonlinear plastic link elements at the beam-to-column and column-to-base connections representing the hysteresis shape presented by Beattie (2006). Rayleigh damping model was used for the damping force calculation in the dynamic analysis and the 5% damping was assumed for both first and second mode for the calculation of mass and stiffness proportional damping coefficient.

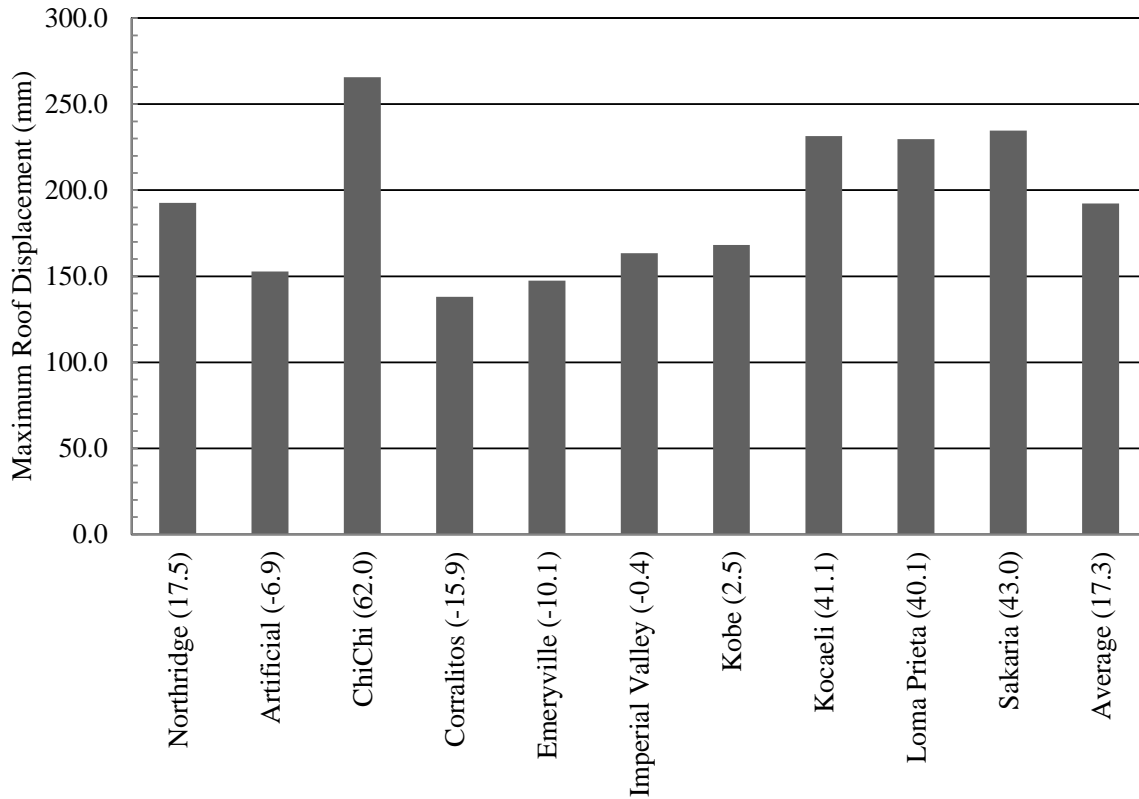


Figure 3.23: Roof displacements and their values percentage higher (value inside bracket) than DDBD displacement profile

It was found out from the analysis that among ten earthquake records, four exceeded the design roof displacement of 164 mm. The remaining three are below the design level. Although the earthquake records were scaled to match the response spectrum for which the frame was designed, the displacement exceeded the limit. The reason behind these high displacement values is that the earthquake records have some large peaks in them. During scaling process these peaks do not get fully attenuated and during analysis these peaks create excessively large deformation compared to response spectrum analysis. Priestley et al (2007) also found out similar results from NLTHA carried out on frames designed using DDBD procedure, and suggested that this type of high peak is acceptable if the mean of the peak displacements remains close to the design displacement. Another reason for this deviation may be attributed to the design process. The

design was carried out without considering the P-delta moment, which rendered the structure slightly more flexible than required for resisting the seismic force, for which the displacement from analysis came higher than the design displacement. From Figure 3.23 it can be observed that the average roof displacement from ten earthquake records is approximately 16.6% above the design displacement, which is reasonable.

3.12 Summary

An extensive study on the previous research works has been carried out and a direct displacement-based seismic design method has been adapted for RCB structures. The assumptions were taken from the studies by Priestley et al. (2007) and Filiatrault et al. (2006a) and new recommendations along with equations and figures necessary for the DDBD of RCB moment resisting frame has been proposed in the current study. After the completion of the design, a response spectrum and several nonlinear time history analyses were carried out to check the performance of the designed structure. The final check of displacement using response spectrum analysis matched the design displacement. Also using NLTHA the average displacement from ten earthquake records was found to be only 17.3% higher than the design displacement. This confirms that the RCB displacement-based design presented in this study is able to produce design that performs as per the set criteria by the designer. This displacement check shows that the DDBD method is able to achieve intended performance level for the RCB structural system. So, the present study recommends the use of DDBD for RCB system.

CHAPTER 4: FORCE BASED DESIGN OF RACK CLAD BUILDINGS

4.1 General

In this chapter overstrength and force reduction factor for rack clad building (RCB) system is evaluated. Current Canadian building code has no overstrength and ductility related force reduction factor for RCB structures. In this study the above mentioned factors have been calculated in the down isle direction of RCB structure, without considering braces. In order to calculate these factors several two dimensional frames of rack clad buildings were modeled in SAP2000 software and analyzed using incremental dynamic and pushover analysis methods. The effect of some parameters such as frame height and width on the ductility related force reduction and overstrength factors has also been investigated. The overstrength and ductility related force reduction factors calculated from this study are 1.05 and 2.06, respectively. These values can be used for ultimate strength design method available in Canadian building code.

There is a widespread construction activity of rack clad building structures all over the world. In countries like Germany the owners get tax write offs as these are not declared as warehouses but are considered to be rack installations with wall and roof cladding (Temesist 2011). This is one of the reasons for which these structures are getting popular in warehouse construction industry. In the present study, pushover and incremental dynamic analysis have been carried out to calculate the two most important parameters for seismic design, e.g. overstrength and ductility related force reduction factor. These two factors are used in Canadian building code to reduce the elastic base shear demand by taking advantage of the structural reserve strength (Overstrength) and its capacity to dissipate energy by going into nonlinear range of response (Ductility). The multiplication of overstrength and ductility factor is also known as the response modification

factor (R) in most of the building codes of the world. The factor ‘ R ’ is the ratio between the elastic base shear demand and the design base shear for a structure. A higher value of ‘ R ’ signifies higher energy dissipation capacity (Kim & Choi, 2005).

RCB structures are currently designed using equivalent lateral force procedures which uses reduced ground motions using the combination of force reduction and overstrength factors also known as response modification/behavior factor. As there are no design guidelines for RCB structures, engineers normally use experience and practical judgment in guessing these factors. Figure 4.1 shows these factors and how they are related to each other.

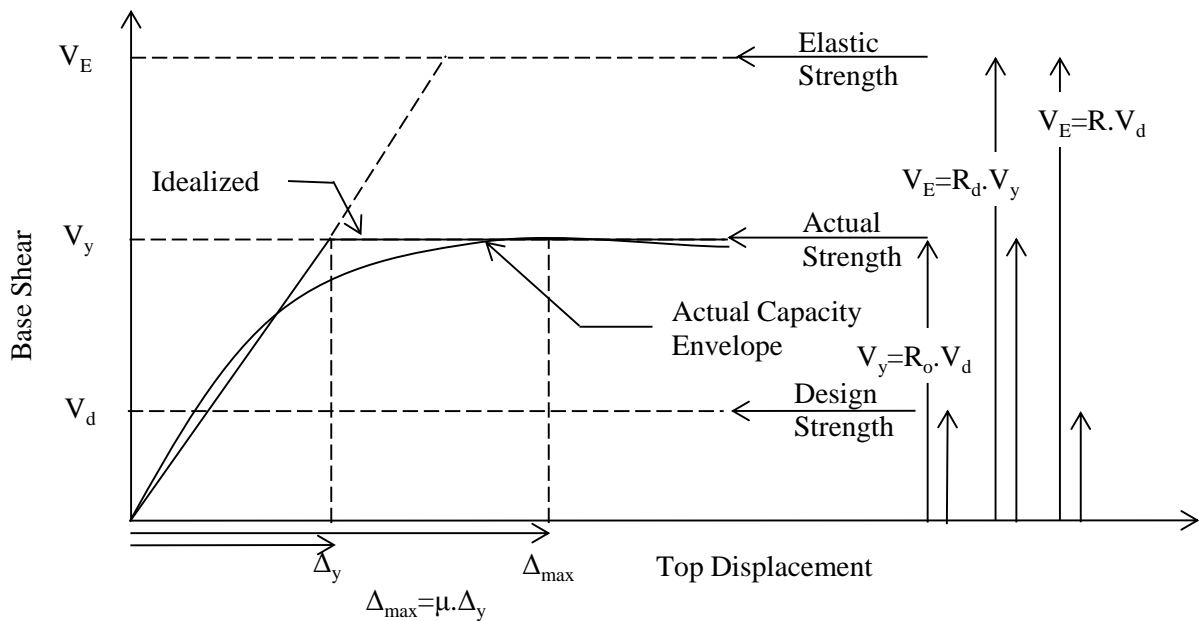


Figure 4.1: Relationships between force reduction (R_d), overstrength (R_o), response modification factor (R) and displacement ductility (μ) (adapted from Mwafy and Elnashai, 2002)

Figure 4.1 shows a representative nonlinear behaviour of a frame structure in terms of base shear versus roof top displacement. In the same figure an idealized bilinear elastic-perfectly plastic representation of this relationship is also presented. The idealization was carried out as per FEMA 356 (2000) recommendations. In NBCC (2005), the design seismic base shear

demand for structure is calculated by dividing the elastic base shear demand by the production of R_d and R_o , also known as the response modification factor (R) (Lee et al. 1999). Another notable parameter in Figure 4.1 is the ductility (μ), which is defined as the ratio of maximum displacement (Δ_{max}) to the displacement (Δ_y) corresponding to global yield of (V_y) of the idealized bilinear curve.

Current building codes all over the world recommend force based seismic design for structures needed to be designed against earthquake load. In Canada, NBCC (2005) also recommends force based design for earthquake resistant design. Force based design is primarily based on estimated seismic demand force which is calculated using empirical equations or simple linear dynamic analysis. In this method, first elastic base shear force demand is calculated then this force is reduced by a reduction factor commonly known as response modification factor (R). Response modification factor is the most important parameter for current force based seismic design. The reduction of base shear is based on the observation that a well-detailed structure is able to sustain lateral force in excess of their design strength and can undergo large amount of deformation without collapse (Kim and Choi 2005). This response modification factor's value is dependent on two other parameters known as overstrength factor (R_o) and ductility related force reduction factor (R_d). Here overstrength is the reserve strength of a structure and ductility is the ability of a structure to undergo nonlinear deformation. The multiplication of R_d and R_o is the response modification factor " R ". In seismic design code " R " or " $R_d * R_o$ " is used to reduce the elastic base shear demand by the following equation available in NBCC (2005).

$$V_d = S(T_d)M_v I_E W / R_d R_o \quad (4.1)$$

Where,

V_d is the design base shear demand

$S(T_d)$ is the spectral acceleration demand

M_v is a factor to account for higher mode effects

I_E is the importance factor

W is the seismic weight of the structure

The numerator of equation 4.1 or $(S(T_d)M_v I_E W)$ is the elastic base shear demand or V_E . This elastic base shear demand is reduced by the overstrength and force reduction factors in this equation. The higher the value of the factor “ R ” the lower the base shear demand is, hence leading to more economic design. Figure 4.2 shows a flow chart describing the force-based design procedure currently followed in most of the building design codes.

A wrong estimation of response modification factor can have catastrophic consequence which might lead to structural collapse and casualty. Applied technology Council (ATC 3-06) first introduced this factor back in 1984. At that time there was no specific guideline for calculating this factor. It was until 1995, when ATC-19 and ATC-34 provided a detailed guideline for calculating the response modification factor from three other factors known as overstrength, ductility reduction and redundancy factor. Current Canadian building code NBCC (2005) takes ductility and overstrength factor into consideration for calculating response modification factor. Outside of Canada, USA also uses similar approach in their building code UBC (1997).

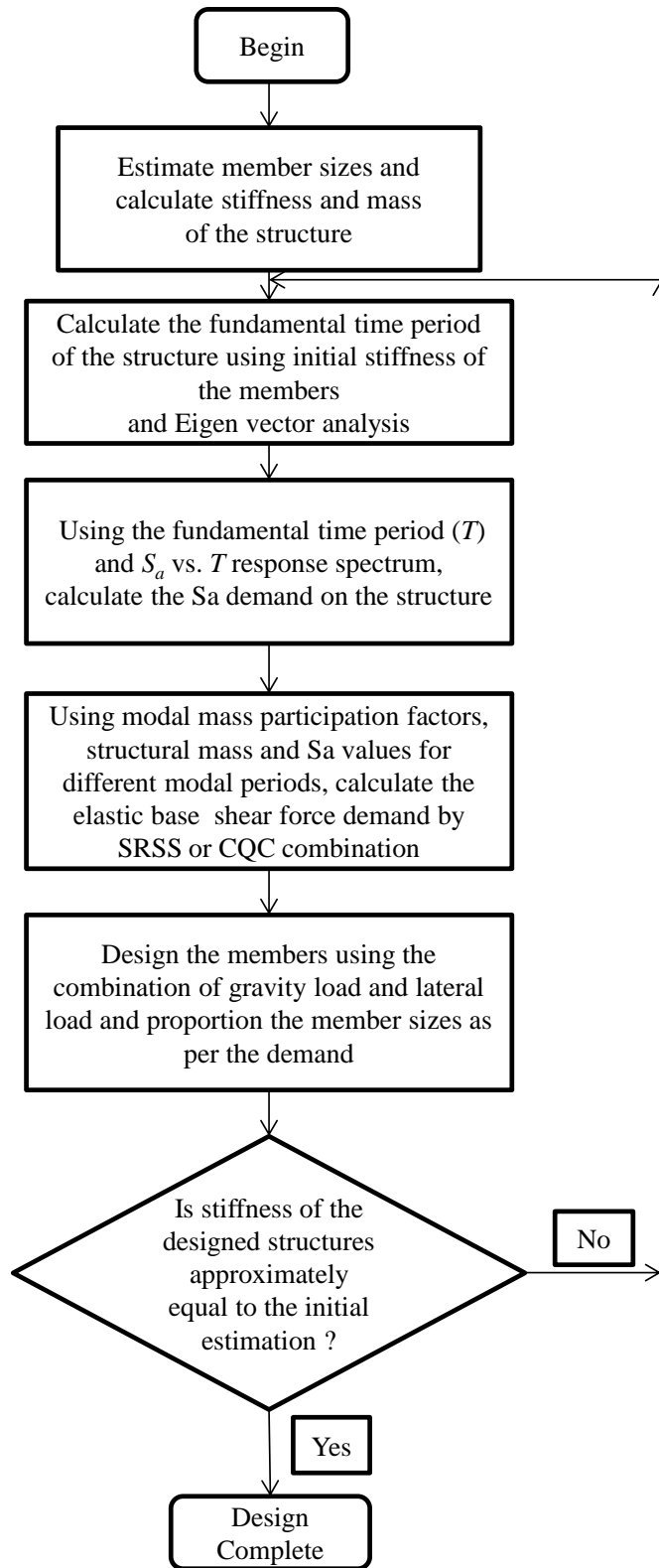


Figure 4.2: Flow chart of force based seismic design procedure

Conventionally response modification factors are calculated in such a way that it allows for adequate amount of energy dissipation through plastic hinge formation without collapse. Traditional steel structures usually employ bolted moment resisting frame connection which allows them to dissipate fairly large amount of earthquake energy without collapse. The nonlinear hinge or plastic hinge forms near the beam-to-column or column-to-baseplate joint. These places are fairly strong as they are part of the structural elements. In case of RCB structures the plastic hinge forms at the beam-to-column joint due to flexibility of the joint. In RCB frames these joint regions are significantly weaker than the members itself, so the energy dissipation capacity is comparatively much lower in RCB structure compared to that of a traditional steel structure.

4.2 Response modification factor calculation in literature

The standard method for calculating force reduction and overstrength factor can be found in many literatures. Asgarian and Shokrgozar (2009) calculated response modification factors for buckling restrained braced frames (BRBF) for Iranian code. They also checked the effect of height and brace configuration on the response modification factor. They carried out nonlinear static analysis to calculate the over-strength factor and incremental collapse analysis to calculate force reduction factor. They found out that the force reduction factor decreases very rapidly with the increase of frame height but the overstrength factor decreases very little for the same change of height.

A more comprehensive analysis for determining the force reduction factor (“R”) can be found in Mwafy and Elnashai, (2001). They carried out a study for the calculation of force reduction or “R” factor “supply” for a wide range of medium rise reinforced concrete buildings.

They compared these supply ‘ R ’ factors with the code and literature provided “design” and “demand” values. In the finite element (FE) analysis they included the “shear” failure criteria for members along with the traditional “moment” failure criteria. Both inelastic pushover and incremental dynamic collapse analysis was carried out for the calculation of the “ R ” factor. They also included the vertical response of the earthquake in their analysis. They found out that it is necessary to include both shear failure and vertical response of the earthquake in the analysis for more accurate calculation. They also stated that the response modification factor presented in ‘Eurocode 8’ are over conservative particularly for regular frames designed to lower peak ground acceleration (PGA) values.

Annan et al. (2009) presented the values and calculation method of overstrength factor for modular steel building (MSB). MSB is a type of structure for which Structural members are made in factories and brought to the site and joined together. One unique feature of MSB frame is that it utilizes two levels of beams at each floor level contrary to regular structures which uses just one. Annan et al. (2009) carried out their research in the context of Canadian building design code. The structural force resisting system under investigation is “braced frame”. They first designed the structure using CSA (2001) and NBCC (2005) guidelines, then modeled them in Seismostruct and carried out nonlinear static analysis. The overstrength factor was found in the range between 1.9 and 2.5, which is much higher than the Canadian code provided value of 1.30. Finally, they concluded that the overstrength factor proposed in Canadian code is over conservative and a single value is not valid for all frame heights. They also calculated ductility of MSB frames and found out that ductility increases with the decrease of frame height.

Kim and Choi (2005) have calculated response modification factors for chevron braced frames using pushover analysis. They took 21 special and 9 ordinary concentric braced frames into consideration for this study. They found out that the response modification factors calculated from pushover analysis came lower than the code specified values except for low rise special concentric braced frames. They also carried out incremental dynamic analysis to validate the pushover results and found good correlation among them.

As RCB moment resisting frames have high flexibility due to their semi rigid connectors, their fundamental time periods tend to elongate. A study on the effect of elongated time period on overstrength and force reduction factor was carried out by Elnashai and Mwafy (2002). The study presents the overstrength of reinforced concrete (RC) buildings designed in Eurocode 8. In their study they designed three types of RC buildings (e.g. regular, irregular and frame wall structure) and carried out pushover and incremental collapse analysis to determine overstrength and force reduction factors. They also carried out an investigation on how the use of cracked moment of inertia for RC frames elements can decrease the elastic seismic demand by increasing the fundamental period of vibration. The contribution of the elongated period on overstrength factor is also discussed. They also showed that the current standards (FEMA (1997), Paulay and Priestley (1992)) of reducing the stiffness of structural elements is over conservative where the stiffness can be safely reduced to a much lower level as proposed by (Mwafy and Elnashai, 2000). Finally, they presented another parameter called inherent overstrength which is the ratio between actual strength and elastic strength of the structure and discussed its importance. So, from this analysis it can be assumed that the use of connection flexibility in design of RCB frame can significantly reduce the seismic base shear demand with safety unaffected.

4.3 Current standard in rack Industry

Rack Manufacturing Institute (RMI 2008) recommends response modification factor, $R = 6$ in the down-isle direction of moment-resisting frame (MRF) and $R = 4$ for the braced frame in the cross-aisle direction. Here, response modification factor is equivalent to the force reduction factor (R_d) multiplied with the overstrength factor (R_o) in National Building Code of Canada (NBCC 2005). The values suggested in RMI (2008) are independent of the structural steel type such as hot-rolled or cold-formed and on the degree of connection flexibility. Eurocode 8 (2004) suggests the same values for class 1 structural steel members, which are used in regular steel buildings. Eurocode 8 (2004) recommends a behavior factor (similar counterpart of response modification factor in European standard) of 6 for MRF and 4 for concentric braced frames. Eurocode 8 (2004) does not explicitly mention rack structures or buildings however, for members made of cold formed steel with semi-compact class 3 sections it assumes a value of behavior factor (Response modification factor) less than or equal to 2 for seismic design. This code does not provide any recommendation for slender class four sections with perforations which are generally used in rack columns. Castiglioni et al. (1996) and Chesi et al. (1999) stated that for racks and regular steel buildings, these behavior factor values often do not sufficiently take the actual frame performance into account.

Beattie (2006)'s proposed a design guideline for steel storage racks where he suggested that for both cross isle and down isle direction the maximum ductility used for design should be 1.25 and in no cases should it go beyond 3.0 for down isle direction except detail study suggest otherwise.

As actual frame performance depends on each type of frame and material, buckling characteristic, structural redundancy, frame section geometry and strength degradation of structural elements, a more sophisticated evaluation of response modification/behavior factor is necessary for RCB structures which should take wide-ranging experimental and numerical studies and different limit states into account (Bernuzzi and Castiglioni 2001).

4.4 Response modification factor

Linear elastic dynamic analysis or response spectrum modal analysis can generate base shear which is many fold greater than the actual response of the structure (Asgarian and Shokrgozar 2009). Several analytical procedures for calculating response modification factor have been described by (Mazzolani and Mandara 2002). They are maximum plastic deformation, energy and low cycle fatigue based approaches. The actual base shear capacity (V_y) of a structure can be determined by carrying out pushover analysis. Using the actual base shear capacity (V_y) and the design lateral strength (V_d) the overstrength factor can be calculated by equation 4.1.

$$R_o = \frac{V_y}{V_d} \quad (4.2)$$

It is very important to quantify the actual overstrength factor as it can be used to reduce seismic forces in design which can lead to more economic structures (Uang 1991, Mitchell and Paulter 1994, Park 1996).

The ductility related force reduction factor (R_d) can be defined as the ratio of the maximum base shear for an elastic structural system (V_E) to the maximum base shear (V_y) for an elastic perfectly plastic structural system. R_d can be calculated using the equation 4.2.

$$R_d = \frac{V_E}{V_y} \quad (4.3)$$

Lastly, the response modification factor (R) can be calculated by dividing the elastic strength (V_e) by the design strength of the structure (V_d). Alternatively this factor can be calculated by multiplying R_d and R_o .

$$R = \frac{V_E}{V_d} = \frac{V_E}{V_y} * \frac{V_y}{V_d} = R_d * R_o \quad (4.4)$$

The computation method of elastic base shear is graphically represented in Figure 4.3. The elastic base shear (V_e) is calculated by performing linear dynamic time history analysis on the structure under consideration using the collapse earthquake for that structure. The collapse earthquake is determined using nonlinear incremental dynamic time history analysis up to the collapse of the structure.

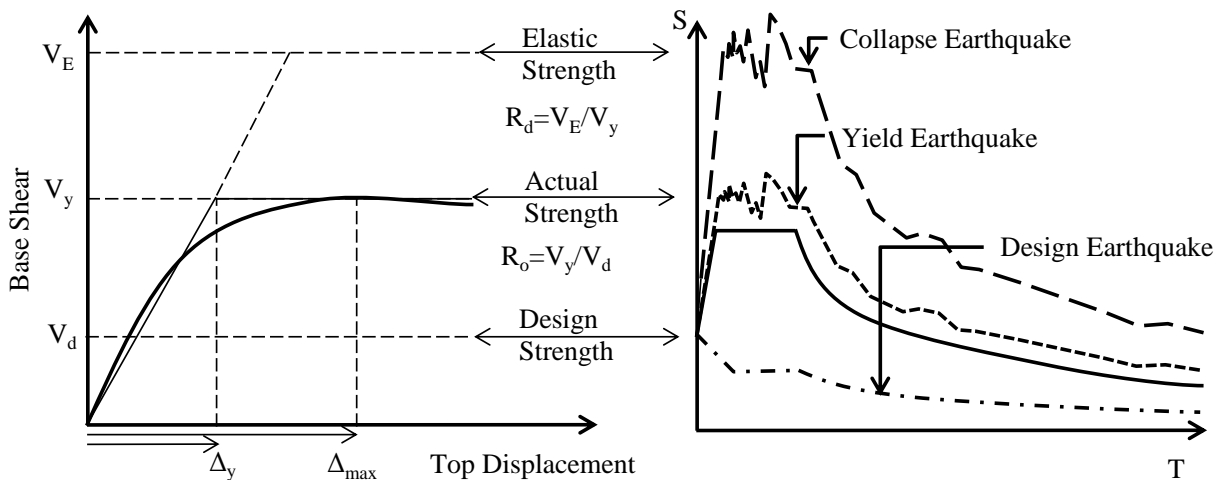


Figure 4.3: Comparison between the ductility reduction factor (R_d) and the definition of R_d (adapted from Mwafy and Elnashai, 2002)

4.5 Overstrength factor

Figure 4.4 shows the selected RCB frames for ductility related force reduction factor calculation. These frames have similar story heights where the first story height is 1767 mm and the subsequent stories are 1600 mm. Each bay width is 2250 mm. Columns have similar cross sectional dimensions as shown in Figure 3.7(a) and all beam are 50mmx100mmx1.5mm

rectangular hollow section. All of these frames have similar beam and column dimensions except beam-to-column connector stiffness, which were designed using tentative R_d and R_o values approximated from a single pushover analysis of one RCB frame.

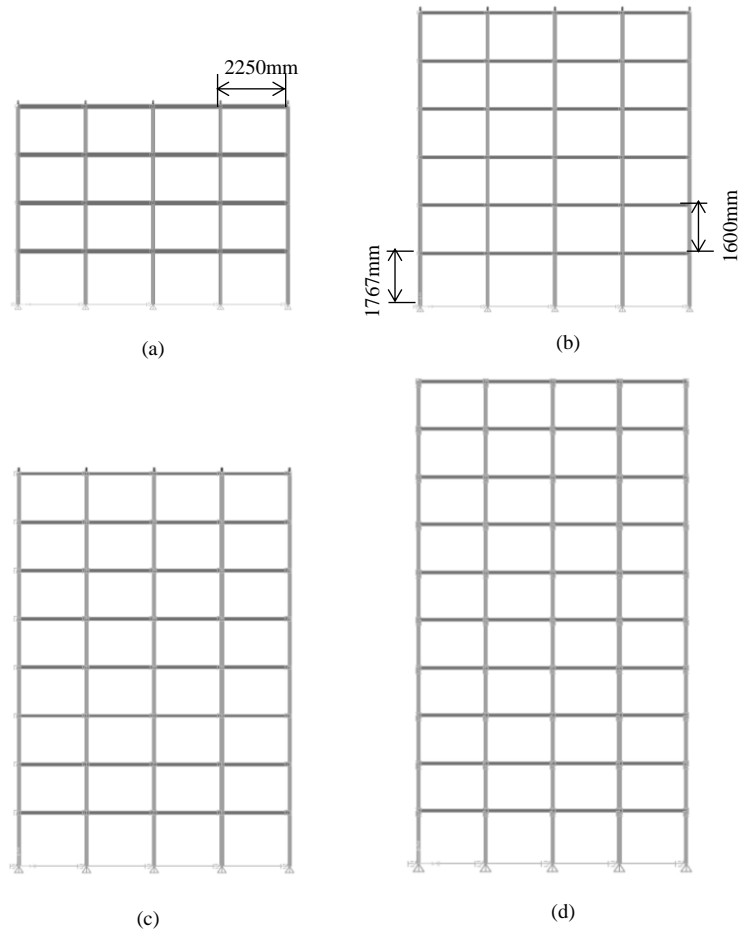


Figure 4.4: Selected frames for incremental dynamic time history analysis (a) four story (b) six story (c) eight story and (d) ten story

Figure 4.5 shows base shear vs. roof displacement curves for the above mentioned 4, 6, 8 and 10 storied RCB frames. The straight line curves drawn along these curves are the idealization of these curves which were created for the calculation of overstrength factors. The area under the actual and idealized curve was approximately the same and it was calculated and presented in

Table 4.1. The area was made approximately equal by adjusting the idealized curve using trial and error method.

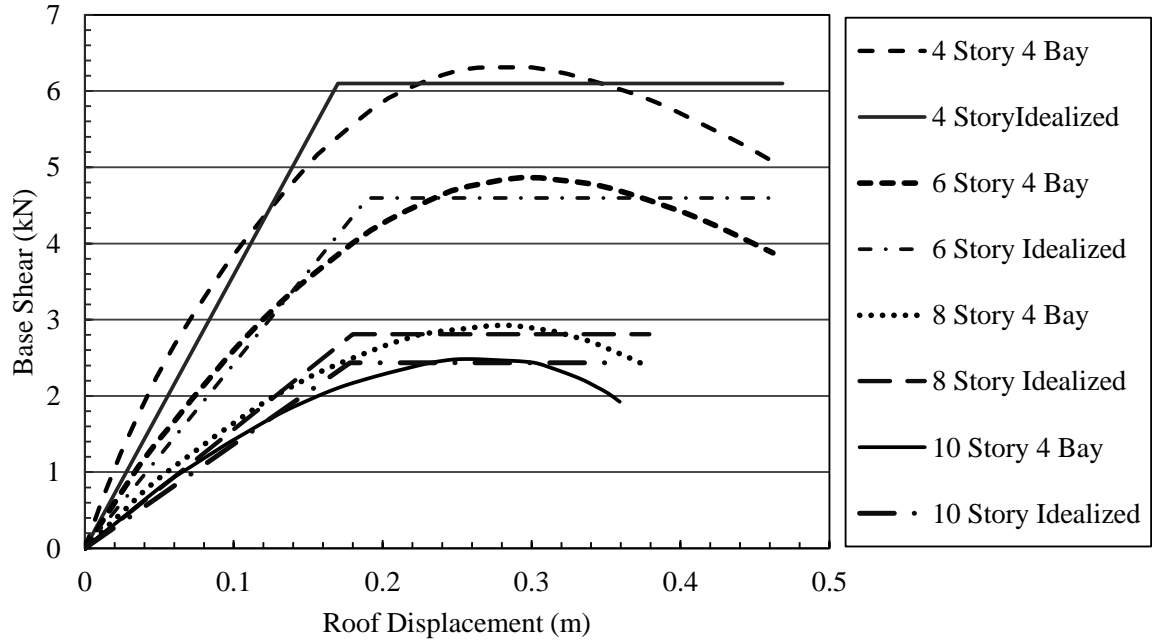


Figure 4.5: Overstrength factor calculation for RCB moment resisting frames using pushover analysis

Table 4.1 presents the values of yield base shear and base shear at first yield along with other values. The base shear at first yield was calculated by observing connector moments along the base shear from the pushover analysis at each step of the analysis. For accurate determination of yield base shear the analysis was carried out under very small displacement increments and finally interpolation was used for precise calculation. From the ratio of the yield base shear determined from idealized curve and base shear at first yield the overstrength factor has been calculated and presented in the same table.

Table 4.1: Overstrength and ductility factor calculation from pushover analysis

	Four Storied	Six Storied	Eight Storied	Ten Storied
Base Shear at Global Yield, V_y (kN)	6.1	4.50	2.85	2.46
Yield Displacement, Δ_y (m)	0.17	0.18	0.19	0.19
Ultimate Displacement, Δ_u (m)	0.47	0.46	0.38	0.36
Connector Yield Moment, M_y (kN-m)	1.12	1.40	1.40	1.65
Base shear at First Yield	5.37	4.17	2.75	2.46
Overstrength Factor, R_o	1.14	1.08	1.04	1.00
Area Under Original Curve (kN-m)	2.31	1.68	0.81	0.64
Area Under Idealized Curve (kN-m)	2.34	1.67	0.81	0.65
Area Variation (%)	1.40	-0.50	0.53	1.20
Ductility ratio	2.76	2.57	2.00	1.89

4.6 Force reduction factor calculation

Force reduction factor is defined as the ratio between the elastic base shear (V_e) and the idealized base shear capacity (V_y) of a structure. The elastic base shear capacities of RCB frames were determined using incremental dynamic time history analysis. Ten earthquake records (Figure 3.21) were selected and were scaled to match the Vancouver response spectrum as per Asgarian and Shokrgozar (2009). The scaling was done using SeismoMatch (2011) software which uses the wavelet algorithm proposed by Abrahamson (1992) and Hancock et al. (2006). Then these earthquake records were scaled with different scaling factors ranging from low to high values. Finally, these scaled records were used to carry out nonlinear dynamic time history analysis on the RCB frames. Before the nonlinear analysis, the frames were designed against the code specified response spectrum. During the design process it was observed that the selected beams and columns had adequate reserve strength and did not require any change in section size but the beam-to-column and column-to-base plate connectors were found inadequate for increasing frame height and required design revision. The connector design was theoretically

revised using scale factor and practical moment rotation limits were checked using the power model developed by Prabha et al. (2010) which is represented by equation 3.14 to 3.16 and also depicted in Figure 3.6. The revised connector designs are presented in Table 4.2.

Table 4.2: Connector design for different frame heights

Rotation (Radians)	Four Storied Moment (kN-m)	Six to Eight Storied Moment (kN-m)	Ten Storied Moment (kN-m)
-0.068	-1.330	-1.663	-1.995
-0.06	-1.329	-1.661	-1.994
-0.05	-1.314	-1.643	-1.971
-0.04	-1.247	-1.559	-1.871
-0.03	-1.084	-1.355	-1.626
-0.02	-0.814	-1.018	-1.221
-0.01	-0.491	-0.614	-0.737
-0.005	-0.295	-0.369	-0.443
0	0.000	0.000	0.000
0.005	0.295	0.369	0.443
0.01	0.491	0.614	0.737
0.02	0.814	1.018	1.221
0.03	1.084	1.355	1.626
0.04	1.247	1.559	1.871
0.05	1.314	1.643	1.971
0.06	1.329	1.661	1.994
0.068	1.330	1.663	1.995

The backbone curve design data represented in Table 4.2 has been illustrated in Figure 4.6. It can be seen that for increase in story height both stiffness and strength of the connector needs to be increased in order to satisfy the increasing moment demand at the beam-to-column joint.

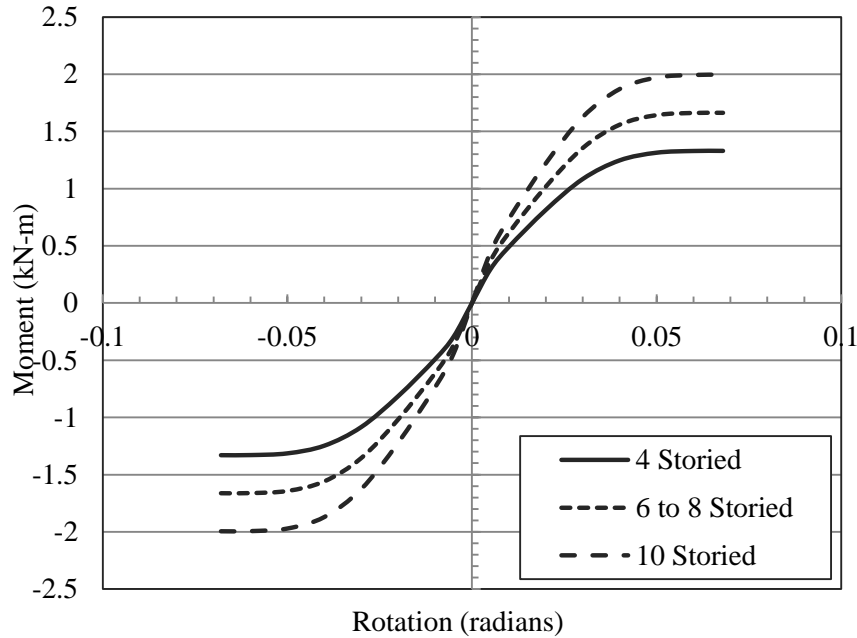


Figure 4.6: Beam-to-column connector backbone curve used for the analysis

During the incremental dynamic analysis the base shear and roof top displacements were recorded for each scaled record and the analysis was carried out with a gradually increasing scale factor until the frame finally became unstable under lateral load. This final base shear was recorded as collapse base shear and denoted as inelastic base shear. The earthquake which initiated collapse of the structure was denoted as collapse earthquake and this earthquake record was used to carry out linear dynamic time history analysis of the RCB frame and the resulting maximum base shear from this analysis is recorded as elastic base shear (V_e). The analysis results are presented in Table 4.3 to Table 4.6.

Table 4.3: R_d values for four storied by four bay moment resisting frame

EQ Record Name	V inelastic	V elastic	Rd	Scale Factor
Northridge	8.60	19.11	2.22	1.82
Artificial	12.71	32.94	2.59	2.9
ChiChi	8.45	31.30	3.70	2.2
Corralitos	11.10	25.33	2.28	2.1
Emeryville	15.03	32.32	2.15	3.5
Imperial Valley	10.02	21.43	2.14	2.3
Kobe	13.96	31.11	2.23	3.4
Kocaeli	8.80	15.35	1.74	0.8
Loma Prieta	10.77	31.44	2.92	2.4
Sakaria	8.07	30.51	3.78	1.5
Average			2.58	

Table 4.4: R_d values for six storied by four bay moment resisting frame

EQ Record Name	V inelastic	V elastic	Rd	Scale Factor
Northridge	9.14	37.20	4.07	2
Artificial	10.44	30.40	2.91	2.6
ChiChi	8.22	25.59	3.11	1.9
Corralitos	8.77	14.83	1.69	1.5
Emeryville	11.12	24.43	2.20	3.3
Imperial Valley	15.00	29.91	1.99	3.6
Kobe	10.31	24.75	2.40	3.4
Kocaeli	6.86	14.64	2.14	0.6
Loma Prieta	11.12	18.37	1.65	2.2
Sakaria	7.86	21.29	2.71	0.9
Average			2.49	

Table 4.5: R_d values for eight storied by four bay moment resisting frame

EQ Record Name	V inelastic	V elastic	Rd	Scale Factor
Northridge	10.14	18.36	1.81	3
Artificial	12.23	16.67	1.36	1.9
ChiChi	9.16	10.49	1.15	1.5
Corralitos	9.44	17.35	1.84	2.2
Emeryville	9.23	13.60	1.47	2.4
Imperial Valley	10.25	10.96	1.07	2.6
Kobe	8.71	15.66	1.80	2.8
Kocaeli	4.39	11.37	2.59	0.7
Loma Prieta	7.30	10.99	1.51	1.6
Sakaria	5.44	10.36	1.90	0.8
Average			1.65	

Table 4.6: R_d values for ten storied by four bay moment resisting frame

EQ Record Name	V inelastic	V elastic	Rd	Scale Factor
Northridge	9.124	15.05	1.65	2.4
Artificial	11.56	16.02	1.39	2.6
ChiChi	6.832	11.16	1.63	1.4
Corralitos	7.331	12.98	1.77	1.8
Emeryville	6.682	9.352	1.40	2.1
Imperial Valley	7.25	7.85	1.08	2
Kobe	6.971	14.39	2.06	2.2
Kocaeli	3.343	5.961	1.78	0.6
Loma Prieta	7.716	9.308	1.21	1.6
Sakaria	4.743	6.467	1.36	0.7
Average			1.53	

On the other hand, the idealized base shear was determined from the idealized curve of the pushover analysis shown in Figure 4.5 and Table 4.1. Figure 4.7 shows eleven base shear vs. roof displacement curve for a four storied RCB frame, two of which are generated from the incremental dynamic analysis using Northridge and Kobe earthquake and the last one is from

nonlinear static (Pushover) analysis. It can be seen that the result from these three curves can have a significant variation with respect to both maximum base shear and roof displacement capacity. For this reason ten earthquake records were selected for the incremental dynamic analysis and the force reduction factor was calculated from averaging their results.

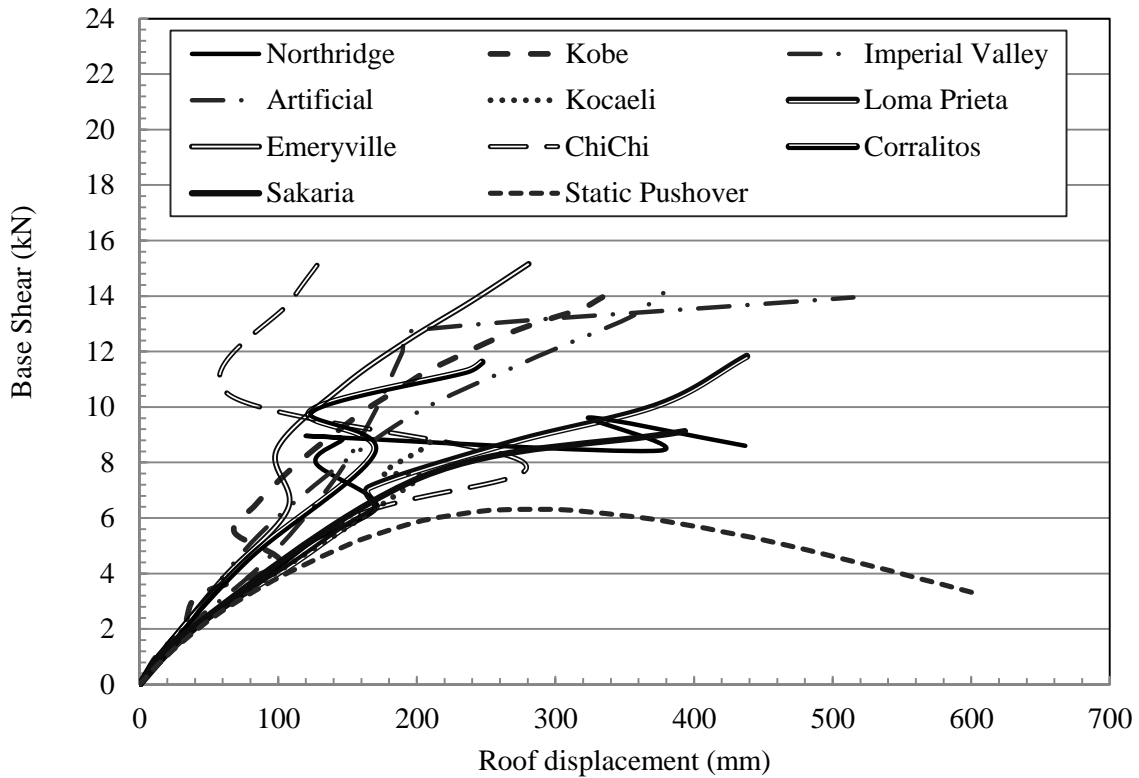


Figure 4.7: Comparison of base shear-roof displacement curve from incremental dynamic and pushover analysis for a four storied RCB frame

Figure 4.8 shows the force reduction factors calculated for the four RCB frames under consideration for ten different earthquake records. From the figure it can be stated that the value of force reduction factor reduces with the increase in number of stories in a frame with some exception observed for some earthquake records e.g. Northridge, Artificial and Kocaeli etc.

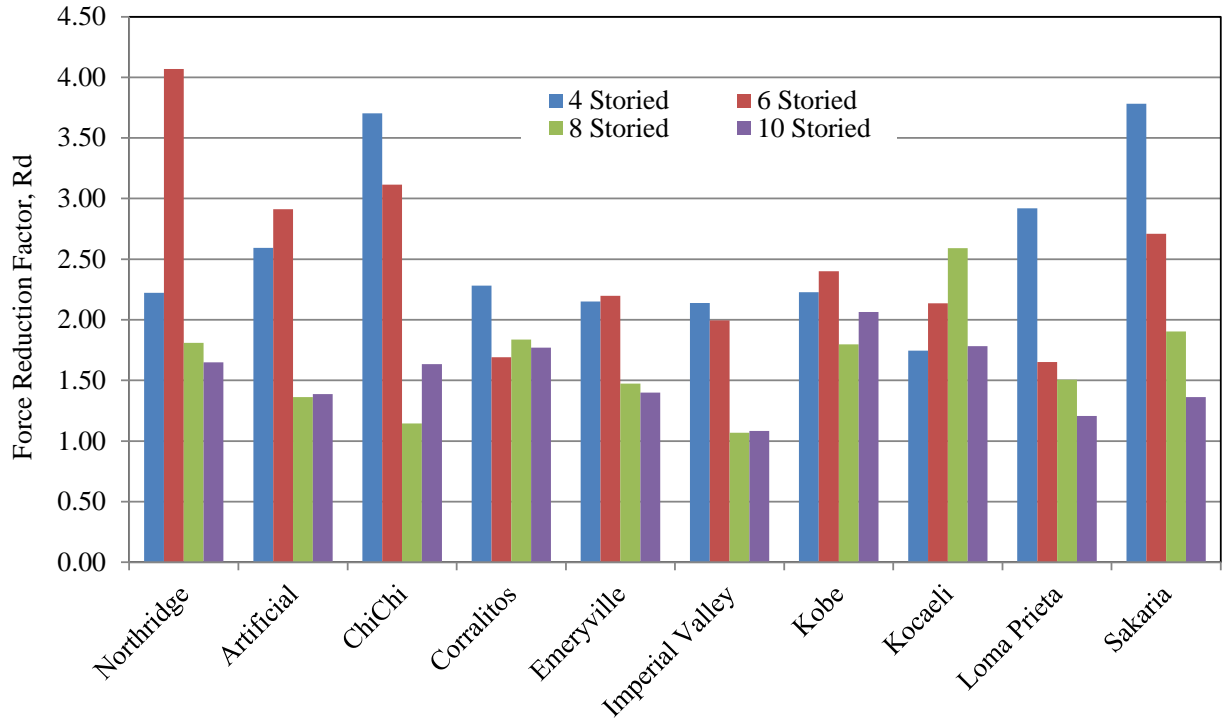


Figure 4.8: Force reduction factors for different earthquake records

Equation 4.5(Table 4.7) and Equations 4.6 and 4.7 (

Table 4.8) show two methods for calculating force reduction factor from ductility values which were developed by Lai and Biggs (1980) and Riddell et al. (1989), respectively. Using these equations and earlier calculated ductility values (Table 4.1) the force reduction factors were calculated and shown in

Table 4.9 and checked against the values obtained from incremental dynamic analysis presented in Figure 4.8.

$$R_{\mu} = \alpha + \beta(\log T) \quad (4.5)$$

Here α and β are two co-efficient.

$$0 \leq T < T^* \quad R_{\mu} = 1 + \frac{R^* - 1}{T^*} \cdot T \quad (4.6)$$

$$T \geq T^* \quad R_{\mu} = R^* \quad (4.7)$$

This cross check determined the effectiveness of the method used in this study and it was observed that the R_d values calculated from IDA are in good agreement with the values calculated from the equations proposed by Lai and Biggs (1980) and Riddell et al. (1989).

Table 4.7: α and β coefficient proposed by Lai & Biggs (1980)

Period Range	Coefficient	$\mu=2$	$\mu=3$	$\mu=4$	$\mu=5$
$0.1 < T < 0.5$	α	1.679	2.229	2.658	3.11
	β	0.329	0.729	1.058	1.430
$0.5 < T < 0.7$	α	2.033	2.772	3.370	3.833
	β	1.505	2.532	3.421	3.832
$0.7 < T < 4.0$	α	1.840	2.482	2.985	3.418
	β	0.264	0.660	0.938	1.149

Table 4.8: R^* & T^* values proposed by Riddell et al. (1989)

Parameter	$\mu=2$	$\mu=3$	$\mu=4$	$\mu=5$	$\mu=6$	$\mu=7$	$\mu=8$
R^*	2	3	4	5	5.6	6.2	6.8
T^*	0.1	0.2	0.3	0.4	0.4	0.4	0.4

Table 4.9: Force reduction factor for four storied by four bay frame

	Four Storied	Six Storied	Eight Storied	Ten Storied
Ductility from Pushover curve	2.76	2.43	2.11	2.00
Time period, T_l (Sec)	1.91	2.72	3.56	4.13
Lai and Biggs (1980)				
α	2.33	2.12	1.91	1.85
β	0.56	0.44	0.31	0.27
R_d	2.69	2.55	2.30	2.00
Riddell et al. (1989)				
R^*	2.76	2.57	2.11	2.00
T^*	0.18	0.16	0.10	0.10
R_d	2.76	2.43	2.11	2.00

From

Table 4.9 it can be seen that the average of R_d values from Lai and Biggs equation is 2.39 and from Riddell et al. equation it is 2.32 and from incremental dynamic analysis it is 2.06. The variation is approximately 12% which can be acceptable if a conversion coefficient is used to convert data from these equations to match with dynamic analysis result. Since incremental dynamic analysis requires large number of earthquake records to be run and is extremely time consuming, the alternative approaches have been utilized on 12 more frames to determine the force reduction factor.

Table 4.10: Ductility overstrength and R_d values of 16 RCB frames

Frame Designation (Story x Bay)	Ductility	Time Period (T_I)	Overstrength factor, R_o	R_d from Lai and Biggs (1980) equation	R_d from Riddell et al.(1989) equation
4x4	2.76	1.91	1.14	2.69	2.76
4x6	3.12	1.93	1.11	3.00	3.12
4x8	3.12	1.94	1.11	3.00	3.12
4x10	3.12	1.95	1.11	3.01	3.12
6x4	2.43	2.72	1.10	2.55	2.43
6x6	2.37	2.75	1.09	2.49	2.37
6x8	2.34	2.76	1.08	2.46	2.34
6x10	2.40	2.76	1.07	2.53	2.40
8x4	2.11	3.56	1.00	2.30	2.11
8x6	2.10	3.57	1.00	2.29	2.10
8x8	2.11	3.59	1.01	2.31	2.11
8x10	2.04	3.59	1.01	2.23	2.04
10x4	2.02	4.13	1.00	2.23	2.02
10x6	2.01	4.15	1.00	2.22	2.01
10x8	2.05	4.09	1.00	2.26	2.05
10x10	2.07	4.11	1.00	2.29	2.07
Average	2.38		1.05	2.49	2.38

Table 4.10 presents the ductility, overstrength factor and force reduction factor values for 16 RCB frames. Riddell et al. (1989) provided equation provided a more conservative result and it is closer to the nonlinear dynamic analysis calculated values. For this reason the average value calculated from this equation has been taken as the final result. As discussed previously this average value can be used with approximately 12% reduction for use in the design. Using a reduction factor of 0.88 yields a value of R_d equal to 2.1 which can be further multiplied by R_o (1.05) and the final response modification factor is 2.2. Figure 4.9, Figure 4.10, Figure 4.11 and Figure 4.12 shows the pushover analysis results of the sixteen frames under consideration.

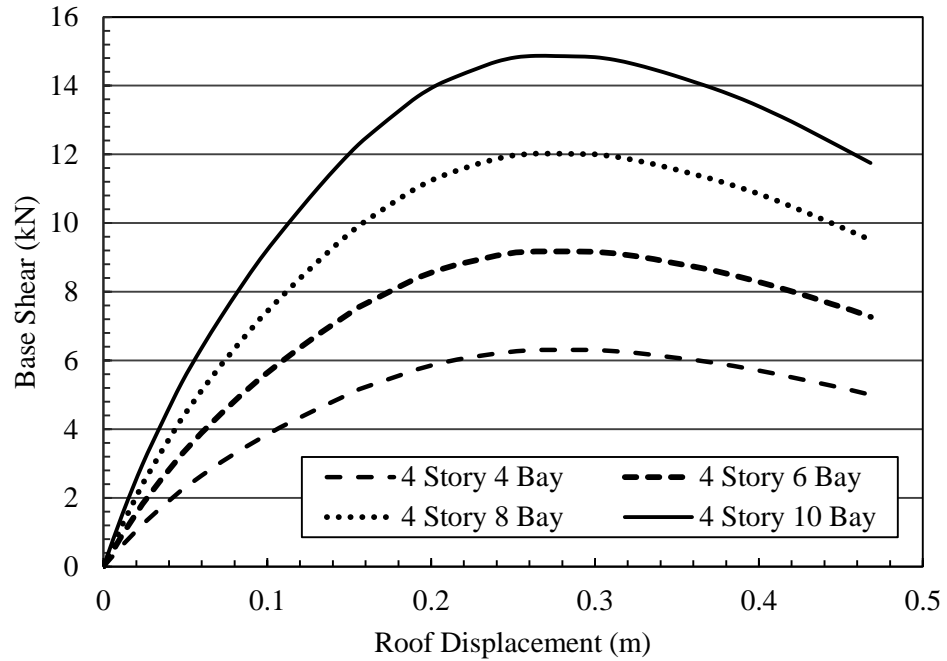


Figure 4.9: Pushover analysis of four storied frame with different bay widths

Figure 4.9 shows four pushover curves for a four storied RCB frame. The top curve is generated from a four storied by ten bay frame. The second one from the top is for four storied by eight bay frame and the bottom two curves are for six and four bay width, respectively. For ductility calculation the curves are drawn up to 20% reduction in base shear from the maximum base shear capacity.

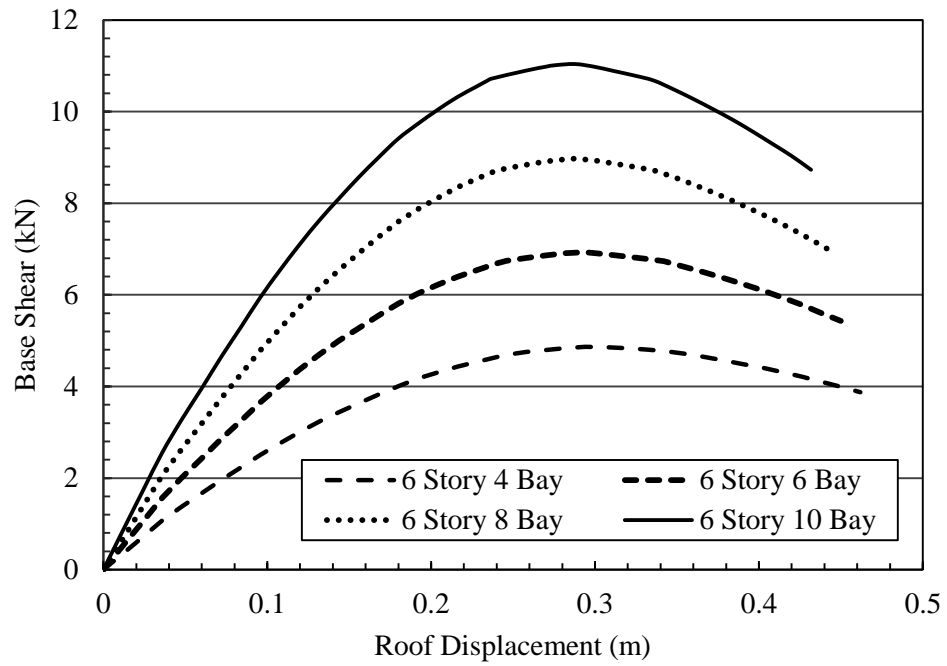


Figure 4.10: Pushover analysis of six storied frame with different bay widths

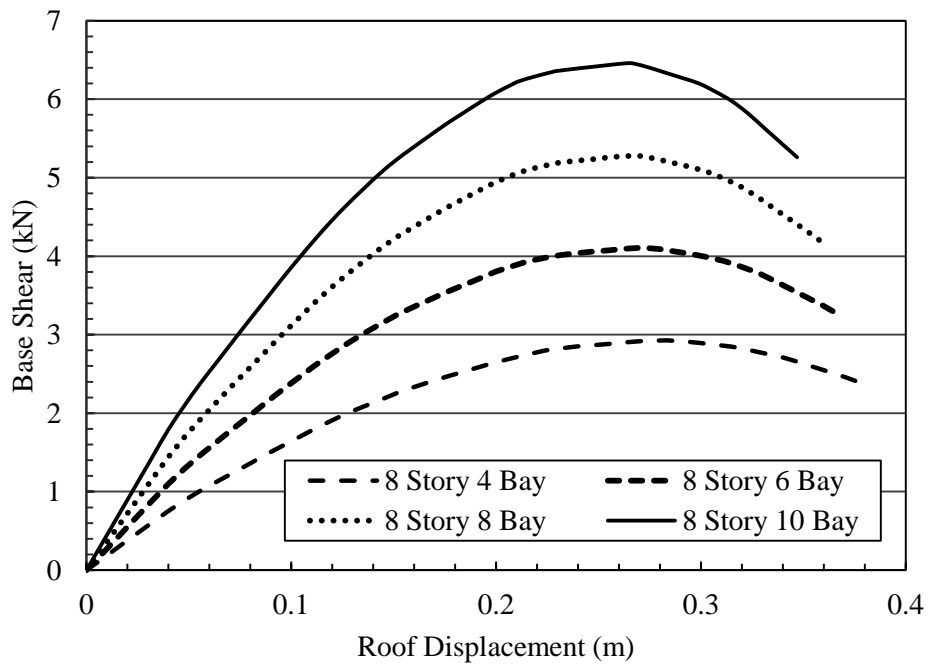


Figure 4.11: Pushover analysis of eight storied frame with different bay widths

A similar trend in pushover curves is also observed for six storied RCB frames shown in Figure 4.10. With higher number of bays the bases shear capacity increases and vice versa. It can be concluded from the above figure that the stiffness increases with increases with increasing number of bays too. Figure 4.11 and Figure 4.12 show similar pushover curves for 8 and 10 storey frames as compared to those of Figure 4.9 and Figure 4.10.

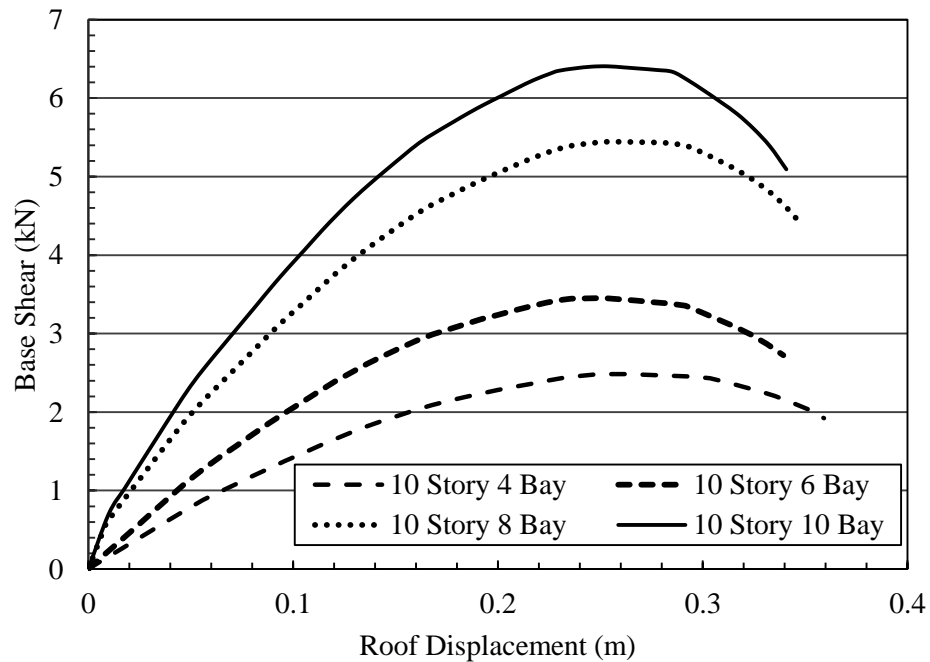


Figure 4.12: Pushover analysis of ten storied frame with different bay widths

4.7 Performance evaluation

A four storied RCB frame shown in Figure 3.15 was chosen to be designed using the overstrength and ductility factor calculated from incremental dynamic analysis. The frame was modeled and analyzed using SAP2000 (2010) software. Vancouver soil class “C” response spectrum was used for the design. From the design it was found out that the initial frame configuration (collected from the documents provided by the industrial partner) was adequate in resisting code specified lateral force level. After the design was complete, the frame was

analyzed using non-linear time history analysis procedure. Ten earthquake records were selected for this analysis. After the analysis was complete, roof drift time history data was collected from the middle point of the roof. Also subsequent story displacements were retrieved from the model for the calculation of interstory and residual drift ratios. The maximum roof drift values are presented in Figure 4.13. It can be seen from the figure that for different earthquake records the roof drift value varies quite significantly which was observed to range from approximately 142mm to 401mm. The average roof drift value was found to be 243mm which is approximately 3.7% of the story height. This average roof drift ratio is significantly higher compared to tradition residential or factory buildings but according to RMI (2008) this is very normal for rack type storage structures for their very high beam-to-column joint connector flexibility.

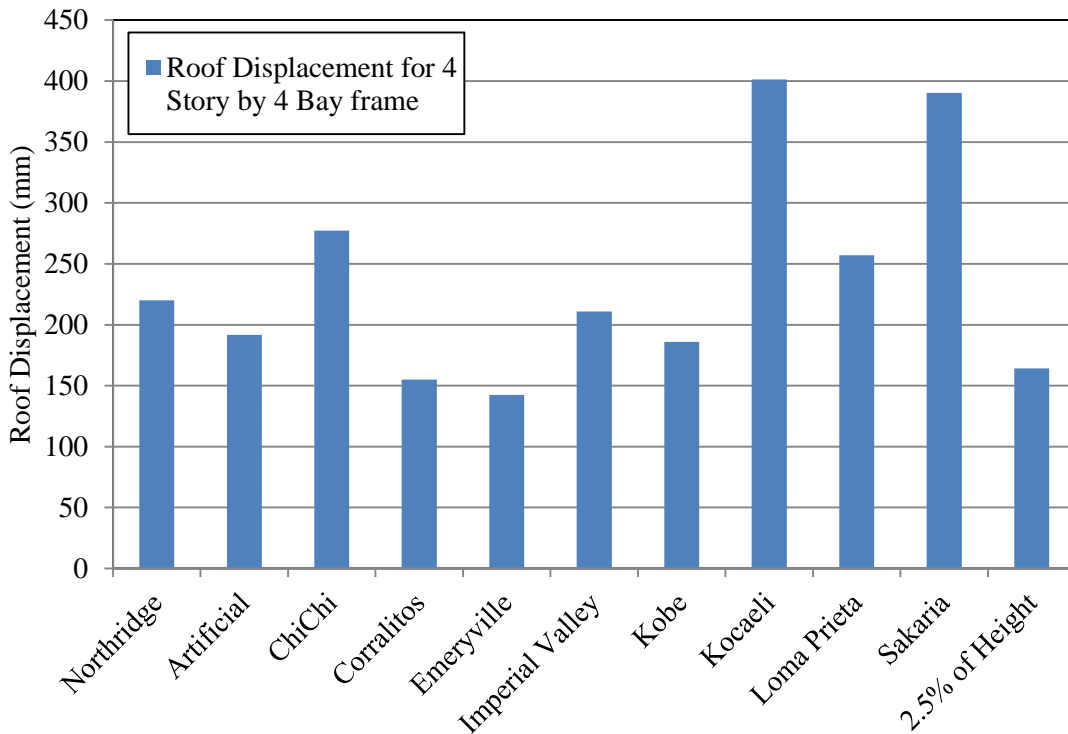


Figure 4.13: Roof drift of the four storied RCB frame from NLTHA

Similar design and analysis was carried out on six, eight and ten storied RCB frames all having a width of four bays. Only top two stories were replicated for the generation of six, eight and ten storied frames from the initially selected four storied frame. Figure 4.14, Figure 4.15 and Figure 4.16 shows the roof displacement values calculated from nonlinear time history analysis. The empty places in these figures (e.g. Kocaeli in Figure 4.14) are due to instability of RCB frame from the nonlinear time history analysis of the corresponding earthquake record. It can be observed from these figures that with increase in frame height the roof displacement values from nonlinear time history analysis comes closer to code specified roof drift limit of 2.5%.

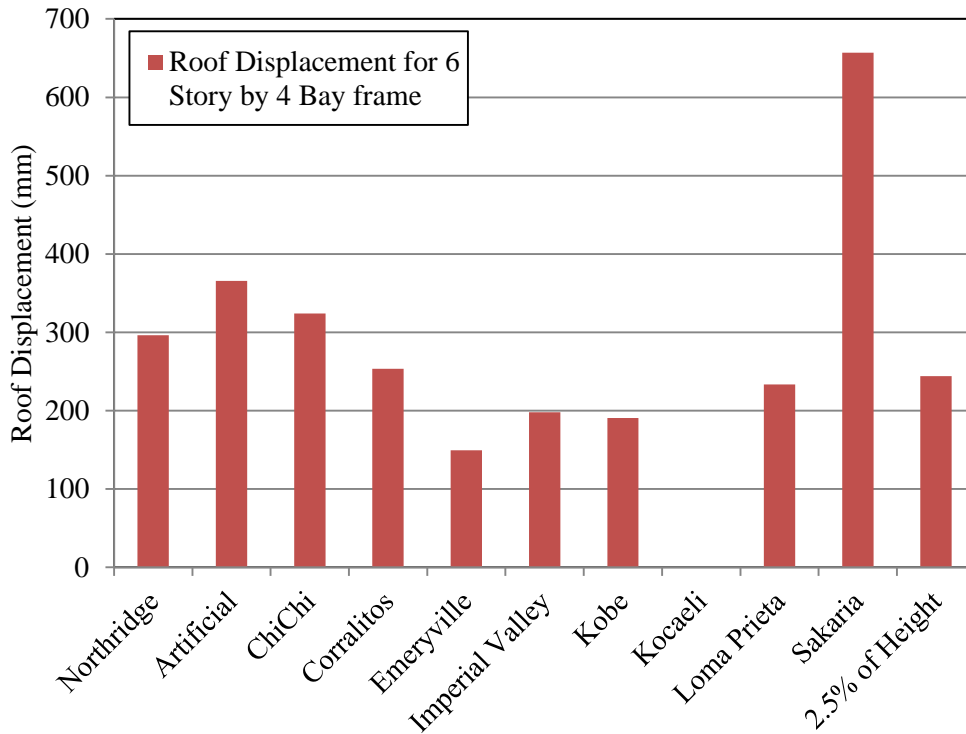


Figure 4.14: Roof drift of the six storied RCB frame from NLTHA

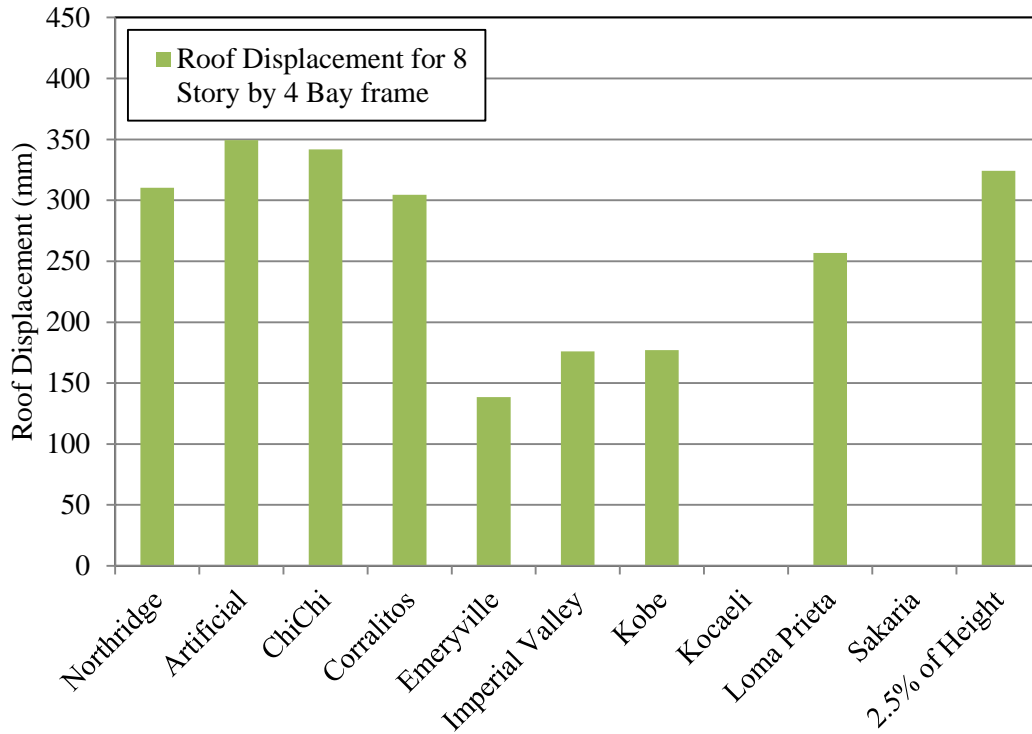


Figure 4.15: Roof drift of the eight storied RCB frame from NLTHA

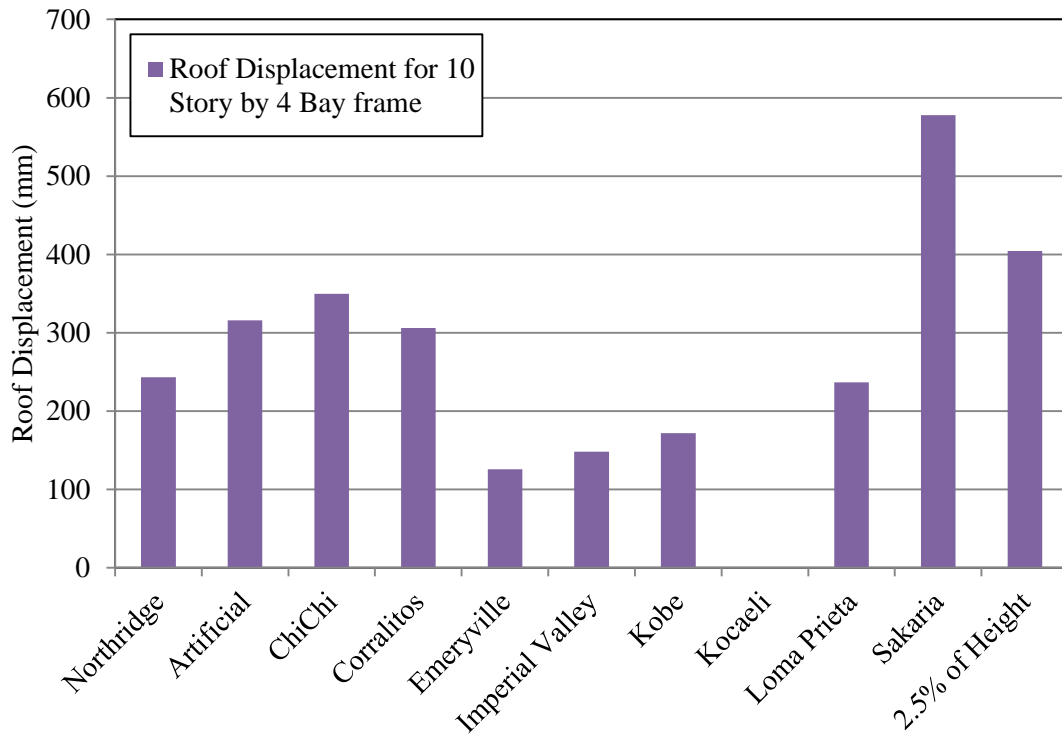


Figure 4.16: Roof drift of the ten storied RCB frame from NLTHA

On the other hand, Figure 4.17, Figure 4.18, Figure 4.19 and Figure 4.20 show the maximum and residual interstory drift ratio for the four, six, eight and ten storied RCB frame. It can be observed from these figures that although the maximum interstory drift ratio values are very high, the residual interstory drift ratio came significantly low. This analysis result confirms the spring back capability of the Rack type frame structures as suggested by (Beattie 2006) and (Filiatrault et al. 2006b). It can be also observed that the maximum interstory drift ratio value came almost twice as that of the roof drift value, and residual interstory drift value came almost one third of the maximum interstory drift ratio. As residual interstory drift ratio represents the residual damage of the structure, a lower value suggests better performance under seismic loading condition.

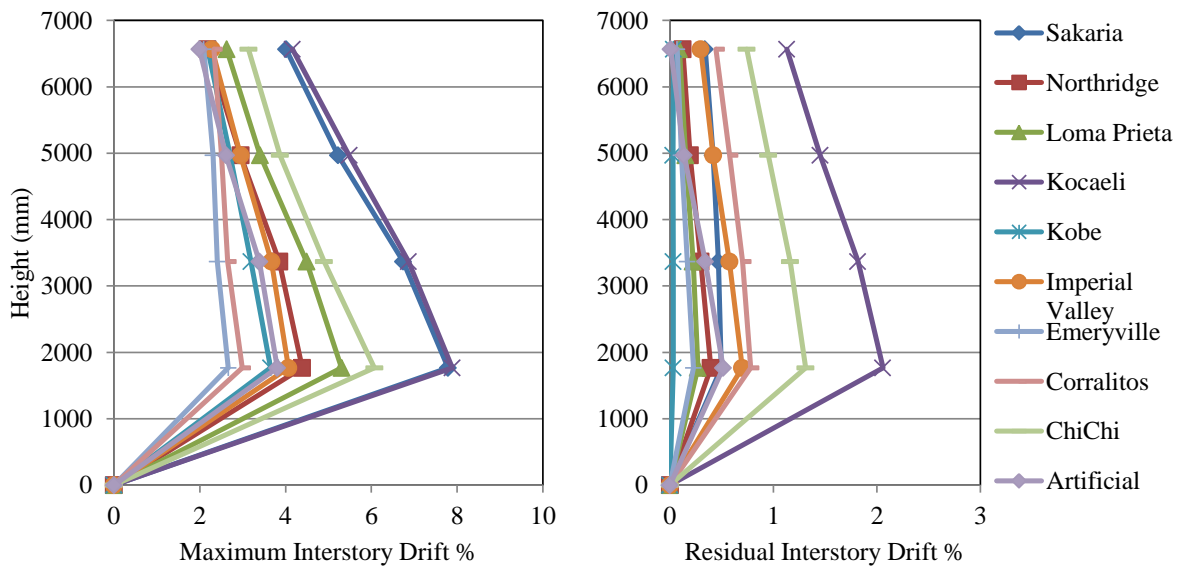


Figure 4.17: Maximum and residual interstory drift ratio of the four storied RCB frame from NLTHA

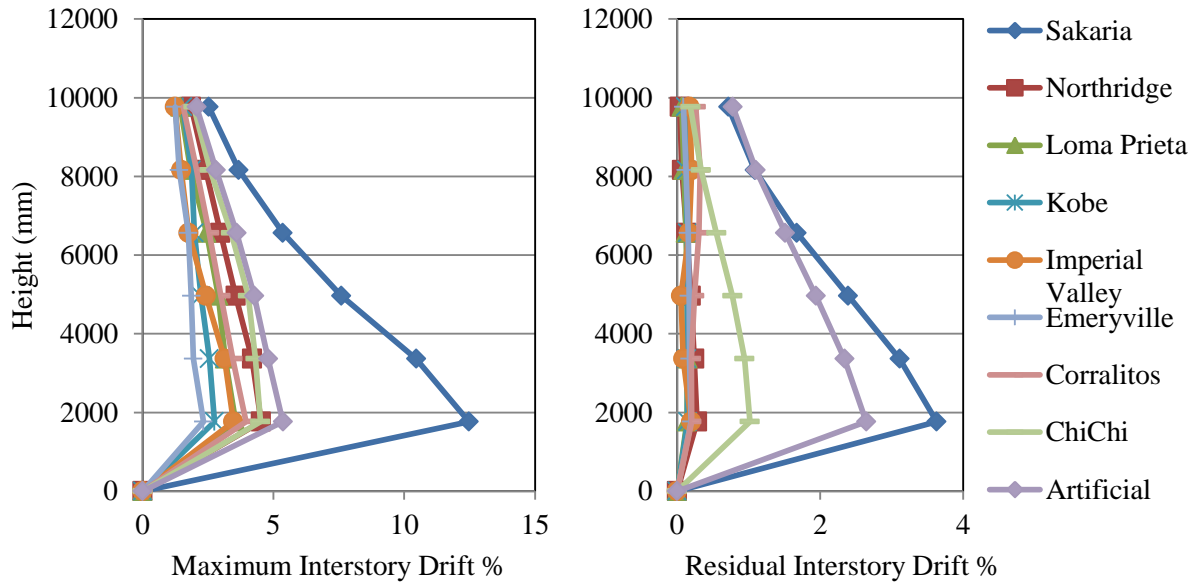


Figure 4.18: Maximum and residual interstory drift ratio of the six storied RCB frame from NLTHA

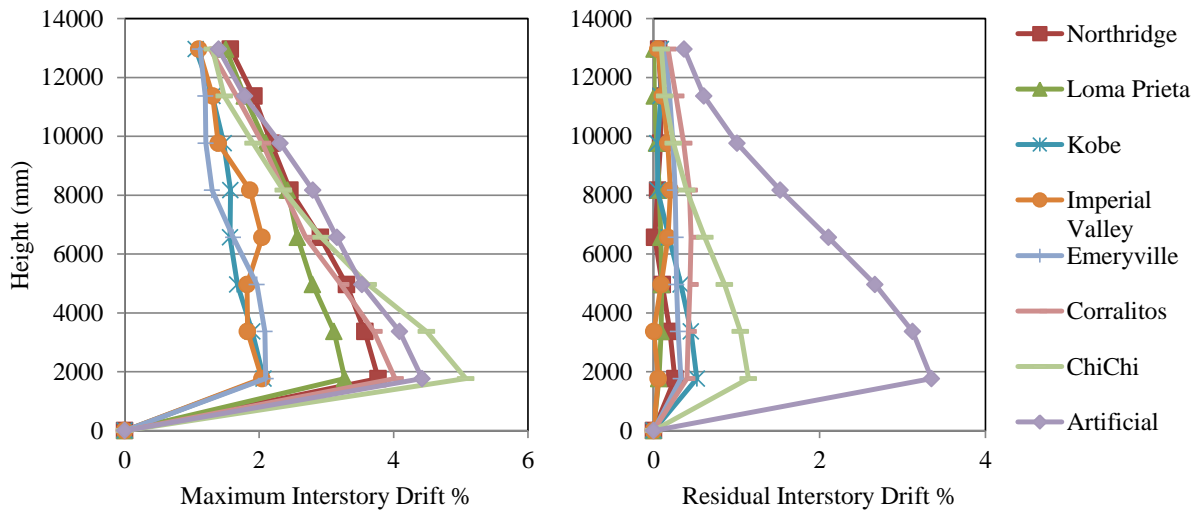


Figure 4.19: Maximum and residual interstory drift ratio of the eight storied RCB frame from NLTHA

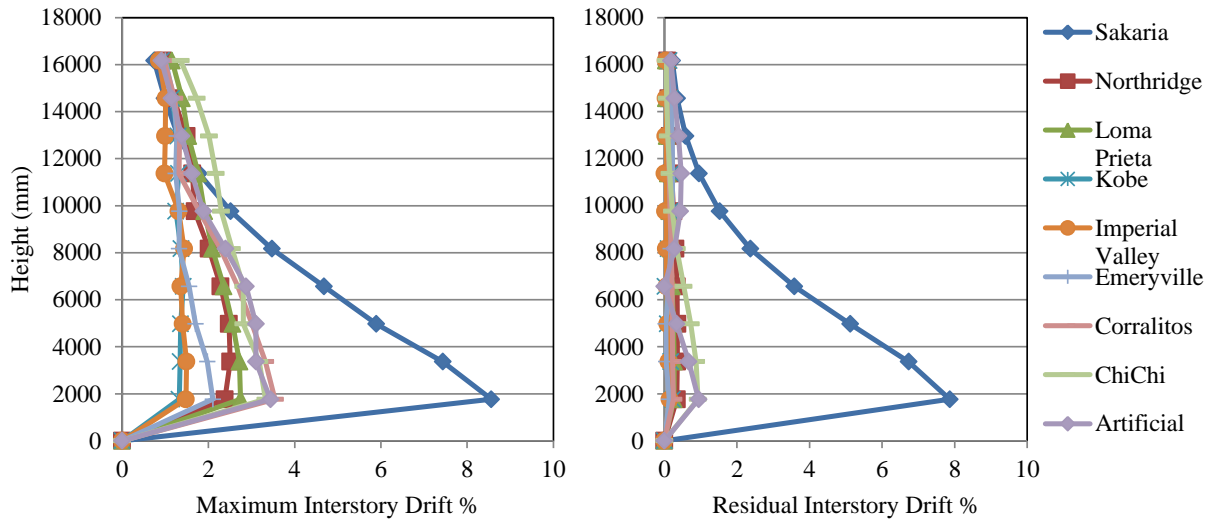


Figure 4.20: Maximum and residual interstory drift ratio of the ten storied RCB frame from NLTHA

4.8 Summary

Several RCB frames were modeled with increasing frame height/stories. Pushover and incremental dynamic time history analysis was carried out on these frames using nonlinear beam-to-column and column-to-base plate connector moment-rotation hysteresis. The overstrength and ductility for these frames were calculated from pushover analysis and force reduction factor from incremental dynamic analysis and it was found out that both overstrength and force reduction factor decreases with the increase of frame height/number of stories. The average R_d value obtained from the dynamic analysis is 2.06 and R_o value from nonlinear static analysis is 1.05. It was also observed that the ductility capacity of the structure reduces with the increase of frame height. The average ductility value obtained from the sixteen frames is 2.38. Also the average value of ductility related force reduction factor from Riddell et al. (1989)'s equation came to be 2.38. Finally, four different RCB frame was designed using the overstrength and ductility factor and analyzed using nonlinear time history with ten earthquake records. The

results from these analyses show acceptable performance with respect to expected rack frame behaviour under seismic loading condition.

CHAPTER 5: COMPARISON BETWEEN FBD AND DDBD OF RCB

5.1 General

Force and displacement based seismic design are two most prominent seismic design methods. However, there are fundamental differences between these two methods which can produce different designs. In this chapter rack clad building (RCB) frames have been designed in both force and displacement based method and their performances were evaluated conducting nonlinear dynamic time history analysis using ten earthquake records. The design and analysis was done using developed excel spreadsheets and SAP2000 (2010) software. This study only considered moment resisting frame in the down-isle direction of RCB frames. It was found out that force-based design produced more economical design due to calculated low base shear compared to displacement based design. On the other hand displacement based design produced stiffer frames because of the higher base shear demand calculated from that method. From the performance evaluation it was found out that the frames designed using displacement based design performed better against earthquake with respect to roof drift ratio, interstory drift ratio and residual interstory drift ratio.

For checking the applicability of displacement and force based design method on RCB frames first the direct displacement based design method developed by Priestley et al. (2000) has been adapted and also the overstrength and ductility related force reduction factors were calculated for force based design.

Using these two methods two RCB frames have been designed with similar geometry and loading condition and their performance have been evaluated under nonlinear time history analysis using ten different earthquake records.

5.2 Force vs. displacement based design

Force based design uses equivalent lateral force or response spectrum analysis procedure which uses reduced base shear forces using force reduction and overstrength factors. The overstrength and ductility can be calculated from nonlinear static analysis procedure. From ductility capacity the force reduction capacity can also be estimated using some empirical equation which depends on the natural time periods of the structure. These empirical equations are based on equal displacement and equal energy concept. As per equal displacement approximation it can be shown that the structural ductility capacity and force reduction factors are equal for specific time period range of the structure. These empirical methods are not very accurate as they are based on static pushover analysis, because static pushover analysis idealizes the structure as a single degree of freedom system and only takes the first mode shape into consideration. Accurate determination of the force reduction factor is a cumbersome process, which requires nonlinear incremental dynamic time history analysis using large number of earthquake records, which is a time consuming process that requires specialized knowledge and tools. Also the finite element models used for these analyses represent beam and columns as line elements, which severely disregards the potential for warping of the thin walls of the uprights. Furthermore, the effect of the perforations cannot be perfectly captured using simple FE models. Therefore, in most cases the empirical methods are being used. Priestley (2000) described that this approach has some limitations because the equal displacement approximation is not valid for

very short and very long period structures. If the hysteresis behavior of a structure significantly deviates from the elasto-plastic action, then equal displacement approximation is not valid because the current force based design cannot take into account the different hysteresis behavior of different materials and structural systems. As the RCB moment resisting frame utilizes semi rigid boltless connectors, the hysteresis behavior largely deviates from the perfectly elasto-plastic behavior. As a result, the force based design will not be able to predict the seismic behavior of these structures.

The current available methods for calculating ductility, which is calculated from the base shear vs. displacement curve of the structure using the ratio between ultimate to yield displacement, are also full of confusion as described by Priestley (2000) because different researchers have different calculation methods for these factors. Therefore, every different method will produce a different ductility capacity of the same structure, which is impractical. Besides, code provides a single ductility factor or force reduction factor to a particular structural system which is an unacceptable approximation because ductility capacity of the structure depends on a large range of factors such as axial load ratio, structural geometry and foundation type.

Due to large differences of the RCB structural systems with regular structures; these factors calculated using the traditional analysis method might not represent the actual energy dissipation capacity of these systems. Various structural configurations, rack height, brace configuration, and brace types and also the connector depth can have significant effect on these factors. The depth, thickness and number of tabs in a connector have great implication on the beam column moment rotation behavior and the hysteresis shape. Due to this large variation in structural

configuration and connection stiffness a single force reduction factor for all RCB structures is impractical as different configuration will have its own ductility.

On the other hand Priestley et al. (2000) suggested that a solution to the above mentioned problem can be the direct displacement based design (DDBD) procedure, which unlike force based design, uses the displacement as the key controlling factor in seismic design. In direct displacement based design the word 'direct' indicates final design with very little or no iteration (Powell 2008). Priestley (2000) showed that the strength of the structure is relatively unimportant parameter. He also showed that the force based procedure is often illogical and can provide non-uniform level of performance to the structure against earthquake.

It is clear from the design steps shown in Figure 4.2 that the force based design does not take displacement into account during the design, which is very unusual because displacement is the indicator of damage, not strength. Now a days force based design includes a displacement check at the end of the design to determine whether the displacement is within code provided limit (Priestley et al. 2007).

Priestley (2000) stated that the use of characteristic force reduction factor in seismic design results in non-uniform risk. Two buildings designed using the same code and same force reduction factor may perform completely different under a seismic event. So uniform-risk design is un-attainable using this method. Since there is a displacement check at the end of the current force based design methods, which usually govern the design, thus force reduction factor assumed at the initial stage of the design can become different than that at the final stage. Thus, the finally designed structure becomes much stiffer or flexible than the one initially designed.

Also the current seismic design codes employ capacity design principle for designing critical structural components against seismic loading. According to the capacity design principle, a structural system should possess sufficient strength, stiffness and energy dissipation capacities during large magnitude earthquakes by developing plastic hinge mechanisms in dissipative zones. However the direct application of capacity design to building based on rack systems is prevented by the limited knowledge on their possible energy dissipative zones (Bernuzzi and Castiglioni 2001).

5.3 Frame design

Initially a four storied four bay RCB frame shown in Figure 3.15 has been selected for the performance comparison. The frame has uniform span length of 2250mm and uniform story height of 1600mm except the 1767mm high first story which is little taller compared to other stories. In the first step the frame has been designed using both force based procedure and displacement based design procedure discussed in Chapter 3 and 4. The selected hazard spectrum is Vancouver response spectrum for both of the design methods. In the second step ten earthquake records have been selected for performance evaluation of the designed frames. These earthquake records were scaled to match Vancouver response spectrum for representing earthquake generated near Vancouver. In the next step nonlinear time history analyses have been carried out on these two frames and subsequently maximum roof displacement, interstory drift and residual interstory drift ratios were recorded. These data have been used to compare the performance of these two frames designed under two different methods. Similar design and analysis exercise was carried out on six, eight and ten storied frames shown in Figure 4.4 and maximum roof displacement, interstory drift and residual interstory drift ratios were recorded.

5.4 Force based design

Figure 3.21 shows the Vancouver response spectrum along the matched earthquake records. This response spectrum was used in SAP2000 (2010) software for calculating seismic base shear demand of the RCB frame. For calculating base shear, modal response spectrum analysis was used which took multiple dynamic mode shapes into consideration. Eigen vector analysis was carried out for the calculation of these mode shapes. Using the modal mass participation ratio and time period of the modes, forces for each mode was calculated and then complete quadratic combination method was used for the calculation of the design base shear demand. SAP2000 (2010) software was used for the calculation of frame forces and the members were designed as per these demand forces. During the design of the RCB frames it was found out that the initial frame configuration (collected from the documents provided by the industrial partner) was adequate in resisting code specified lateral force level except the beam-to column connectors initial stiffness and strength. For this reason the stiffness and strength of the connector was changed as per the calculated bending moment demand at beam ends.

5.5 Direct displacement based design

The author has adapted direct displacement based design for RCB frame and it has been used for the design of the frame under consideration. The developed step-by-step procedure was followed for the calculation of the demand seismic base shear force. Using the developed procedure by Priestley et al. (2007) the base shear force was distributed for each story and then the frame was analyzed using SAP2000 (2010) software and the frame forces were calculated. From the frame analysis it was found out that the beam end moments came higher than the capacity of the beam-to-column connector. For this reason the connector design was revised. So,

like force based design the beam-to-column and column-to-base plate connector required design revision. After the design the frame was analyzed using time history analysis method of ten different earthquake records similar to that used for the force based design.

5.6 Performance comparison

After the design was completed using force and direct displacement based design procedures, the frames were analyzed using ten earthquake records through non-linear dynamic time history analysis. The connector design data are shown in Table 5.1. All columns have same dimension as shown in Figure 2.6 and all beams are 50mm x 100mm x 1.5mm rectangular hollow sections. After the analysis, roof drift time history data was collected from the middle point of the roof. Also subsequent story displacements were retrieved from the model for the calculation of interstory and residual drift ratios. The maximum roof drift value comparison between force and direct displacement based designed frames are presented in Figure 5.1, Figure 5.2, Figure 5.3 and Figure 5.4 for four, six, eight and ten storied RCB frames respectively. All of these frames have a width of four bays.

Table 5.1: Beam-to-column connector design data for the designed frames

Connector Parameter	4 story 4 Bay	6 story 4 Bay	8 story 4 Bay	10 story 4 Bay
Initial Stiffness (FBD) (kN-m/radian)	98.82	115.29	125.17	125.17
Yield moment (FBD) (kN-m)	1.68	1.96	2.13	2.13
Initial Stiffness (DDBD) (kN-m/radian)	131.76	197.65	214.12	263.53
Yield moment (DDBD) (kN-m)	2.24	3.36	3.64	4.48

Figure 3.21 shows ten earthquake records but not all of their results are presented for roof drift, maximum and residual interstory drift ratio calculation. For some earthquake records the only force-based designed RCB frame became unstable during the time history analysis (e.g.

Sakaria and Kocaeli earthquake records) and for some other records both force and displacement based designed frame became unstable. But it was found out that the force based designed frame became unstable for more cases compared to the displacement based designed frames. It can be seen from Figure 5.1 that for different earthquake records the roof drift varies quite significantly that range from approximately 142mm to 401mm for force based design and 151mm to 271mm for displacement-based design. The average roof drift value was 243mm for force based design which is approximately 3.7% of the story height contrary to 201mm i.e. 3.05% achieved from the displacement based design. Similar trend can be observed in Figure 5.2 where for most of the earthquake records the displacement based designed frame showed lower displacement. But this trend is not observed for eight and ten storied frames. For eight storied frames roof displacement values shown in Figure 5.3 it can be observed that the values are almost similar for both force and displacement based designed frames. For Kocaeli and Sakaria earthquake records the force based designed frame became unstable so displacement based designed frame is a better performer in case of eight storied frame as it was able remain stable for all earthquake records. For ten storied frame it has been found out that the force based designed frame outperformed the displacement based designed frame by a little margin for eight out of nine earthquake records. Both of the force and displacement based designed frames became unstable under Kocaeli earthquake record's time history analysis.

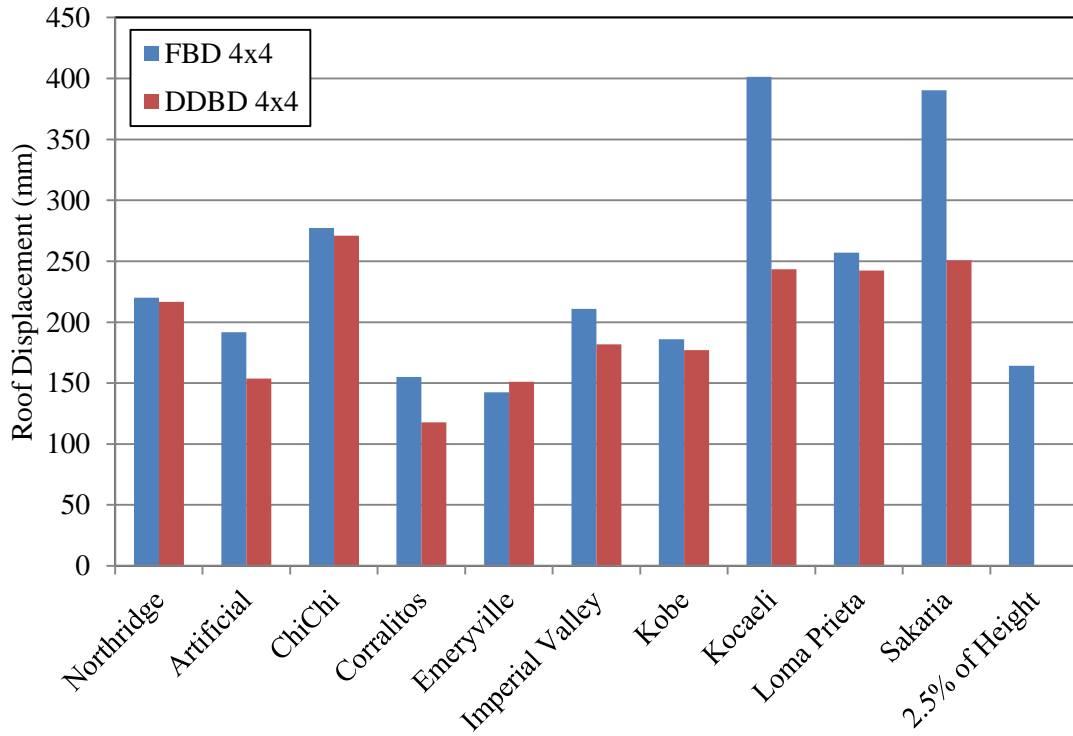


Figure 5.1: Roof drift of the four storied RCB frame from NLTHA

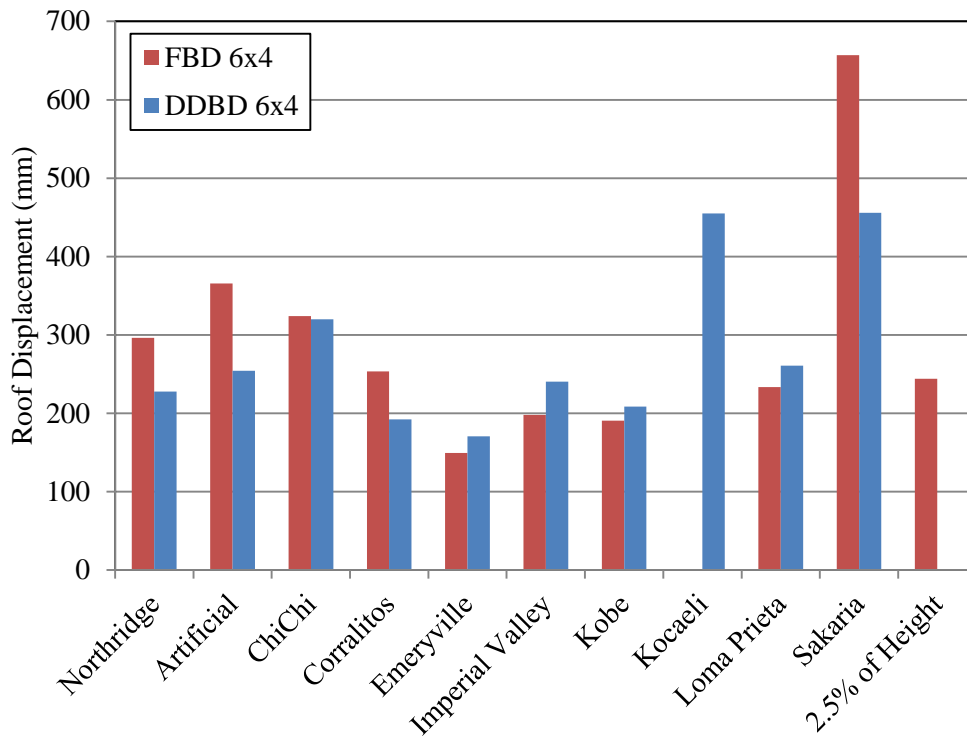


Figure 5.2: Roof drift of the six storied RCB frame from NLTHA

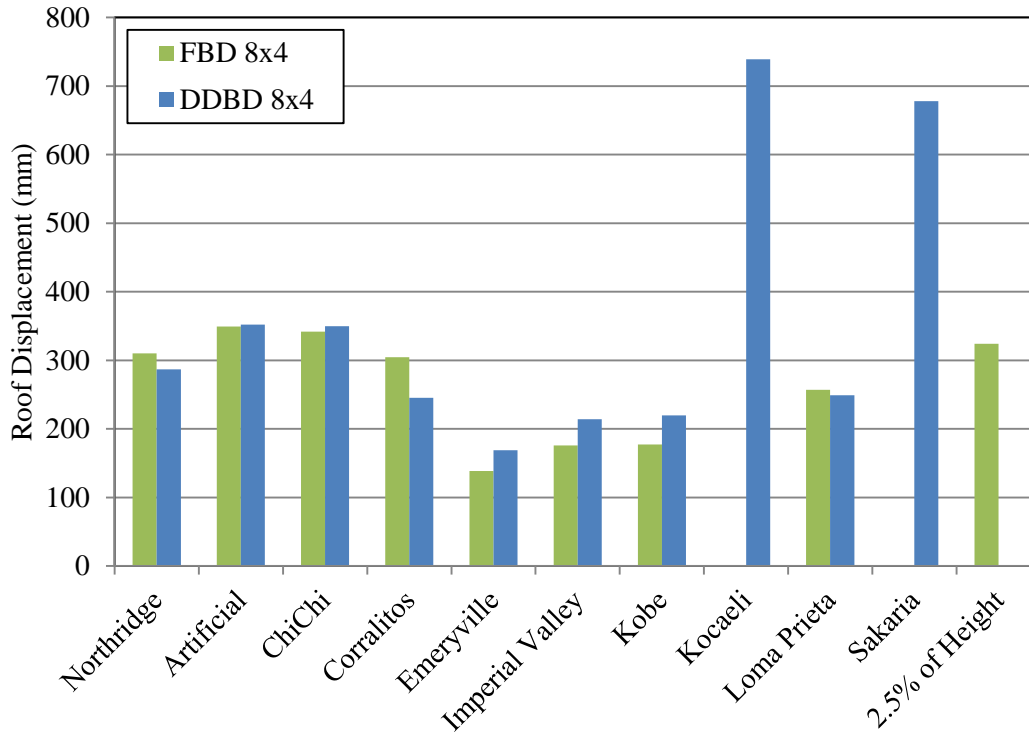


Figure 5.3: Roof drift of the eight storied RCB frame from NLTHA

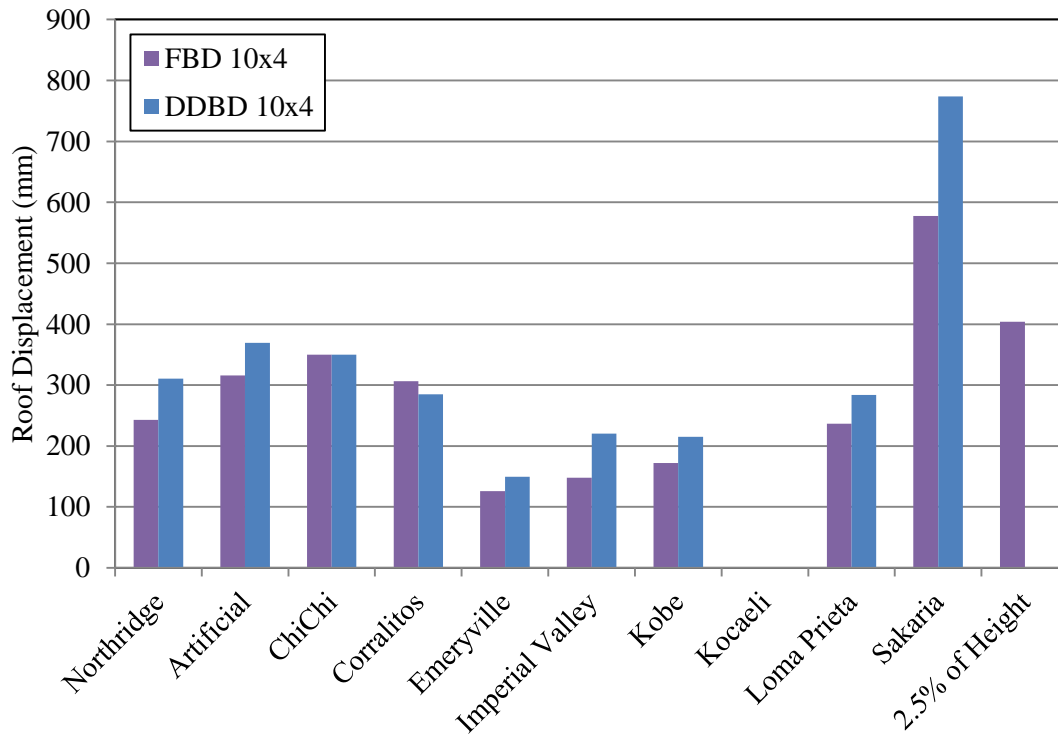


Figure 5.4: Roof drift of the ten storied RCB frame from NLTHA

On the other hand, Figure 5.5 to Figure 5.12 show the maximum and residual interstory drift ratio respectively for four, six, eight and ten storied RCB frame designed under force and displacement based design methods. From these comparative figures it can be observed that although the maximum interstory drift ratio values are very high, the residual interstory drift ratio came low for both force and displacement based design methods. From these figures it can be observed that the maximum interstory drift ratio observed for the frame designed under displacement-based design procedure came lower than that of the force-based design for four and six storied frame but for eight storied frame they are almost similar and for ten storied frame the force based designed frame shows somewhat lower interstory drift ratio compared to displacement based designed frame.

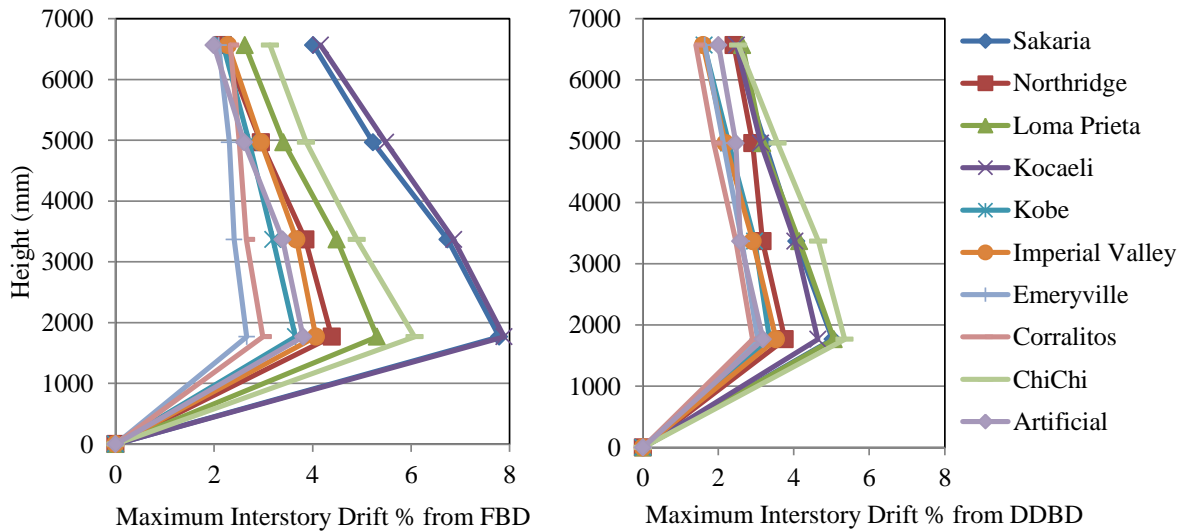


Figure 5.5: Maximum interstory drift ratio of the four storied RCB frame designed using FBD and DDBD methods

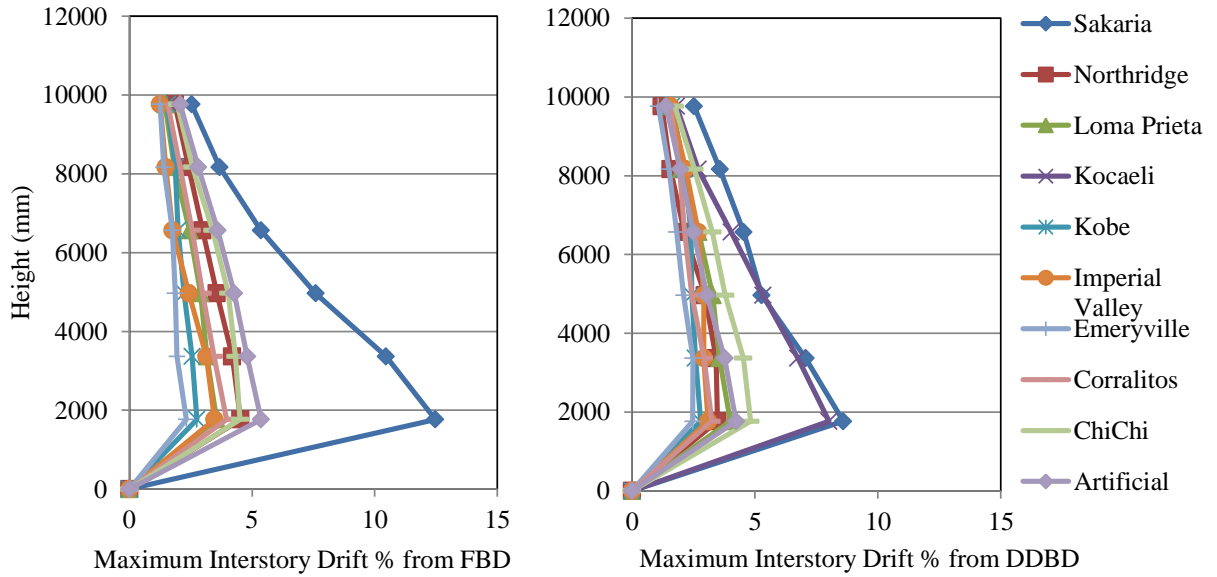


Figure 5.6: Maximum interstory drift ratio of the six storied RCB frame designed using FBD and DDBD methods

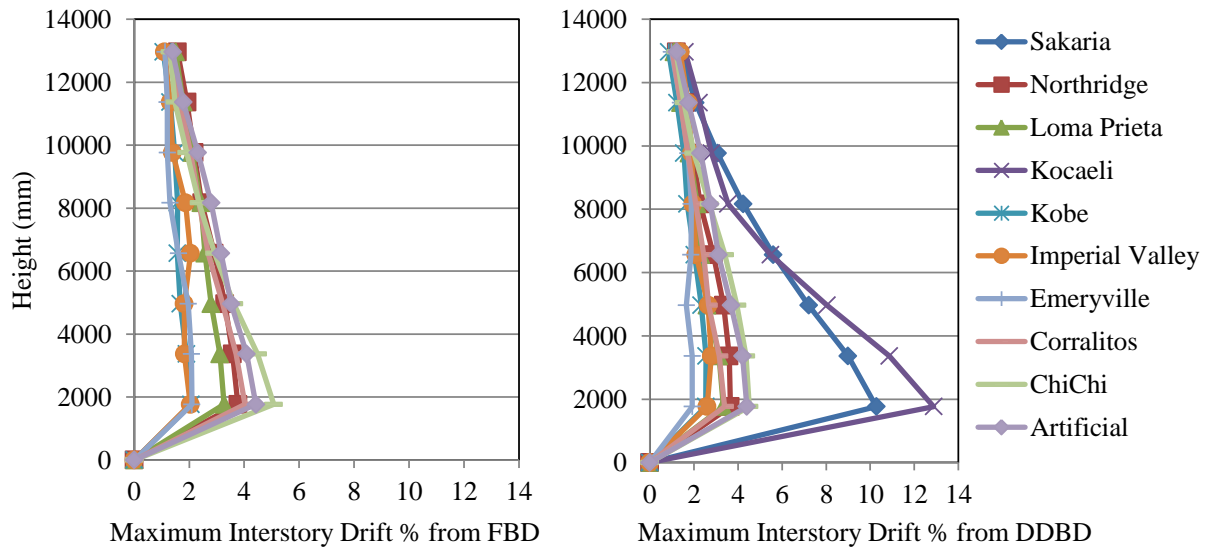


Figure 5.7: Maximum interstory drift ratio of the eight storied RCB frame designed using FBD and DDBD methods

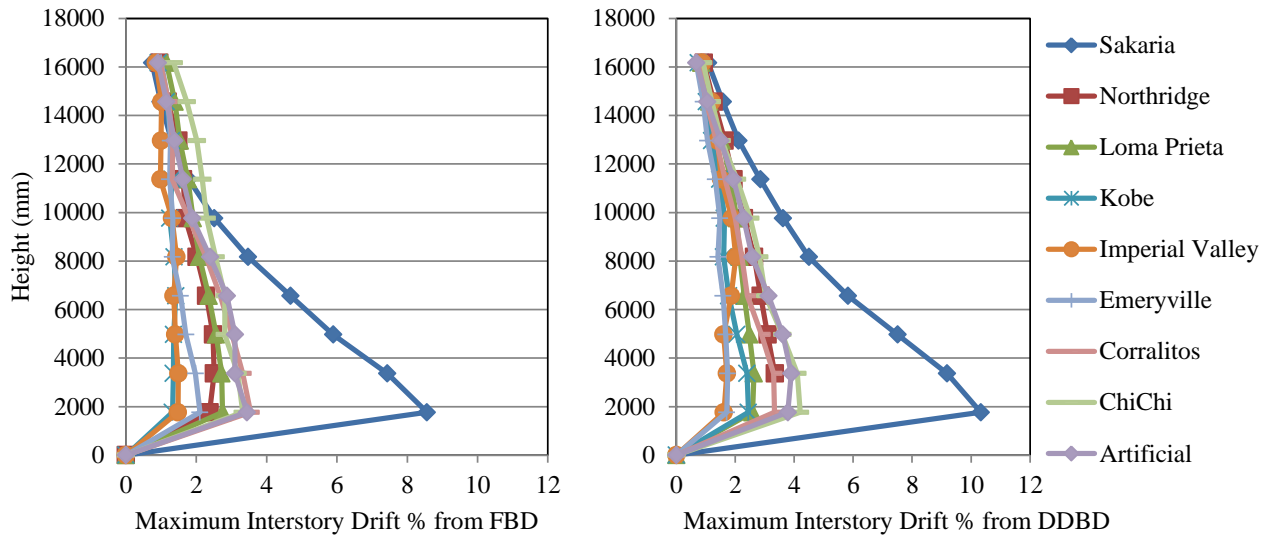


Figure 5.8: Maximum interstory drift ratio of the ten storied RCB frame designed using FBD and DDBD methods

Figure 5.9 to Figure 5.12 shows the residual interstory drift ratio of the force and displacement based designed frames. It can be observed that the residual interstory drift ratio came almost one fourth to half times of the maximum interstory drift values for both displacement and force based designed frames. As residual interstory drift ratio represents the residual damage of the structure, a lower value suggests better performance under seismic loading condition. Similar trend compared to maximum interstory drift ratio is observed for residual interstory drift ratio. For both four and six storied frames the displacement based design showed lower interstory drift and displacement based designed frame was able to withstand all ten earthquake record without being unstable unlike force based design which became unstable under Kocaeli earthquake record for six storied frame. Also for eight storied RCB frame the displacement based designed frame was stable for all ten earthquake records but the force based designed frame became unstable for Kocaeli and Sakaria records. In case of ten storied frame both force and direct displacement based designed frames became unstable under Kocaeli earthquake record. For the remaining nine earthquake records the displacement based designed

frame showed lower residual interstory drift ratio compared to the other. For force based designed frame the maximum residual interstory drift came 7.86% which is much higher than the maximum residual drift observed (2.75%) for displacement based designed frame.

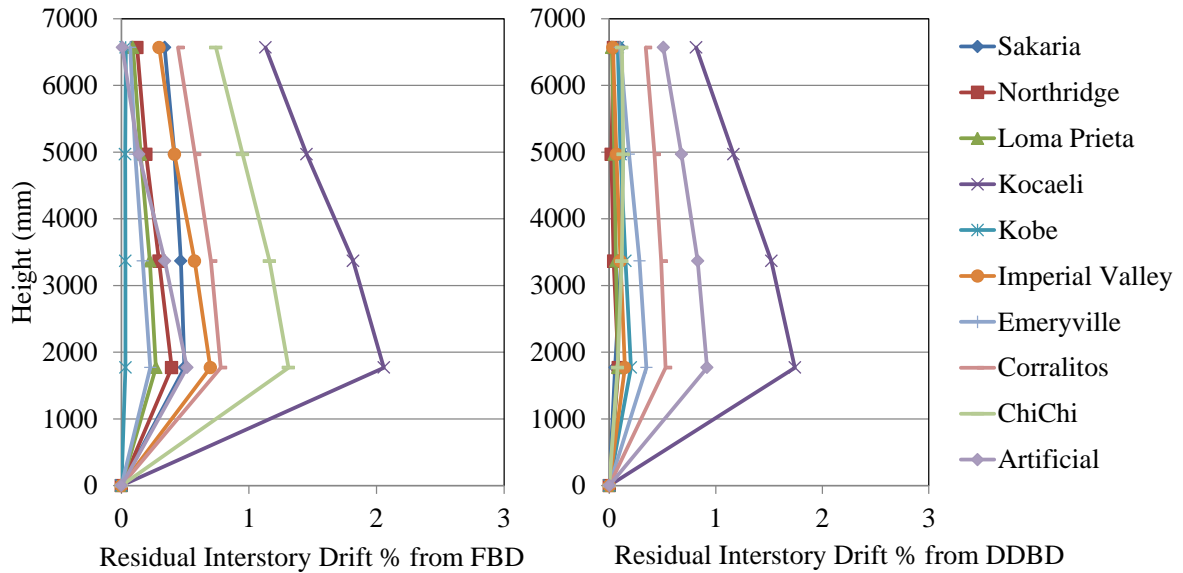


Figure 5.9: Residual interstory drift ratio of the four storied RCB frame designed using FBD and DDBD methods

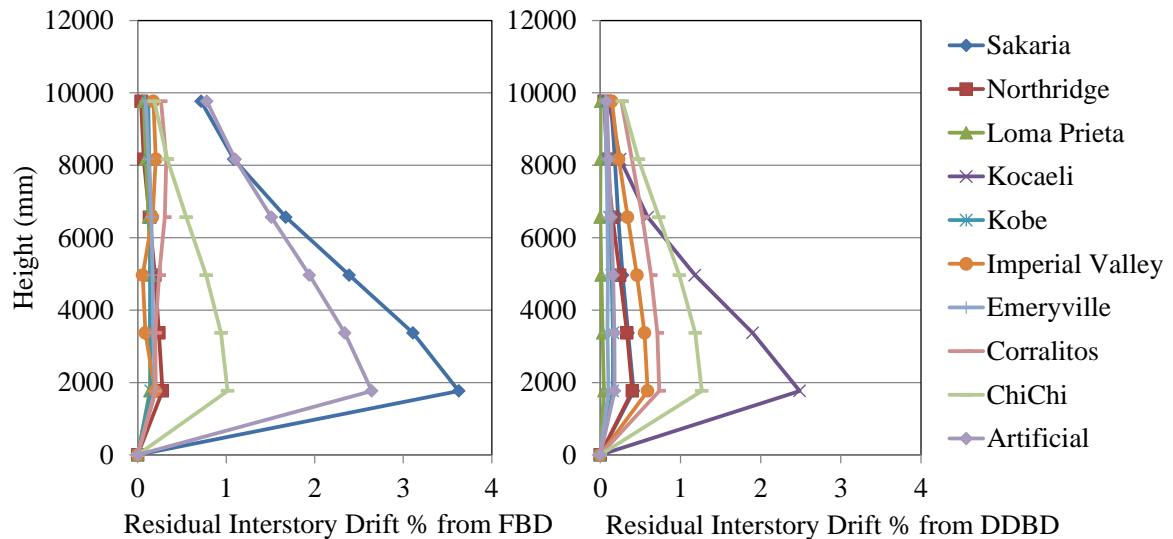


Figure 5.10: Residual interstory drift ratio of the six storied RCB frame designed using FBD and DDBD methods

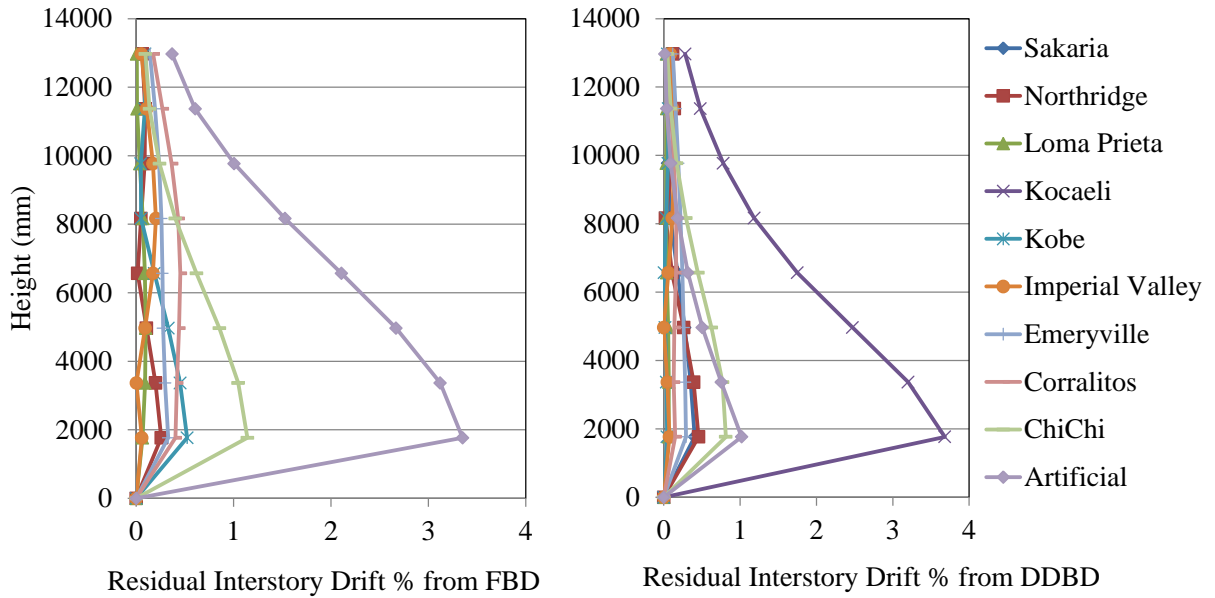


Figure 5.11: Residual interstory drift ratio of the eight storied RCB frame designed using FBD and DDBD methods

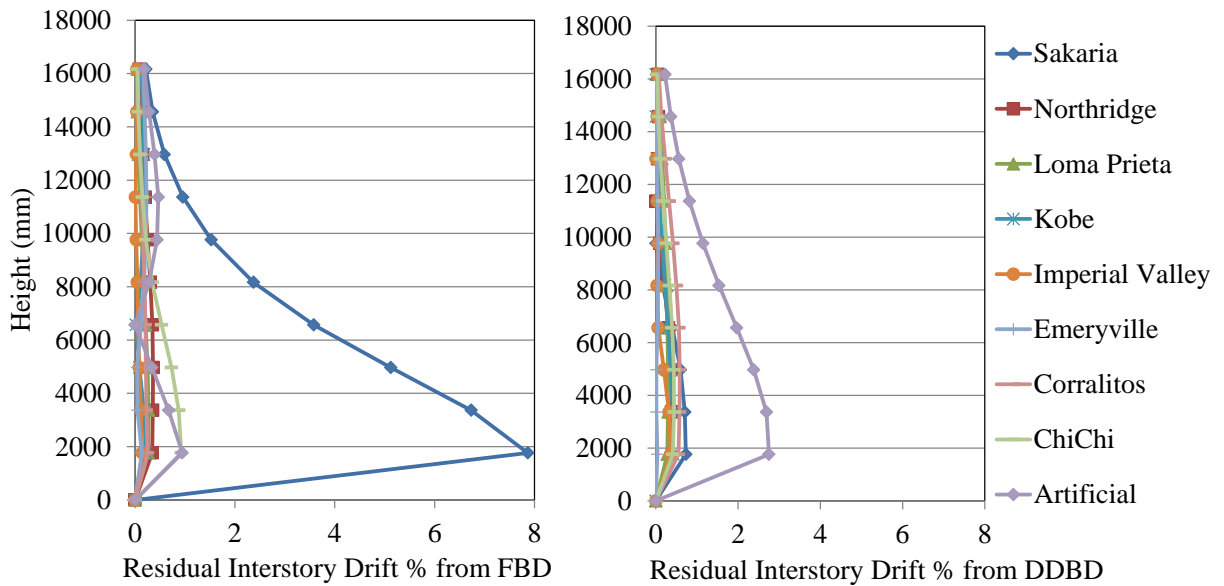


Figure 5.12: Residual interstory drift ratio of the ten storied RCB frame designed using FBD and DDBD methods

5.7 Summary

Four frames were chosen for the comparative study of the force and displacement based design procedures adapted for RCB structural system. These frames have been designed using

these two methods and modeled in finite element (FE) software for element force calculation. From these forces the frames were designed and finally analyzed using ten different earthquake records which were matched with Vancouver soil class “C” response spectrum. It was found out that for most of the frames designed using displacement based design procedure performed particularly well against seismic loading in the areas of maximum roof, interstory and residual interstory drift ratios. These ratios came smaller than those of the force based designed frame in majority of the cases. Although force based designed frame showed slightly better performance in case of ten storied RCB frame, it can be seen from the roof drift comparison (Figure 5.4) that displacement based designed frames displacements are lower than the code drift limit for which it is designed for, which means it performed as per design. As lower drift ratios signifies lower damage it may be concluded that the frame designed using displacement based design process can perform better compared to the counterpart under seismic loading condition.

CHAPTER 6: CONCLUSIONS

6.1 Summary

Seismic design codes warrant that during earthquakes structural members and systems will behave in a ductile manner and dissipate adequate amount of energy through cyclic load reversal of the energy dissipative zones. This type of behavior ensures occupant safety and economy of construction. Since no prior seismic design guideline exists for Rack Clad Building (RCB) structures, this thesis is an initial effort in providing such a guideline for RCB structures. A literature review on RCB structural elements and its framing system has also been carried out in this thesis.

The author has carried out research in the areas of force and direct displacement-based seismic design and provided the required equations, parameter values and figures for designing RCB structures. In the case of force-based design the most important parameters are overstrength and force reduction factor. Author has carried out pushover and incremental dynamic time history analysis on several RCB frames and calculated the values of these parameters. The proposed values of overstrength and ductility factors are 2.06 and 1.05, respectively. This study also presents ductility vs. damping relationship for RCB frames and also provides an equation for calculating the yield displacement of these frames. Using the yield displacement equation, ductility-damping relationship and direct displacement-based design method, structural design practitioners can systematically design RCB moment resisting frames.

This study also presents the performance comparison of RCB frames designed under force and direct displacement-based design methods. It was observed that the direct displacement-

based designed frame outperformed the counterpart in most of the performance checks e.g. roof, interstory and residual interstory drift ratios. As force-based design (FBD) is common in current building codes and can be carried out by the use of computer software, the design practitioners are more inclined to use this method although it seems less safe compared to that of DDBD. This study advocates structural engineers in choosing DDBD over FBD method while designing RCB frame structures in seismic regions.

6.2 Limitations of this study

The limitations of this study are as follows:

1. Only one hysteresis shape has been considered in this study.
2. Only down-isle direction moment resisting frame has been considered.
3. Only two dimensional frames have been considered.
4. No experimental investigation has been carried out for the RCB frame elements.
5. Only ten earthquake records have been used for incremental dynamic time history and nonlinear time history analysis.
6. Beam-to-column connector hysteresis has been used for column-to-base plate connection.

6.3 Conclusion

The following conclusions can be drawn from this study

1. RCB moment resisting frames are much more flexible than the traditional steel moment resisting frames. As a result, they have higher fundamental period, which significantly lower their spectral acceleration demand from the response spectrum

- analysis compared to those of traditional steel structures. Also due to this high flexibility, RCB moment resisting frames sway in large magnitude compared to those of their traditional counterparts.
2. RCB moment resisting frames experience much larger displacements under seismic loading conditions. Their interstory drift ratio was observed more than two times than that of traditional steel structures.
 3. For tall RCB frames the design moment for beam-to-column connectors can be much higher than the practical capacity of the connectors. For these tall frames it is not possible to resist seismic loading only by semi-rigid connectors. For this case, bracings are necessary.
 4. Although the interstory drift ratios of RCB moment resisting frames are high, the residual interstory drift is much lower.
 5. The direct displacement-based design produces somewhat stiffer RCB frame design compared to force-based design, which results in better seismic performance compared to force based design.

6.4 Recommendations for future research

The RCB structural system is highly complex as it employs two different framing systems in its two orthogonal directions and also a large number of structural configurations are also possible depending upon the combination of braces and moment resisting frames. For this reason more research is necessary for the development of a complete seismic design guideline. Following are some of the areas that the author wishes to work on in his future studies.

1. Displacement and force-based design for down-isle braced frame: It was observed from some trial designs (Chapter 3.10) of RCB structures with different heights that the seismic design base shear force drastically increases with the increase in Story height. So, designing tall RCB structures using thin walled perforated sections and teardrop connector against this large base shear can be difficult. So, it becomes necessary to use braces to reduce the displacement demand. A study should be carried out to provide a displacement and force-based design guideline for RCB braced frame.
2. Force-based design in the cross isle direction: Cross isle direction only employs braced frames which are connected by spacer bars. The structure is much more brittle in this direction. So it is necessary to suggest overstrength and force reduction factor in the cross isle directions with bracings.
3. A more general ductility damping relationship: In this study only one ductility damping relationship has been established for a single connector hysteresis although it represents the general shape of the connector hysteresis. For an accurate real world application more ductility damping relationship is necessary depending on connector depth, beam height, column dimension and material properties etc. Moment-rotation analysis should be carried out for different types of beam-end connectors and using these data several ductility-damping curves should be generated for a broader spectrum of hysteresis shapes.
4. Improvement of the developed DDBD method: Modification of design equation is necessary for taking into account the extra base shear force which generates from P- Δ effect.

5. SAP2000 v14.2.3 (2010) software uses initial stiffness instead of tangent stiffness for stiffness proportional damping calculation for its Rayleigh damping model during dynamic analysis. By this method the damping forces calculated after yielding of the joints can be come much higher compared to the actual situation. This can produce wrong impression of the frame performance. In future research a more realistic damping force calculation from tangent stiffness should be carried out possibly with other dynamic analysis software package.

REFERENCES

- Abrahamson, N.A. (1992). "Non-stationary spectral matching," *Seismological Research Letters*, 63(1), 30.
- Affolter, C., Piskoty, G., Wullschleger, L., and Weisse, B. (2009). "Collapse of a high storage rack." *Engineering Failure Analysis*, 16(6), 1846-1855.
- Aguirre, C. (2005). "Seismic behavior of rack structures." *Journal of Constructional Steel Research*, 61(5), 607-624.
- Alavi, B., and Gupta, A. (2008). "Performance-Based Seismic Design of an Industrial Storage Rack System." *Crossing Borders*, Asce, pp. 1-10.
- Alhan, C., and Gavin, H.P. (2005). "Reliability of base isolation for the protection of critical equipment from earthquake hazards." *Engineering Structures*, 27(9), 1435–1449.
- Annan, C., Youssef, M., and El Naggar, M. (2009). "Seismic Overstrength in Braced Frames of Modular Steel Buildings." *Journal of Earthquake Engineering*, 13(1), 1–21.
- Applied Technology Council. (1985). "Tentative Provisions for the Development of Seismic Regulations for Buildings." ATC-3-06, Redwood City, CA.
- Applied Technology Council. (1995). "Structural Response Modification Factors." ATC-19, Redwood City, CA.
- Applied Technology Council. (1995). "A Critical Review of Current Approaches to Earthquake-Resistant Design." ATC-34, Redwood City, CA.
- AR Storage Solutions. (2012). "Clad Rack Building." <http://www.ar-storage.com/index.php?option=com_content&task=view&id=200&Itemid=326&lang=en> (March 20, 2012)
- Asgarian, B., and Shokrgozar, H. R. (2009). "BRBF response modification factor." *Journal of Constructional Steel Research*, 65(2): 290-298.

- Baldassino, N. and Bernuzzi, C. (2000). "Analysis and behaviour of steel storage pallet racks." *Thin-Walled Structures*, 37(4), 277-304.
- Baldassino, N., Bernuzzi, C., Zandonini, R. (n.d.). "Performance of joints in steel storage pallet racks."
<<http://courseweb.xu.edu.ph/courses/ics100/ENG/AISC%20Code/Special%20Connections/382.pdf>> (October 25, 2011]
- Bajoria, K. M., Sangle, K. K., and Talicotti, R. S. (2010). "Modal analysis of cold-formed pallet rack structures with semi-rigid connections." *Journal of Constructional Steel Research*, 66(3), 428-441.
- Beattie, G.J., (2006). "A Design Guide for High Level Storage Racking with Public Access." NZSEE Conference, Paper no. 40, 8p.
- Bernuzzi, C., Chesi, C., and Parisi, M. A. (1989). "Seismic behaviour and design of steel storage racks." *13th world conference on earthquake engineering*, 18(1), 141-143.
- Bernuzzi, C. and Castiglioni, C.A. (2001). "Experimental analysis on the cyclic behaviour of beam-to-column joints in steel storage pallet racks." *Thin-Walled Structures*, 39(10), 841-859.
- Canadian Standards Association CSA. (2001). "Limit states design of steel structures." CAN/CSAS16.1- 01, Rexdale, Ontario, Canada.
- Casafont, M., Pastor, M.M., Roure, F., and Peköz, T. (2011). "An experimental investigation of distortional buckling of steel storage rack columns." *Thin-Walled Structures*, 49(8), 933-946.
- Castiglioni, C. A., Calado, L., (1996). "Comparison of two cumulative damage approaches for the assessment of behaviour factor for low-rise steel buildings." *Journal of Constructional Steel Research*, 40(1), 39-61.

- Castiglioni, C. A., Carydis, p., Negro, P., Calado, L., Degee, H., and Rosie, I. (2009). "Seismic behaviour of steel storage racking systems." *Proceedings of the STESSA 2009 Conference*, pp.757-764.
- Comite Europeen de Normalisation (CEN). (2004). "Eurocode 8 earthquake resistant design of structures, part 1-1 — General rules and rules for buildings." Brussels, Belgium
- Chen, C., Scholl, R., and Blume, J., (1980). "Earthquake simulation tests of industrial steel storage racks." *Proceedings of the Seventh World Conference on Earthquake Engineering, Istanbul, Turkey*, 379–386.
- Chesi, C., Parisi, M. A., (1999). "Recent developments and perspectives for the seismic design code in Europe." *Proceedings of the XVII Italian Conference on Steel Structures*, 2,189–96.
- Davies, M. and Jiang, C. (1998). "Design for Distorsional Buckling." *Journal of Constructional Steel Research*, 46(1-3), 174-175
- Dowell, R. K., Seible, F., and Wilson, E. L. (1999). "Pivot Hysteresis Model for Reinforced Concrete Members." *Aci Structural Journal*, (95), 607-617.
- Dwairi, H., Kowalsky, M., and Nau, J. M. (2007). "Equivalent damping in support of direct displacement-based design." *Journal of Earthquake Engineering*, 11(4), 512–530. Taylor & Francis.
- Elnashai, A. S., and Mwafy, A. M. (2002). "Overstrength and force reduction factors of multistory reinforced-concrete buildings." *The Structural Design of Tall Buildings*, 11(5), 329-351.
- European Committee for Standardization (CEN). (2009). "Steel static storage systems – Adjustable pallet racking systems – Principles for structural design." EN 15512. Brussels ,Belgium.

- European Racking Federation. (2005). "Recommendations for the design of static steel pallet racks under seismic conditions." prFEM 10.2.08. Birmingham.
- Fédération Européenne de la Manutention (FEM). (1998). "Section X—Recommendations for the design of steel static pallet racking and shelving." FEM, Brussels, Belgium.
- Federal Emergency Management Agency (FEMA). (1997). "NEHRP provisions for the seismic rehabilitation of buildings." FEMA273 (Guidelines) and FEMA274 (Commentary). Department of Homeland Security, Washington, DC.
- Federal Emergency Management Agency (FEMA), (2000). "Prestandard and Commentary for the Seismic Rehabilitation of Buildings." FEMA356, Department of Homeland Security, Washington, D.C.
- Federal Emergency Management Agency (FEMA), (2004). "The 2003 NEHRP Recommended Provisions for New Buildings and Other Structures—Part 1: Provisions." FEMA450, Department of Homeland Security, Washington, D.C.
- Federal Emergency Management Agency (FEMA), (2005). "Seismic Considerations for Steel Storage Racks Located in Areas Accessible to the Public," FEMA460, Department of Homeland Security, Washington, D.C.
- Filiatrault, A., Bachman, R. E., and Mahoney, M. G., (2006a). "Performance-Based Seismic Design of Pallet-Type Steel Storage Racks." *Earthquake Spectra*, 22(1), 47-64.
- Filiatrault, A., Higgins, P. S., and Wanitkorkul, A. (2006b). "Experimental Stiffness and Seismic Response of Pallet-Type Steel Storage Rack Connectors." *Practice Periodical on Structural Design and Construction*, 11(3), 161.
- Filiatrault, A., Higgins, P. S., Wanitkorkul, A., and Courtwright, J. (2007). "Experimental Stiffness of Pallet-Type Steel Storage Rack Teardrop Connectors." *Practice Periodical on Structural Design and Construction*, 12(4), 210-215.

- Filiatrault, A., Higgins, P. S., Wanitkorkul, A., Courtwright, J. A., and Michael, R. (2008). "Experimental Seismic Response of Base Isolated Pallet-Type Steel Storage Racks." *Earthquake Spectra*, 24(3), 617-639.
- Frazier Industrial. (n.d). "Pre-Engineered Solution." <<http://www.frazier.com/Pre-Engineered-Solutions.asp>> (Dec 14, 2011)
- Freitas, a, Freitas, M., and Souza, F. (2005). "Analysis of steel storage rack columns." *Journal of Constructional Steel Research*, 61(8), 1135-1146.
- Freitas, A.M.S., Souza, F.T., Freitas, S.R. (2010). "Analysis and behavior of steel storage drive-in racks." *Thin-Walled Structures*, 48(2),110–117.
- Gilbert, B. P., and Rasmussen, K. J. R. (2010). "Bolted moment connections in drive-in and drive-through steel storage racks." *Journal of Constructional Steel Research*, 66(6), 755-766. Elsevier Ltd.
- Godley, M.H.R. (1991). "Storage Racking, chapter 1, Design of Cold Formed Steel Members." Rhodes ed. Elsevier Applied Science, London, UK, 361-399.
- Godley, M.H.R. (1997). "Plastic design of pallet rack beams." *Thin-Walled Structures*, 29(1–4), 175–188.
- Ghobarah, A. (2001). "Performance-based design in earthquake engineering: state of development." *Engineering Structures*, 23(8), 878-884.
- Hancock, G.J. (1985). "Distortional Buckling of Steel Storage Rack Columns." *Journal of Structural Engineering*, ASCE, 111(12), 2770-2783.
- Hancock, J., Watson-Lamprey, J., Abrahamson, N.A., Bommer, J.J., Markatis, A., McCoy, E., Mendis, R. (2006). "An improved method of matching response spectra of recorded earthquake ground motion using wavelets." *Journal of Earthquake Engineering*, 10, 67–89.

- Kilar, V., Petrovic, S., Koren, D., and Silih, S. (2011). "Seismic analysis of an asymmetric fixed base and base-isolated high-rack steel structure." *Engineering Structures*. In press.
- Kim, J., and Choi, H. (2005). "Response modification factors of chevron-braced frames." *Engineering Structures*, 27(2), 285-300.
- Lai, S.P. and Biggs, J.M.(1980). "Inelastic Response Spectra for Aseismic Building Design." *Journal of Structural Engineering*, ASCE., 106(6).
- Lee, L.H., Han, S.W., and OH, Y.H. (1999). "Determination of ductility factor considering different hysteretic models." *Earthquake engineering & structural dynamics*, 28(9), 957-977.
- Markazi, F.D., Beale, R.G. and Godley, M.H.R. (1997). "Experimental Analysis of Semi- Rigid Boltless Connectors." *Thin-Walled Structures*, 28(1), 57-87
- Mitchell, D. and Paulter, P. (1994). "Ductility and overstrength in seismic design of reinforced concrete structures." *Canadian Journal of Civil Engineering*, 21, 1049–1060.
- Mwafy AM. (2000). "Seismic Performance of Code-designed RC Buildings." PhD thesis, Imperial College, London
- Mwafy, A.M., and Elnashai, A.S., (2001). "Calibration of Force Reduction Factors of RC Buildings." *Journal of Earthquake Engineering*, 6(2), 239-273.
- National Research Council of Canada (NRCC). (2005). "National building code of Canada." Ottawa, Ontario.
- Ng, A.L.Y., Beale, R.G., Godley, M.H.R. (2009). "Methods of restraining progressive collapse in rack structures." *Engineering Structures*, 31(7),1460–1468.
- Park R. (1996). "Explicit incorporation of element and structure overstrength in the design process." In Proceedings 11th WCEE. IAEE, Acapulco, Mexico. Paper 2130.

- Paulay T, Priestley MJN. (1992). “Seismic Design of Reinforced Concrete and Masonry Buildings.” John Wiley, New York.
- Powell, G. H. (2008). “Displacement-based seismic design of structures.” *Earthquake Spectra*, 24(2), 555-557.
- Prabha, P., Marimuthu, V., Saravanan, M., and Arul Jayachandran, S. (2010). “Evaluation of connection flexibility in cold formed steel racks.” *Journal of Constructional Steel Research*, 66(7): 863-872.
- Priestley, M. J. N., (2000). “Performance based seismic design.” *Bulletin of the New Zealand Society for Earthquake Engineering*, 33(3), 325–346.
- Priestley, M., and Grant, D. (2005). “Viscous damping in seismic design and analysis.” *Journal of Earthquake Engineering*, 9(2): 229–255.
- Priestley, M. J. N., Calvi, G. M., and Kowalski, M. J., (2007). “Displacement-based seismic design of structures.” IUSS press, Pavia.
- Rack Manufacturers Institute RMI. (2008). “Specification for The Design, Testing, and Utilization of Industrial Steel Storage Racks.” Charlotte, NC.
- Riddell, R., Hidalgo, P. and Cruz, E. (1989). “Response Modification Factors for Earthquake Resistant Design of Short Period Structures.” *Earthquake Spectra*, 5(3).
- Temesist Rack and Storage Systems. (2011). ”Rack Clad Buildings.” < <http://www.temesist-raf.com/en/about.html>> (November 20, 2011).
- SAP2000. (2010). “SAP2000 Integrated Software for Structural Analysis and Design.” Analysis Reference Manual, Computers and Structures Inc. Berkeley, California, U.S.A.
- Saar Lagertechnik GmbH. (2010). “XL Pallet Racking.” <www.saar-lagertechnik.com/download/XL-Pallet-Racking.pdf> (October 10, 2010).

SeismoMatch. (2011). "A program for adjusting earthquake records, through wavelet addition, to match a specific target response spectrum." Seismosoft, Pavia, Italy.

Sideris, P., Filiatrault, A., Leclerc, M., and Tremblay, R. (2010). "Experimental investigation on the seismic behavior of palletized merchandise in steel storage racks." *Earthquake Spectra*, 26(1):209–33.

Standards Australia. (1993). "Steel storage racking." AS 4084. Sydney, Australia.

Uang, C.M. (1991). "Establishing R (or R_w) and Cd factors for building seismic provisions." *ASCE Journal of Structural Engineering*, 117(1), 19–28.

APPENDICES

Appendix A: Incremental dynamic analysis output

Some sample calculation for incremental dynamic analysis of four storied by four bay RCB frame is shown in Table A.1, Table A.2, Table A.3 and Table A.4. The detail of the frame is shown in Figure 3.15. For the analysis of this frame the chosen joint hysteresis backbone has the same initial and post elastic stiffness as that of the original data collected from Beattie (2006) shown in Figure 2.4. For six, eight and ten storied frame the backbone curve was revised based on design moment demand. The first column of the above mentioned tables show the scaling factor for the corresponding earthquake record and the remaining two columns show the roof displacement and base shear force calculated from the collapse analysis using that earthquake record.

Table A.1: Incremental dynamic analysis data for Northridge earthquake

Scale factor	Displacement (mm)	Base Shear (kN)
0	0.0	0.00
0.05	9.3	0.51
0.1	18.5	1.02
0.2	37.3	1.93
0.4	81.0	3.45
0.6	124.7	5.15
0.8	170.6	6.46
1	127.2	7.98
1.2	146.7	8.87
1.4	122.8	8.95
1.6	374.6	8.43
1.8	324.0	9.62
1.82	437.0	8.60

Table A.2: Incremental dynamic analysis data for Kobe earthquake

Scale factor	Displacement (mm)	Base Shear (kN)
0	0	0
0.1	18.17941	1.28553
0.2	32.51382	2.19026
0.4	43.35812	3.25423
0.6	101.41142	4.352
0.8	68.34974	5.49301
1	83.355	6.45927
1.2	101.79838	7.41465
1.4	121.70148	8.30478
1.6	142.03594	9.10489
1.8	163.16192	9.90526
2	184.89189	10.58705
2.2	206.37287	11.26103
2.4	228.03336	11.78677
2.6	250.08274	12.31571
2.8	272.66847	12.78202
3	295.66032	13.17665
3.2	319.07735	13.54903
3.4	334.01774	13.96377

Table A.3: Incremental dynamic analysis data for Emeryville earthquake

Scale factor	Displacement (mm)	Base Shear (kN)
0	0	0
0.1	12.82	0.94
0.5	59.86	3.8
1	107	6.34
1.5	98.98	8.465
2	146.7	10.75
2.5	192.6	12.38
3	239	13.8
3.5	280.7	15.16

Table A.4: Incremental dynamic analysis data for Loma Prieta earthquake

Scale factor	Displacement (mm)	Base Shear (kN)
0	0	0
0.1	24	1.325
0.25	58.01	2.736
0.5	108.1	4.277
0.75	147	5.646
1	170.6	6.407
1.5	165.6	7.1
2	269.7	8.744
2.2	374.9	10.09
2.4	438	11.83

Table A.5 shows detail data from incremental dynamic analysis for all four RCB frame. This table also shows the idealized and elastic base shear forces which were used to calculate the force reduction factor values shown in Table A.6.

Table A.5: Idealized (V_y) and elastic (V_e) base shear values from IDA

EQ Record Name	4 Story		6 Story		8 Story		10 Story	
	V_y	V_e	V_y	V_e	V_y	V_e	V_y	V_e
Northridge	8.60	19.11	9.14	37.20	10.14	18.36	9.124	15.05
Artificial	12.71	32.94	10.44	30.40	12.23	16.67	11.56	16.02
ChiChi	8.45	31.30	8.22	25.59	9.16	10.49	6.832	11.16
Corralitos	11.10	25.33	8.77	14.83	9.44	17.35	7.331	12.98
Emeryville	15.03	32.32	11.12	24.43	9.23	13.60	6.682	9.352
Imperial Valley	10.02	21.43	15.00	29.91	10.25	10.96	7.25	7.85
Kobe	13.96	31.11	10.31	24.75	8.71	15.66	6.971	14.39
Kocaeli	8.80	15.35	6.86	14.64	4.39	11.37	3.343	5.961
Loma Prieta	10.77	31.44	11.12	18.37	7.30	10.99	7.716	9.308
Sakaria	8.07	30.51	7.86	21.29	5.44	10.36	4.743	6.467

Table A.6: Force reduction factor (R_d) values from incremental dynamic analysis

EQ Record Name	Force Reduction Factor (Rd)			
	4 Storied	6 Storied	8 Storied	10 Storied
Northridge	2.22	4.07	1.81	1.65
Artificial	2.59	2.91	1.36	1.39
ChiChi	3.70	3.11	1.15	1.63
Corralitos	2.28	1.69	1.84	1.77
Emeryville	2.15	2.20	1.47	1.40
Imperial Valley	2.14	1.99	1.07	1.08
Kobe	2.23	2.40	1.80	2.06
Kocaeli	1.74	2.14	2.59	1.78
Loma Prieta	2.92	1.65	1.51	1.21
Sakaria	3.78	2.71	1.90	1.36
Average	2.58	2.49	1.65	1.53
Standard Deviation	0.65	0.70	0.42	0.28

Appendix B: Screenshots of the DDBD spreadsheet

Figure B.1, Figure B.2 and Figure B.3 show the screen shots of the developed spreadsheet for direct displacement based design of rack clad buildings which was used in this study for the design exercise.

Input		
Description	Value	Unit
Length of Beam C/C, L_b	2.25	m
Depth of Beam, h_b	0.1	m
width of the beam	0.05	m
Beam thickness, t	0.0015	m
No of storeys, n	4	Nos
Storey height, h_i	1.6	m
Bottom Storey height, h_1	1.77	m
E_s	2.00E+11	N/m ²
Yield moment of the connector, M_{ey}	2.24E+03	N-m
Yield stiffness of the connector, k_{ey}	131764	N-m/rad
Seismic gravity load on the beam per meter, w	2370	N/m
Code/Target drift limit, θ_c	0.025	rad
Column dimension in direction of load, h_c	0.11	m
No of column lines in direction of seismic load	5	nos
Equivalent Viscous damping, ζ	5.40	%
Effective time period, T_e	1.44	sec

Figure B.1: Input data table of the excel spreadsheet

Calculation		
Description	Value	Unit
Second moment of Area of the beam, I_b	5.92031E-07	m ⁴
Beam end stiffness, $K_{be} = 6EI/L_b$	315749.7333	N-m/rad
Rotation due to gravity load, $\theta_i = wL^2/(12(k_{cy}+2EI/L))$	0.0042	rad
Yield rotation of the connector, $\theta_{cy}=M_{cy}/k_{cy}$	0.0170	rad
Beam end rotation, $\theta_{be}=M_{cy}/k_{be}$	0.0071	rad
Yield rotation of the beam column joint, $\theta_{yc} = \theta_{cy} + \theta_{be} - \theta_i$	0.0199	rad
Critical storey displacement, $\Delta_c = \Delta_1$ (Displacement of the first storey)	0.0443	m
Critical storey normalized inelastic drift, δ_c	0.2694	m
Drift amplification factor, $\omega\theta = 1.15 - 0.0034H_n$	1.0000	
Substitute Structure effective height, H_e	4.9374	m
Equivalent System yield displacement, Δ_y	0.0981	m
Substitute Structure Design displacement, Δ_d	0.123	m
Displacement Ductility demand, μ	1.26	
Effective connector stiffness for finite element analysis	104756.6744	N-m/rad
Individual storey masses, m_i	2.0680	Tonne
Total mass of the structure	8.2720	Tonne
Effective mass, m_e	6.9864	Tonne
Effective Stiffness, K_e	133.0108	KN/m
Base Shear Force, $V_{base} = K_e * \Delta_d$	16.4181	KN
Extra force at roof level, $F_t = 0.1V_{base}$	1.6418	KN
Remaining Base Shear other than roof, $0.9V_{base}$	14.7763	KN
Analysis Based on Relative stiffness of Members		
No of interior columns	3	nos
Exterior column shear, V_{c1}	2.05	KN
Interior column shear, V_{c2}	4.10	KN
Exterior column Design moment, M_{c1}	2.18	KN-m
Interior column Design moment, M_{c2}	4.36	KN-m

Figure B.2: Preliminary calculation table of the excel spreadsheet

